

CO₂- SEQUESTRATION ON LABORATORY SCALE:

GEOCHEMICAL INTERACTIONS BETWEEN
INJECTED CO₂, SALINE FLUID PHASES, AND
POTENTIAL RESERVOIR MATERIALS

Dissertation

zur Erlangung des Doktorgrades
der Mathematisch-Naturwissenschaftlichen Fakultät
der Christian-Albrechts-Universität zu Kiel

vorgelegt von

Dipl.-Geol. Katja Beier

Kiel, 2012

Referentin: Prof. Dr. Astrid Holzheid

Koreferent: Prof. Dr. Volker Schenk

Tag der mündlichen Prüfung: 21. Mai 2012

Zum Druck genehmigt: 21. Mai 2012

gez. Prof. Dr. Lutz Kipp, Dekan

Zusammenfassung

Aufgrund des zunehmenden globalen Energieverbrauchs stellt die CO₂-Emission aus Kraftwerken ein weltweites Problem dar. Das während des Verbrennungsprozesses von fossilen Brennstoffen entstehende CO₂ trägt dabei maßgeblich zur Veränderung des Klimas bei. Als eines der Verbundprojekte innerhalb des deutschen Forschungsprogramms GEOTECHNOLOGIEN hat sich das CO₂-MoPa Projekt die Modellierung und Parametrisierung eines virtuellen, subterrestrischen Raumes zum Ziel gesetzt, in welchem verschiedene CO₂-Speicherszenarien untersucht und Methoden zur Dimensionierungs- und Risikoabschätzung erstellt werden sollen. Neben der numerischen und prozessorientierten Modellierung sowie der Erfassung und Validierung von bereits bekannten Daten, sollen experimentelle Laborstudien durchgeführt werden. Die vorliegende Arbeit beschreibt einen Teil dieser Laborstudien, in der die Ermittlung geochemischer Wechselwirkungen zwischen injiziertem CO₂, salinen fluiden Phasen und potentiellen Reservoirmaterialien vorgestellt wird. Vier Hauptziele werden dabei verfolgt: (i) die Ermittlung des geochemischen Reaktionsverhaltens innerhalb eines virtuellen CO₂-Speichers, (ii) die Ermittlung geochemischer und/oder struktureller Veränderungen der beteiligten Reaktionspartner, (iii) die Ableitung kinetischer Daten aus den durchgeführten Experimenten und (iv) der Vergleich der experimentell ermittelten Daten mit Literaturwerten.

Die in der vorliegenden Arbeit dargestellten Daten und Ergebnisse basieren auf Experimenten in geschlossenen, statischen Teflonreaktoren. Alle Versuche sind in Anlehnung an natürliche Bedingungen eines 600 – 700 m tiefen potentiellen Reservoirs konzipiert. Unter Anwendung von Trockeneis als Druckmedium wird innerhalb der Reaktoren ein Gesamtdruck von 85 bar erzeugt. Die für die betrachtete Reservoirtiefe angenommene Temperatur von 35 – 40 °C wird in den durchgeführten Experimenten aus Gründen der schnelleren Kinetik und somit verkürzten Versuchsdauer auf 100 °C bzw. 150 °C erhöht. Durch die Verwendung zweier Temperaturen kann eine Temperaturabhängigkeit der verwendeten Materialien in Bezug auf deren Lösungsverhalten ermittelt werden.

Zur Abbildung des Formationswassers innerhalb eines Reservoirs wird in den Experimenten eine synthetische Na-Ca-K-Mg-Cl Sole (2.6 M) eingesetzt. Diese wird in Anlehnung an ein natürliches Formationswasser (Unterkreide) des Norddeutschen Beckens hergestellt. Das Reservoir an sich wird nicht durch Sandsteinproben möglicher Speicherformationen dargestellt. Zur Vereinfachung der ablaufenden Reaktionen werden natürliche, monomineralische Startmaterialien verwendet. Calcit, Dolomit, Anorthit und Orthoklas charakterisieren daher mögliche Bestandteile natürlicher Reservoirs. Um ein korngößenabhängiges Reaktionsverhalten zu untersuchen, wurden je nach Ausgangsmaterial bis zu vier verschiedene Korngrößen verwendet. Die Injektion von CO₂ in das Reservoir wird durch die Zugabe von Trockeneis realisiert.

Zur Beantwortung der oben genannten Ziele werden verschiedene Analysemethoden und Rechenverfahren eingesetzt.

So lassen sich chemische und strukturelle Veränderungen der festen und fluiden Phasen mittels EMP-, REM-, μ -CT und ICP-OES Analysen nachweisen. Die dabei ermittelten Messergebnisse sind in der Regel mit Literaturwerten vergleichbar. Die Oberflächen post-experimenteller Feldspat-Proben weisen beispielsweise gängige Verwitterungserscheinungen, wie die Bildung von Stufen, Ätzgruben oder Sekundärmineralen, auf. Auch die Ausbildung von Nadeln auf den Oberflächen der Calcit-Proben werden durch Literaturangaben bestätigt. Des Weiteren lassen sich die in der Literatur beschriebenen temperatur- und korngrößenabhängigen Lösungserscheinungen durch ICP-OES Analysen der post-experimentellen fluiden Phasen sowohl für die Versuche mit Feldspäten als auch für die Versuche mit Carbonaten bestätigen. Der Einsatz von EMP- und μ -CT Analysen ist nur bedingt möglich. Die chemischen bzw. strukturellen Veränderungen der eingesetzten Materialien sind zu gering, um signifikante Unterschiede zwischen Edukt und Produkt mit diesen Methoden detektieren zu können.

Die rechnerische Ermittlung kinetischer Daten, wie Lösungsrate oder Aktivierungsenergie, ist unter Verwendung der vorliegenden Messergebnissen in der Regel möglich. Alle ermittelten Daten liegen im Bereich der bekannten Literaturdaten.

Zusammenfassend ist zu sagen, dass mit Hilfe der genutzten Reaktoren geochemische Verhaltensweisen einzelner Mineralphasen innerhalb eines Reservoirs nachgebildet werden können. Im Besonderen ist dabei hervorzuheben, dass innerhalb der vorliegenden Arbeit eine Erweiterung des bisher üblichen, beschriebenen Systems vorgenommen wird. Während frühere Studien zur Ermittlung von Lösungs- und Fällungsprozessen niedrige pT-Bedingungen annahmen, werden in dieser Arbeit pT-Bedingungen ähnlich denen eines potentiellen Reservoirs genutzt. Des Weiteren ist aus früheren Studien die Verwendung geringkonzentrierter Solen, Säuren und Basen oder sogar destillierten Wassers bekannt. Innerhalb dieser Arbeit kommt hingegen eine synthetische Modellsole zum Einsatz, die ein potentielles Formationswasser innerhalb des Reservoirs widerspiegeln kann. Die Auswertung der ermittelten Daten zeigt, dass der Einsatz unterschiedlicher pT-Bedingungen bzw. realitätsnäherer Startmaterialien durchaus einen Einfluss auf das Reaktionsverhalten hat. Die ermittelten Daten bieten daher eine Verbesserung der Güte hinsichtlich ihrer Nähe zu natürlichen Bedingungen.

Mit Hilfe der gewonnenen Daten ist es möglich, weitere noch komplexere Fragestellungen zu beantworten, welche die Natur noch deutlicher wiedergeben (z.B. Einsatz von polymineralischen Startmaterialien). Des Weiteren können die ermittelten Daten in Datenbanken numerischer Modelle eingespeist werden. Eine Verbesserung in der Berechnung verschiedener Speicherszenarien durch realitätsnähere Grundlagendaten ist möglich.

Abstract

Due to the increasing global energy consumption the CO₂ emission of fossil fuel burning power plants is a worldwide problem and contributes significantly to the climate change. As one of the joint research projects within the German GEOTECHNOLOGIEN program the CO₂-MoPa project represents the aim of dimension and risk analyses for subterrestrial CO₂ sequestration by virtual scenario investigations. In addition to numerical and process oriented modeling as well as the compilation and validation of known data, laboratory experiments were accomplished. Within the present work experimental studies about geochemical interaction processes between injected CO₂, saline fluids and potential reservoir materials were accomplished in regard to four main objectives: (i) determination of geochemical reaction behaviors in virtual CO₂ reservoirs, (ii) determination of geochemical and/or structural changes of the reacting agents by using different analytical methods, (iii) derivation of kinetic data from laboratory experiments and (iv) comparison of collected experimental and existing literature data.

The data and results mentioned in the present study are generally based on closed, static teflon autoclave experiments. To reflect natural conditions within reservoirs of 600 – 700 m depth a total pressure of 85 bar were triggered by dry ice (solid carbon dioxide snow). The prevailing temperature of 35 – 40 °C for these reservoir depths is increased to 100 °C and 150 °C to accelerate the kinetic of the ongoing geochemical reactions and thus to reduce the experimental run duration. Using these two temperatures the determination of temperature dependent dissolution behaviors of the used materials is possible.

To mimic the formation water within the reservoir a synthetic Na-Ca-K-Mg-Cl brine (2.6 M) is used and is based on a natural formation water of a Lower Cretaceous sandstone in the Northern German Basin. Within the present study the reservoir itself is not represented by natural sandstone samples of possible reservoirs. In contrast natural, monomineralic starting materials are used to simplify the ongoing chemical reactions. Thus, calcite, dolomite, anorthite and orthoclase characterize possible constituents of natural reservoirs. To determine grain size dependent dissolution behaviors up to four different grain size fractions are used in regard to the starting material. The injection of CO₂ into the reservoir is realized by the addition of dry ice.

To answer the objectives mentioned above different analytical and calculation methods are applied.

Chemical and/or structural changes of solid and fluid phases are detected by EMP-, SEM-, μ -CT and ICP-OES analyses. In general the determined results are comparable with literature data. For example, the mineral surfaces of post-experimental feldspar samples exhibit common dissolution features like steps, etch pits and/or mineral precipitations. Furthermore the development of needles on

post-experimental calcite surfaces can be affirmed by literature data. In addition, temperature as well as grain size dependent dissolution behaviors as described in literature are detected by ICP-OES analyses for both, experiments with carbonates and feldspars. The application of EMP- and μ -CT measurements is limited due to the minor chemical and structural changes of the used materials. Significant differences between reactants and products are therefore not detectable with these methods.

The determination of kinetic data like dissolution rate and activation energy is generally possible by using the measuring results mentioned above. All detected experimental data are comparable with known literature data.

In conclusion, it has to be noted that geochemical behaviors of single mineral phases can be simulated with the used experimental setup. In particular it is to be pointed out that an enhancement of the commonly described system is carried out within the present study. Previous dissolution and precipitation studies were accomplished at low pT-conditions. In contrast all experiments accomplished in the present study run under pT-conditions comparable with pT-conditions within potential reservoirs. Furthermore it is known that previous studies were carried out with low-concentrated brines, acids and bases or distilled water. Within the present study a synthetic model brine is used and mimics the composition of natural formation water within a potential reservoir. The evaluation of the determined data shows a clear influence of the geochemical reaction behavior by using different pT-conditions and more realistic starting materials. Consequently, the determined data exhibit an advanced quality in regard to their more realistic conditions.

Therefore, the collected data provide a basis for more complex scientific questions – e.g. the use of polymineral starting materials. Furthermore the collected data can be included into databases for the numerical modeling. An enhancement of different storage scenario calculations is possible due to more realistic, adapted data.

Contents

Contents	I
List of Figures	III
List of Tables	VII
1 Introduction	1
1.1 Motivation	1
1.2 Aim of the Study	3
2 Influencing Experimental Variables	5
2.1 Experimental Setup	8
2.2 Experimental Conditions	18
2.2.1 Temperature	18
2.2.2 Pressure	22
2.3 Material Properties	25
2.3.1 pH - value	26
2.3.2 Ionic Strength	29
3 Experimental Techniques & Materials	32
3.1 Experimental Technique	32
3.1.1 Teflon Reactor Experiments	33
3.1.2 PARR Reactor Experiments	35
3.2 Materials	37
3.3 Analytical Methods	40
3.3.1 Analyses of Solid Materials	40
3.3.2 Solution Analyses	41
4 Experimental Results & Interpretation	43
4.1 Teflon Reactor Experiments at Carbonatic Samples	43
4.1.1 Analyses of the Solid Samples	44
4.1.2 Analyses of the Fluid Samples	50

4.2	Teflon Reactor Experiments at Feldsparic Samples	73
4.2.1	Analyses of the Solid Samples	74
4.2.2	Analyses of the Fluid Samples	84
5	Summary & Outlook	97
	Bibliography	103
	Appendix	
A	Figures	A 1
B	Tables	B 1

List of Figures

1.1	Structure and linkages between individual sub-projects within the joint project CO ₂ -MoPa	4
2.1	Influence of three important experimental parameters on the carbonate dissolution process	7
2.2	Various reactor types and their possible capabilities for experimental studies on CO ₂ -sequestration aspects	10
2.3	Starting point for a dissolution process (t = 0)	12
2.4	Beginning of the dissolution process (t = 1) within a closed reactor system without stirring or fluid flow	13
2.5	Ongoing dissolution process within a closed reactor system without stirring or fluid flow (t = 2)	14
2.6	Influence of a movement process within a closed reactor system (t = 3)	15
2.7	Literature data of stirring rate depending calcite dissolution processes in batch reactors	16
2.8	Influence of a faster movement process within a closed reactor system (t = 4)	17
2.9	Temperature as influencing parameter for calcite dissolution rates: a detailed comparison	19
2.10	Temperature as influencing parameter for feldspar dissolution rates	19
2.11	Detailed description of the temperature dependency on feldspar dissolution rates	20
2.12	Partial CO ₂ pressure as influencing parameter for calcite dissolution rates: a detailed comparison	23
2.13	pH-value as influencing parameter for calcite dissolution rates	27
2.14	Ionic strength as influencing parameter for calcite dissolution rates	30

3.1	Schematical sketch of the used teflon reactors	33
3.2	Schematical sketch of the used PARR reactor	36
3.3	Photo-micrographs and backscattered electron images of the starting materials	38
3.4	Composition of the used synthetic model brine	40
4.1	CaO content of pre- & post-experimental calcite samples as function of the experimental run duration and the applied grain size	45
4.2	SEM photomicrographs of the starting materials calcite & dolomite	46
4.3	SEM images of post-experimental calcite grains after a 1-day run duration	47
4.4	SEM images of post-experimental calcite grains after a 30-day run duration	48
4.5	SEM images of post-experimental dolomite grains after a 1-day run duration	49
4.6	SEM images of post-experimental dolomite grains after a 30-day run duration	49
4.7	Temperature dependent alteration of the model brine in regard to the Ca-concentration and corresponding calcite dissolution rates	55
4.8	Comparison of calculated dissolution rates and literature data (temperature dependent)	56
4.9	Derivation of the activation energy of calcite	60
4.10	Grain size dependent alteration of the model brine in regard to the Ca-concentration and corresponding calcite dissolution rates	63
4.11	Gas-phase dependent alteration of the model brine in regard to the Ca-concentration and corresponding calcite dissolution rates	68
4.12	Comparison of calculated dissolution rates and literature data (pH-value dependent)	69
4.13	Material dependent alteration of the model brine in regard to the Ca- and Mg-concentration	71
4.14	Photo-micrographs of the starting materials anorthite & orthoclase	76
4.15	SEM images of post-experimental anorthite grains after a 30-day run duration	77
4.16	SEM images of post-experimental orthoclase grains after a 30-day run duration	78

4.17 Grain volume distribution compared to the grain size (constant grey thresholds)	81
4.18 Grain volume distribution compared to the grain size (variable grey thresholds)	82
4.19 Schematical illustration of the grain size determination by μ -CT analyses	83
4.20 Temperature dependent alteration of the model brine in regard to the Si-concentration (starting material: orthoclase)	87
4.21 Grain size dependent alteration of the model brine in regard to the Si-concentration (starting material: orthoclase)	91
4.22 Grain size dependent development of orthoclase dissolution rates	92
4.23 Comparison of calculated dissolution rates and literature data	93
4.24 Theoretical development of dissolution rates by using different values for the reactive surface	94
4.25 Schematic illustration of reactive surfaces	95
A.1 Various construction elements of the used teflon reactor as well as used preparation equipments	A 2
A.2 p-T characteristics of nine reference experiments	A 2
A.3 Experimental setup of the used PARR reactor	A 3
A.4 SEM analyses of the used teflon meshes before and after a teflon reactor experiment	A 3
A.5 Chemical composition of the initial model brine and their endurance over the period of storage	A 4
A.6 Backscattered electron images of reacted calcite grains and the points of measuring	A 5
A.7 Simplified illustration of the functionality of the micro computertomography	A 6
A.8 Temperature dependent alteration of the model brine with increasing run duration (starting material: calcite)	A 7
A.9 Grain size dependent alteration of the model brine with increasing run duration (starting material: calcite)	A 8
A.10 Temperature dependent alteration of the model brine with increasing run duration (starting material: orthoclase) – single measurements	A 9
A.11 Temperature dependent alteration of the model brine with increasing run duration (starting material: orthoclase) – average values	A 10

A.12 Grain size dependent alteration of the model brine with increasing run duration (starting material: orthoclase) – single measurements	A 11
A.13 Grain size dependent alteration of the model brine with increasing run duration (starting material: orthoclase) – average values	A 12

List of Tables

2.1	Comparison of three injection projects and their reservoir conditions	11
3.1	Comparison of Reynolds numbers described in the literature and calculated within the present study	35
3.2	Chemical formula of the used mineral phases	37
4.1	Determined parameters as basis of activation energy calculations	59
4.2	Determined reactive surfaces for carbonatic materials described in the literature	64
4.3	Experimental conditions of experiments at orthoclase samples analyzed by μ -CT measurements	80
4.4	Determined grey values using the manual threshold detection	82
B.1	Overview of compared mineral dissolution experiments and their corresponding references	B 2
B.2	EMP measurements of unreacted carbonate samples regarding their chemical composition	B 4
B.3	EMP measurements of unreacted feldspar samples regarding their chemical composition	B 5
B.4	Overview of the accomplished monomineralic experiments and the appendant experimental conditions	B 6
B.5	EMP measurements on a subset of reacted calcites grains	B 7
B.6	Results of ICP-OES measurements on post-experimental fluid samples (<i>calcite: 250 – 500 μm, T: 100°C</i>)	B 8
B.7	Validation of the reproducibility of experimental data (<i>calcite: 250 – 500 μm, T: 100°C</i>)	B 11
B.8	Results of ICP-OES measurements on post-experimental fluid samples (<i>calcite: 250 – 500 μm, T: 150°C</i>)	B 12

B.9	Validation of the reproducibility of experimental data (<i>calcite</i> : 250 – 500 μm , T : 150°C)	B 15
B.10	Results of ICP-OES measurements on post-experimental fluid samples (<i>calcite</i> : 160 – 250 μm , T : 150°C)	B 16
B.11	Validation of the reproducibility of experimental data (<i>calcite</i> : 160 - 250 μm , T : 150°C)	B 18
B.12	Results of ICP-OES measurements on post-experimental fluid samples (<i>calcite</i> : 63 – 160 μm , T : 150°C)	B 19
B.13	Results of ICP-OES measurements on post-experimental fluid samples (<i>calcite</i> : <63 μm , T : 150°C)	B 21
B.14	Results of ICP-OES measurements on post-experimental fluid samples (<i>calcite</i> : 250 – 500 μm , T : 150°C, <i>without</i> CO_2) . . .	B 23
B.15	Calcite dissolution rates and related parameters for determination	B 24
B.16	Results of ICP-OES measurements on post-experimental fluid samples (<i>dolomite</i> : 250 – 500 μm , T : 150°C)	B 26
B.17	Validation of the reproducibility of experimental data (<i>dolomite</i> : 250 – 500 μm , T : 150°C)	B 29
B.18	Dolomite dissolution rates and related parameters for determination	B 30
B.19	Results of ICP-OES measurements on post-experimental fluid samples (<i>orthoclase</i> : 250 - 500 μm , T : 100°C)	B 31
B.20	Validation of the reproducibility of experimental data (<i>orthoclase</i> : 250 - 500 μm , T : 100°C)	B 34
B.21	Results of ICP-OES measurements on post-experimental fluid samples (<i>orthoclase</i> : 250 - 500 μm , T : 150°C)	B 35
B.22	Validation of the reproducibility of experimental data (<i>orthoclase</i> : 250 - 500 μm , T : 150°C)	B 38
B.23	Results of ICP-OES measurements on post-experimental fluid samples (<i>orthoclase</i> : 160 - 250 μm , T : 150°C)	B 39
B.24	Validation of the reproducibility of experimental data (<i>orthoclase</i> : 160 - 250 μm , T : 150°C)	B 42
B.25	Orthoclase dissolution rates and related parameters for determination	B 43

Chapter 1

Introduction

1.1 Motivation

Due to the increasing global energy consumption the CO₂ emission of fossil fuel burning power plants is a widespread problem. As one of the most important greenhouse gases CO₂ contributes significantly to the climate change. For several years scientists as well as the energy producing industry are concerned with the topic of CO₂ sequestration and work on methods and techniques to minimize the CO₂ emission that is directly related to fossil fuel burning power plants. In general CO₂ sequestration includes the separation of CO₂ from power plants, the transport and the storage of CO₂ in capable reservoirs. To make the storage technique as safe as possible it is important to study the processes in the reservoir and the surrounding rock formations in detail. This results in quite diverse fields of scientific research. One example is the modeling of different CO₂ injection and expansion scenarios in the reservoir. Therefor existing software is partly adapted or newly generated with regard to the topic of CO₂ sequestration. Furthermore geomechanical and geochemical interactions between the injected CO₂ and coexisting phases in the reservoir have to be study either in laboratory experiments or with the help of field/pilot projects. All these methods are developed with the aim to design a new technique to reduce the emission of greenhouse gases and to estimate the dimension, the risk and the sustainability of this technique.

As described above, the knowledge of geochemical interactions, like dissolution and/or precipitation processes, between injected CO₂ and coexisting phases (e.g. reservoir material, formation fluids) as well as the displacement of reservoir particles during and/or after the CO₂ injection is very important for potential reservoir sites. These potential injection sites generally consist of reservoir rocks (e.g. sandstones, coalbeds) and cap rocks (e.g. mudstones,

limestones, shales) which include silicates like quartz, feldspar, pyroxene or olivine, carbonates like calcite, dolomite or magnesite, and/or clay minerals like kaolinite, montmorillonite, illite or smectite. All these natural mineral phases exhibit different properties in contact with CO₂-bearing fluids. Therefore a reliable statement about geochemical interactions in a capable reservoir requires detailed information about kinetic processes of the individual mineral and possible reaction partners.

In the past numerous dissolution experiments on natural monomineralic materials like the mineral phases mentioned above were accomplished by different research groups. A complex literature survey exhibits a high diversity of scientific questions. In the determination of carbonate dissolution processes the following observations can be noticed. Earlier studies for example dealt with (i) exchange and/or replacement reactions on carbonates (Chou et al. (1989)), (ii) relationships between active sites on strained calcites and the dissolution rate (Schott et al. (1989)), or (iii) the understanding of simple CaCO₃-CO₂-H₂O system processes to resolve various questions in the aqueous modeling (Plummer and Busenberg (1982)). In general the aim of these studies was to understand fundamental mineral dissolution processes at simple experimental conditions (e.g. atmospheric pressure; deionized water or low ionized salt solutions). In contrast numerous recent publications deal with the subject of CO₂ sequestration. The research group of Pokrovsky (Toulouse, France) for example studies with the characterization of the reactivity of carbonates under elevated pressures (Pokrovsky et al. (2005)) or the influence of inorganic and organic ligands on the calcite/magnesite dissolution process (Pokrovsky et al. (2009)). Other authors describe dissolution processes on carbonates as functions of (i) the fluid composition and the ionic strength, respectively (Finneran and Morse (2009), Gauteliet al. (2007), Gledhill and Morse (2006a)), (ii) mineral impurities (Eisenlohr et al. (1999)) or (iii) various experimental parameters like pH-value, temperature or pressure (Druckenmiller et al. (2006), Yadav et al. (2008)). In general the accomplished experiments were adapted to more natural conditions (pressure, temperature, fluid composition, sophisticated apparatuses) during the last years. Furthermore the modeling of complex processes during the CO₂ sequestration plays an important role in recent publications.

The described scientific questions result in a large number of various experimental parameters – reactor type, experimental conditions, starting materials to name a few – which distinguish the diverse studies and generate to some extent very different kinetic data. This observation raises the following questions: Which experimental setups and/or conditions describe certain natural circumstances? Which parameters influence the kinetic data and how strong are these effects? Which literature data is suitable to compare to own data?

One main part of the present work was to describe the differences of scientific questions and the consequential changes of experimental conditions and parameters. Furthermore the degree of influence of each single experimental parameter as well as the influence of various parameters to other parameters should be estimated. The second part of this work consisted of the accomplishment of static laboratory experiments by using existing and new apparatuses, to improve the knowledge of dissolution and/or precipitation mechanisms related to the subject of CO₂ sequestration. With the help of different analytical methods the changes of the solid material and the fluid phase during the experiment were determined and placed into the context of CO₂ sequestration.

1.2 Aim of the Study

The present PhD thesis was performed as part of the CO₂-MoPa¹ project, which is funded by the German Federal Ministry of Education and Research (BMBF), EnBW Energie Baden-Württemberg AG, E.ON Energie AG, E.ON Ruhrgas AG, RWE Dea AG, Vattenfall Europe Technology Research GmbH, Wintershall Holding AG and Stadtwerke Kiel AG within the framework of the special program GEOTECHNOLOGIEN. The overall aim of the still ongoing CO₂-MoPa project is to investigate dimension and risk analyses for subterrestrial CO₂ sequestration on virtual scenarios. Therefor the following objectives and main questions were established and were examined with the help of the following approaches. The development of numerical, process-oriented and integral model tools provides quantitative conclusions about long-term retention of dense CO₂ in deep geological formations. Furthermore, in consideration of hydraulic, geometrical, geochemical and geomechanical processes, prognoses on the migration of CO₂ in deep as well as in shallow subsurfaces could be established. To support the model development accompanying geochemical and geomechanical laboratory experiments were accomplished. The compilation of a validated, consistent and comprehensive database is essential (i) to provide a base for numerical modeling and (ii) to collect and safe data, which were determined within the project. Synthetic virtual-type scenario simulations depict the assessment of usable CO₂ storage capacities (dimensional analyses) and possible influences of protected resources during a CO₂ leakage (risk analyses). All mentioned objectives and approaches were realized by 11 sub-projects of various geoscientific institutes in Kiel, Leipzig and Stuttgart as well as the State Agency for Agriculture,

¹Modeling and Parameterization of CO₂ storage in deep saline formations for dimension and risk analyses

Environment and Rural Areas. Figure 1.1 shows the structure and linkages between the individual sub-projects.

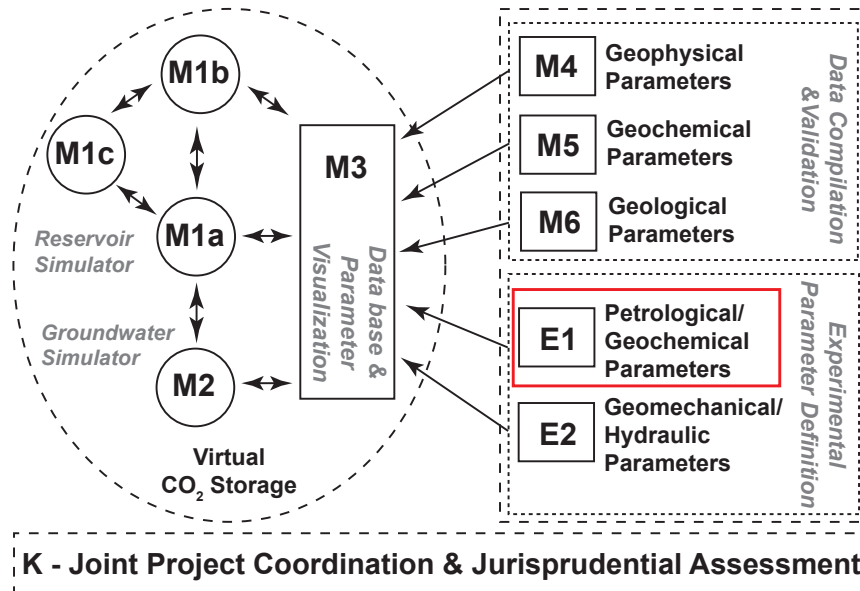


Figure 1.1: Structure and linkages between individual sub-projects within the joint project CO₂-MoPa; red square: present work as part of the sub-project E1 "Petrological/Geochemical Parameters"

The present work (red square within figure 1.1) was one part of the subproject E1 with the working title "Experimental simulation of chemical interactions between injected CO₂, saline fluids and reservoir rocks as well as the influence of chemical interactions on reservoir rock microstructures". In relation to experimental laboratory simulations the following objectives and approaches were handled. To determine geochemical reaction behaviors and interactions in virtual CO₂ reservoirs static laboratory experiments with CO₂-bearing brines and potential reservoir materials were accomplished under p-T conditions similar to CO₂ reservoir rocks far from injection sites. Based on these laboratory experiments the knowledge about dissolution and/or precipitation processes during the reaction progress was expanded and kinetic data like dissolution/precipitation rates or activation energies was derived. A summarizing comparison of collected data and literature data completed the present work.

Chapter 2

Influencing Experimental Variables and their Impact on Kinetic Data

As mentioned in chapter 1.1 numerous dissolution experiments on natural monomineralic materials were accomplished in the past by different research groups. To exhibit the high diversity of scientific questions and to estimate the influence of individual experimental parameters on the dissolution behavior, a detailed literature study was accomplished. The following comparisons and observations are based on 30 representative publications, which present an overview of the experimental work of the last forty years. According to possible reservoir and cap rock materials the present literature survey includes mineral dissolution reactions of quartz and various feldspar group members, carbonates and clay minerals, respectively. All used references are listed in appendix B.1.

Publications including experiments with carbonates were chosen for a first comparison to provide a general view about influencing parameters on dissolution processes. In the past this mineral group was preferred because of the distinct solubility and therefore the fast kinetic of these minerals. Thus numerous experimental studies result in a substantiated data base which allows a detailed comparison of various influencing parameters. Furthermore in respect to CO₂ sequestration processes carbonates are able to represent mineral phases of reservoir materials as carbonates in grain assemblages and also as part of the bonding cement. In the course of the literature study it can be noticed that the pH-value, the temperature and the fluid composition are the most varying parameters. Figure 2.1 shows these three parameters as influencing factors on the dissolution rate. The most obvious dependence is caused by the pH-value (c.f. figure 2.1A), which ranges from -1.099 to 11.7

with most experiments in the low acid to neutral pH-milieu. The decreasing dissolution rate with increasing pH-value is caused by the proton induced dissolution of carbonates. During the dissolution process in a $\text{H}_2\text{O}-\text{CO}_2-\text{CaCO}_3$ system multiple consecutive and parallel reactions took place. For example the dissociation of water and the dissociation of CO_2 in water. Consequently protons were released, which consumed CO_3^{2-} from the carbonate dissolution. Compared to the pH-value the temperature (c.f. figure 2.1B) does not show such a pronounced dependence. The commonly used temperatures range from 3°C to 150°C . Noticeable not all temperatures had the same significance. Most experiments run at room temperatures (25°C) followed by temperatures of 50°C and 80°C . These three temperatures exhibit a large spreading of dissolution rates. For example the temperature of 25°C describes a spreading in the dissolution rate of about 12 orders of magnitude. Detailed information in the literature suggest that other parameters like the pH-value, the pressure or the experimental setup cause this wide range. The same phenomena can be described for the ionic strength (c.f. figure 2.1C). The ionic strength used most often ranged from 0 to 0.1 M. Within this range the dissolution rate also spread between 12 orders of magnitude. One reason for this large difference results from varying compositions of the fluids. Whereas a fluid with an ionic strength of 0 M is generally described by deionized water, fluids with higher ionic strength can include different acids and bases, salts or organic ligands. These varying compositions result in different dissolution rates. Stronger solutions up to an ionic strength of 5.5 M were used considerably less.

Based on this first comparison the following observation can be made: the wide spreading of dissolution rates for single parameters approves no clear general information about the influence of these parameters on dissolution rates. Dissolution experiments include a lot of variables which can be changed because of the large number of scientific questions. Therefore it is important to describe the influences of parameters (pH-value, temperature, ionic strength, etc.) in more detail.

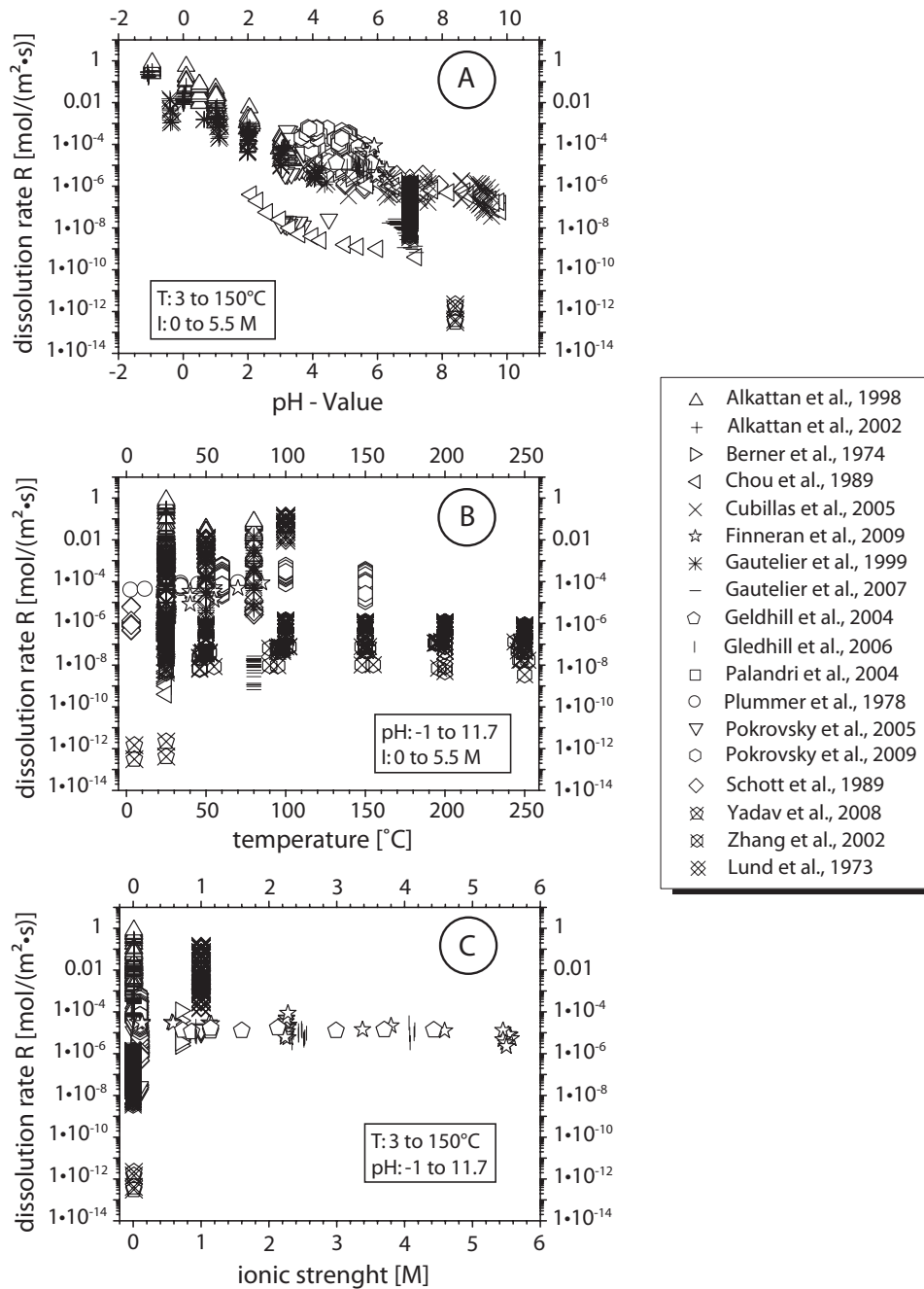


Figure 2.1: Influence of three important experimental parameters on the carbonate dissolution process: **A** – pH-value vs. dissolution rate, **B** – temperature vs. dissolution rate, **C** – ionic strength vs. dissolution rate. Detailed information see text. References see appendix B.1.

2.1 Experimental Setup

To utilize a capable experimental setup it is important to describe natural procedures as true as possible. In the case of CO₂ sequestration figure 2.2 shows a schematical cross section of one possible virtual geological storage scenario - the geological trapping in oil/gas deposits and saline aquifers, respectively. Porous rock formations like sandstones build up the reservoir where dense CO₂ from industrial separation processes will be injected. These layers are surrounded by cap rock formations like mudstones, which trap the injected CO₂ in the reservoir. Based on the figure it can be noticed that different locations in the reservoir exhibit different geomechanical, geochemical and flow through regimes. At the point of injection dense CO₂ displaces most of the formation water and gas/oil, respectively, and causes a disturbed fluid flow. In contrast phases like dissolved CO₂, CO₂ bubbles and formation water or gas/oil dominate the reservoir far from the injection site, where a natural fluid flow arises. With the help of various CO₂ sequestration pilot projects and the knowledge of oil/gas productions information of the underground can be provided. Table 2.1 shows exemplary three different injection projects and their reservoir conditions. The wide range of injection site parameters becomes apparent already on these three examples. Whereas the Permian coalbed of the Qinshui Basin (China) resides at about 471 m depth, the carboniferous sandstone formation in Algeria resides in a depth of more than 1800 m. Directly related to the reservoir's depth the temperatures varied between 25 °C and 90 °C as well as the reservoir pressures ranged from 12 to 179 bar. The knowledge of these conditions already describe the spread of possible experimental setups.

Despite the various scientific questions which have to be answered in the literature, mainly two different reactor types were described: flow through reactors (c.f. figure 2.2 left box, e.g. after Gautier et al. (2000)) and batch reactors (c.f. figure 2.2 right box, e.g. present work: chapter 3.1). Depending on the regulated stirring rate and fluid flow, respectively, both reactor types are able to reproduce laminar as well as turbulent fluid regimes. In the case of CO₂ sequestration reactions close to the injection site can be simulated by flow through reactors (also called mixed flow reactors in some publications). This experimental setup permits a fluid flow (e.g. brine, gas phase or brine-gas mixture) through a rock body (e.g. sandstone drill core, selected bulk solids). In general flow through reactors are open systems, where unreacted fluids were injected and reacted fluids were separated during the entire run duration. The accomplished fluid flow rates as well as stirring rates mentioned in the literature range from 2.5×10^{-4} to 20 ml/min and 100 to 1000 rpm, respectively. The fluid flow is induced by various pump systems and

the stirring is induced by impeller systems, magnetic stirrer or the rotating disk method. For the latter method a monomineral solid or a pressed powder tablet is installed in a fastener and rotated continuously. Data about the volume of the used reactors varied between 75 and 550 ml. At sufficiently small stirring rates or fluid flow rates, flow through reactors are also able to simulate processes far from the injection site, where a natural fluid flow regime arises (e.g. coefficient of hydraulic conductivity of sandstones: 10^{-5} to 10^{-10} m/s). In contrast to flow through reactors the also mentioned batch reactors are only able to reproduce processes far from the injection site. Caused by their static experimental conditions the limited exchange between fluid and solid in a natural reservoir with undisturbed flow regime can be simulated. In literature batch reactors with magnetic stirrer, impeller systems or the rotating disk method are described, where the accomplished stirring rates range from 10 to 2630 rpm. Occasionally an internal circulation of the fluid is described. Volume data for the used batch reactors range from 30 to 550 ml. Both reactor types – flow through reactors and batch reactors – are able to simulate high temperature and high pressure conditions. In literature accomplished temperatures range from 2.5 °C to 300 °C. The total pressure ranges from 1 to 124 bar. The experimental parameters summarized in this literature review cover the natural conditions mentioned in table 2.1. In consequence possible CO₂ sequestration scenarios could be simulated by the mentioned experimental setups.

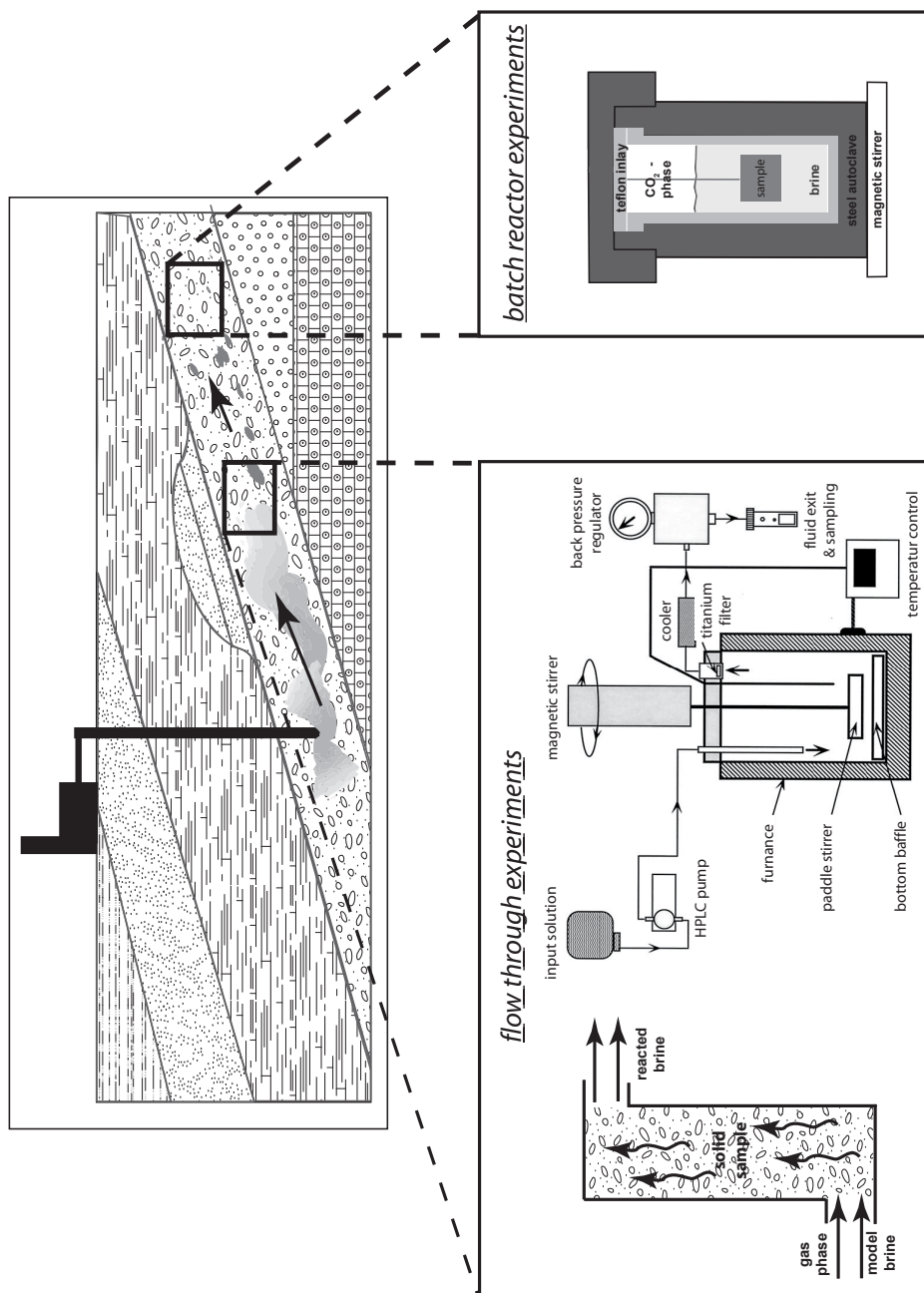


Figure 2.2: Various reactor types and their possible capabilities for experimental studies on CO₂-sequestration aspects: left - flow-through column; middle - mixed flow reactor after Gautier et al. (2000); right - closed batch reactor (present work: chapter 3.1).

Table 2.1: Comparison of three injection projects and their reservoir conditions

Ketzin (Germany)^a	
reservoir material	Triassic sandstone (Stuttgart Fm.)
reservoir depth	630–650 m
reservoir thickness	80 m
reservoir temperature	34 °C
pressure	73 bar
injection rate	86 t/day
utilization	pilot project

Qinshui (China)^b	
reservoir material	Permian coal
reservoir depth	471 m
reservoir thickness	6 m
reservoir temperature	25 °C
pressure	12.96 bar
injection rate	22.65 m ³ /day
utilization	pilot project

In Salah (Algeria)^a	
reservoir material	Carboniferous sandstone (Krechba Fm.)
reservoir depth	1850 m
reservoir thickness	29 m
reservoir temperature	90 °C
pressure	179 bar
injection rate	3500 t/day
utilization	commercial

^a Michael et al. (2010)^b Canadian International Development Agency (2007)

To compare literature data the knowledge of dissolution mechanism during different flow regimes is very important. Various authors like Plummer et al. (1978); Dreybrodt and Buhmann (1991); Raines and Dewers (1997) and Pokrovsky et al. (2005) describe these dissolution mechanisms for different experimental setups. Following explanations describe the main mechanism of dissolution processes in closed undisturbed systems, closed systems with laminar fluid flow and closed systems with turbulent fluid flow without paying attendance to possible pH- or temperature effects. All listed dissolution mechanisms are basically explained by carbonate dissolution processes, although some of them can also be extended to other minerals. The starting point ($t = 0$) of each experiment - regardless of the reactor type - is illustrated in figure 2.3.

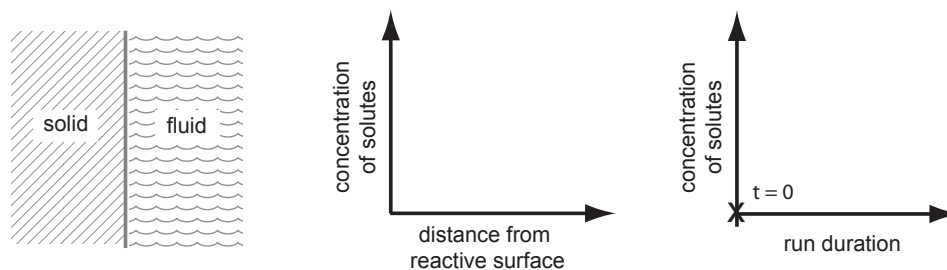


Figure 2.3: Starting point for a dissolution process ($t = 0$): solid and fluid are in direct contact with each other. The mineral surface and the fluid composition are well-defined. The fluid is present in its original composition and does not include solutes from mineral dissolution. The initial concentrations of possible solutes within the original fluid are far from the saturation concentrations of these solutes. Existing p-T conditions in the reactor allow dissolution processes.

A solid sample (e.g. individual mineral crystal, mineral powder or pressed mineral powder tablet) with known surface and a fluid with known composition are in direct contact to each other. At the beginning of the experiment the fluid is present in its original composition and does not include any solutes from mineral dissolution processes. In addition the initial concentrations of possible solutes within the original fluid are far from the saturation concentrations of these solutes to allow dissolution processes. Furthermore existing p-T conditions accomplished in the experiment permit mineral dissolution processes. With the initiation of dissolution ($t = 1$) in undisturbed systems, like batch reactors without stirring and/or fluid flow, transport controlled processes will start (see Plummer et al. (1978); Raines and Dewers (1997), Pokrovsky et al. (2005)). After Raines and Dewers (1997) these transport

controlled mechanisms are controlled by a five-step process, where chemical and hydrodynamical interactions between mineral and fluid take place. At first the reactants of the initial fluid have to reach the mineral surface. Adjacent these reactants have to be adsorbed on the mineral surface to trigger a chemical reaction between fluid and solid. As final steps the reaction products have to be transported and included into the initial solution. During this perseverative and to some extent coexisting five-step process a diffusion layer forms, where a gradient of solute concentration within the fluid develops (see figure 2.4).

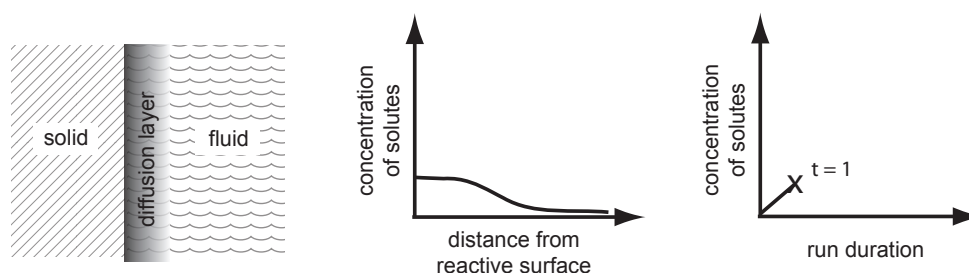


Figure 2.4: Beginning of the dissolution process ($t = 1$) within a *closed reactor system without stirring or fluid flow*: caused by a five stage dissolution process a diffusion layer builds up whereat a concentration gradient of solutes arise (detailed information see text). The overall concentration of solutes in the fluid increase as result of the dissolution process. The slowest dissolution step determines the rate of the overall reaction progress.

Close to the reactive surface the solute concentration is the highest. With increasing distance to the reactive surface the solute concentration decreases. With proceeding run duration ($t = 2$) the concentration gradient between the reactive surface and the fluid becomes steeper due to the ongoing release of solutes (see figure 2.5). Along with these phenomena the diffusion layer also expands. Dreybrodt and Buhmann (1991) ascribe two inhibiting effects of the diffusion layer: (i) thicker diffusion layers result in slower diffusion velocities of reactants and reaction products, respectively and (ii) the heterogeneity of the chemical reaction onto the reactive surface. Caused by these limiting effects reactions within undisturbed closed reactor systems are termed "transport controlled" processes. Even at slow diffusion velocities in the presence of thick diffusion layers an exchange of reactants and reaction products takes place and results in an increase of solutes in the total fluid volume. Within an appropriate run duration it is possible to achieve equilibrium conditions between solid and fluid, where the dissolution rate approaches zero.

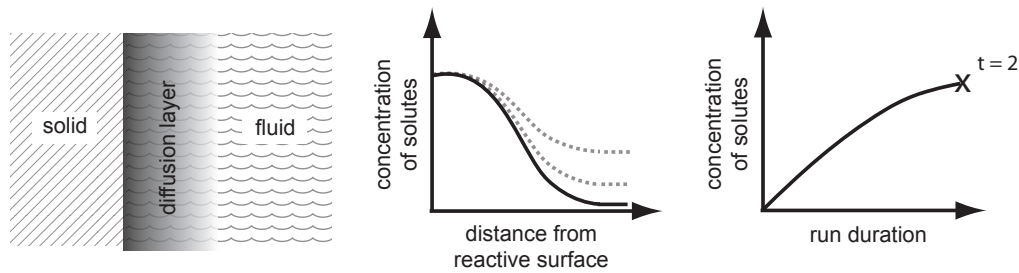


Figure 2.5: Ongoing dissolution process within a *closed reactor system without stirring or fluid flow* ($t = 2$): proceeding dissolution processes result in an increase of the diffusion layer thickness. The concentration of solutes near the solid surface increase with increasing run duration: the concentration gradient gets steeper. With ongoing run duration the overall solute concentration within the fluid increases because of diffusion effects. Reaching the saturation concentration is possible.

Starting a movement process - stirring the fluid, rotating the sample or fluid flow through - the hydrodynamic conditions in the described closed batch reactor systems change extremely in some cases. In the case of a laminar flow regime ($Re \leq 12.050$ after Raines and Dewers (1997)) following changes can be observed (see figure 2.6). As a consequence of the initiating movement the transport of reactants and reaction products, respectively, is not only determined by diffusion processes but also determined by hydrodynamic processes. Therefore Raines and Dewers (1997) describe the interface between fluid and solid as hydrodynamic boundary layer instead of diffusion layer. Due to the movement the mass transport of reactants/reaction products accelerates, which results in a decrease of the hydrodynamic boundary layer thickness. Accompanying this fact the dissolution rate increases. Furthermore the concentration gradient of solutes between mineral surface and fluid phase becomes steeper. Within the hydrodynamic boundary layer the transport of reactants/reaction products is still determined by diffusion processes. Whereas a perfect mixing of reactants/reaction products beyond the hydrodynamic boundary layer takes place by convective fluid flow (Dreybrodt and Buhmann (1991)). With adequate dissolution of the mineral phase the achievement of an equilibrium state becomes faster in experiments including stirring/fluid flow than in completely static experiments, because of higher dissolution rates within stirred/flow through systems.

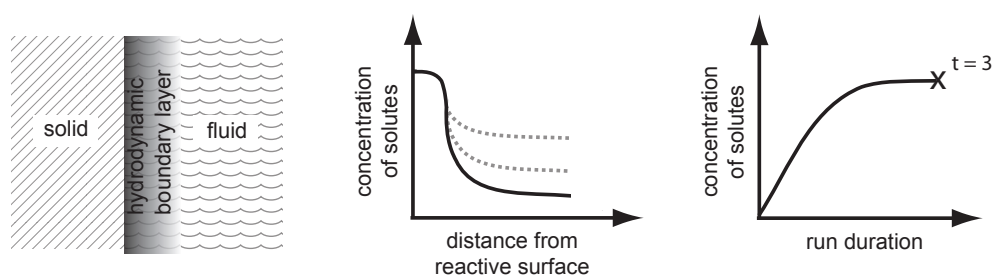


Figure 2.6: Influence of a movement process within a *closed reactor system* ($t = 3$): stirring and/or fluid flow induces *laminar fluid flow* ($Re \leq 10.000$). Merging of the fluids results in a decrease of the hydrodynamic boundary layer thickness. At the beginning of the movement process the solute concentration gradient within the hydrodynamic boundary layer is steep. The ongoing movement effects an increase of the overall solute concentration and therefore a flatter solute concentration gradient develops. Since the reaction products are not removed, a saturation concentration and consequently an equilibrium between mineral and fluid can be reached.

Various authors not only describe changes in dissolution rates between static and stirred/flow through systems but also describe dependencies of the dissolution rate regarding the stirring rate/disk rotation speed/fluid flow rate. Dreybrodt and Buhmann (1991), Raines and Dewers (1997) as well as Pokrovsky et al. (2005) for example describe a linear increase of the dissolution rate with increasing stirring rate/disk rotation speed/fluid flow under laminar fluid flow conditions (see figure 2.7). In addition Plummer et al. (1978) as well as Alkattan et al. (1998) describe an influence of the dissolution rate by the position of the sample or stirring propeller within the reactor. Similar configurations resulted in linear dependencies of the dissolution rate with regard to the stirring rate/flow rate. However, small changes in the configuration already reflected an impact on the dissolution behavior (see figure 2.7B).

A further increase in the stirring rate/fluid flow within closed batch reactor systems induces a turbulent flow regime (see figure 2.8). This turbulent fluid flow could cause a complete breakdown of the hydrodynamic boundary layer which results in higher dissolution rates. Raines and Dewers (1997) demonstrated this phenomena with accomplished experiments whereat the linear development of the dissolution rate at laminar fluid regimes changes into a parabolic development of the dissolution rate at turbulent fluid regimes. In the previous mentioned phases the transport of reactants/reaction products through the diffusion layer and the hydrodynamic boundary layer, respec-

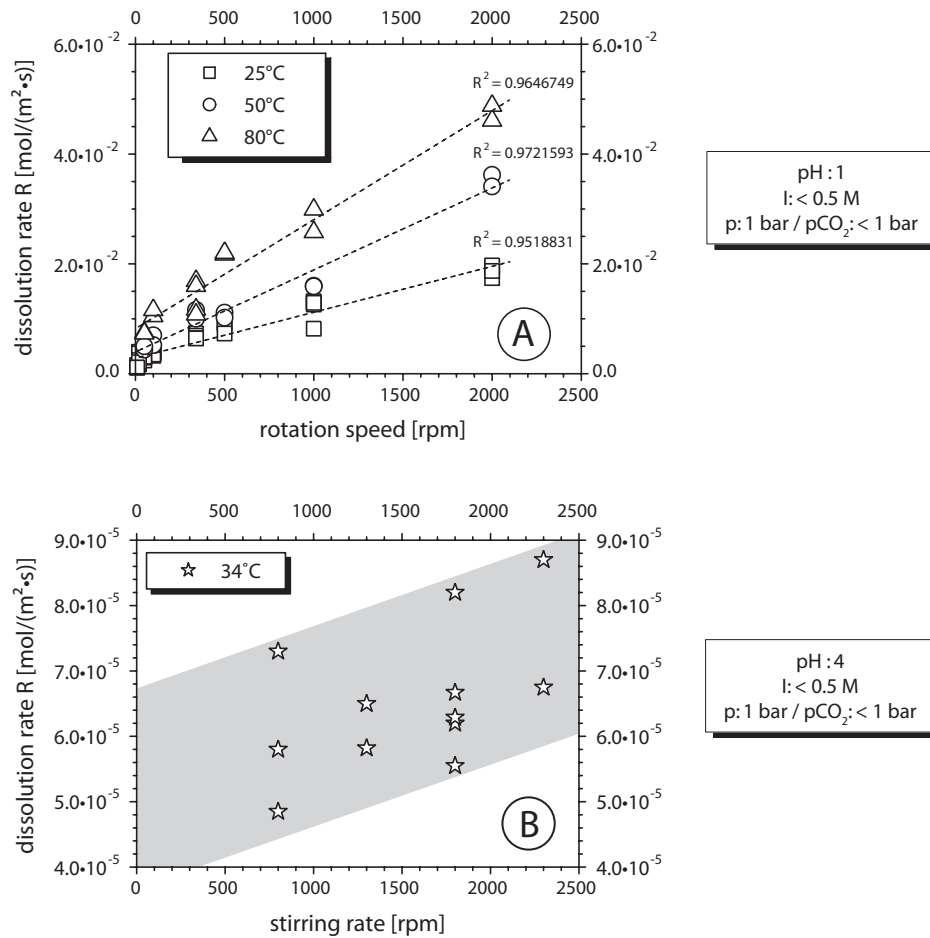


Figure 2.7: Literature data of stirring rate depending calcite dissolution processes in batch reactors: **A** – after Alkattan et al. (1998); **B** – after Plummer et al. (1978).

tively was the limiting factor of the dissolution processes. Due to fast velocities within the fluid the mass transport of reactants/reaction products is so high, that chemical reactions on the mineral surface are the limiting factor which significantly influences the dissolution rate (Dreybrodt and Buhmann (1991)). Therefore the occurring processes were no longer determined as transport controlled processes but rather as surface controlled processes (Raines and Dewers (1997)). Based on the movement process all reaction products which are released during the dissolution process dispersed evenly in the fluid. A solute concentration gradient between mineral surface and fluid cannot be formed.

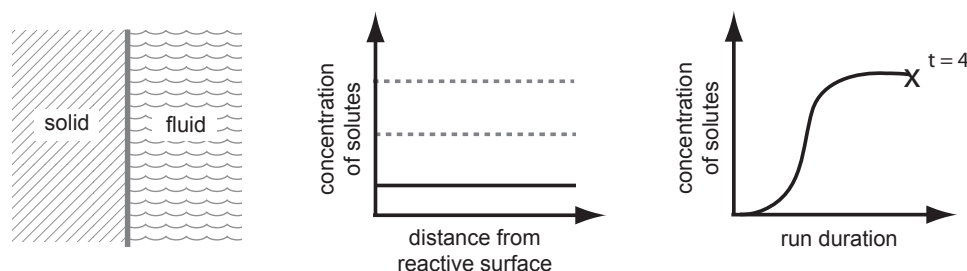


Figure 2.8: Influence of a faster movement process within a *closed reactor system* ($t = 4$): stirring and/or fluid flow induces *turbulent fluid flow* ($Re \geq 10.000$). Due to the fast velocities a complete breakdown of the hydrodynamic boundary layer is possible. Dissolution processes change from transport controlled into surface controlled processes. The increasing rate of feed of the reaction products results in a faster achievement of the solute saturation concentration within the fluid.

In regard to the above mentioned processes within closed batch reactor systems - with and without stirring/fluid flow - well defined differences of the dissolution rate can be observed. Within a completely static reactor a diffusion layer builds up and consequently decelerates the dissolution process. Once a movement mechanism initiates, the diffusion layer/hydrodynamic boundary layer shrinks. At laminar flow regimes the shrinking diffusion layer/hydrodynamic boundary layer results in a linear increasing dissolution rate with increasing stirring rate/disk rotation speed/fluid flow. During experiments with turbulent flow regimes the hydrodynamic boundary layer disappears completely with the result of a parabolic increase of dissolution rates with increasing stirring rate/disk rotation speed/fluid flow. The initial transport controlled dissolution processes change into surface controlled dissolution processes. Different experimental setups exhibit different levels of difficulty of the characterization of the dissolution processes within the literature. Dreybrodt and Buhmann (1991) conclude that rotating disk experiments are the best possibility to determine kinetic data because of well defined hydrodynamic conditions and simple calculations. However, the choice of sample volumes has to be taken into account. If the fluid - solid ratio is too large, an increase of the experimental run duration can be observed due to slow dissolution processes. Less suitable to determine kinetic data are experiments where solid and fluid build up a suspension and are exposed to a continuously stirring. In this case hydrodynamic processes are not well defined. In contrast Raines and Dewers (1997) see so called mixed-flow reactors as the method of choice to determine kinetic data. If the system has

achieved steady state conditions dissolution rates can be directly determined by changes of influent and effluent solute concentrations. Just as Dreybrodt and Buhmann (1991) Raines and Dewers (1997) see also advantages of using rotating disk setups due to the simple geometry as well as the well known hydrodynamic conditions. Each scientist who uses an experimental setup - regardless of the individual type - should be aware of differences within the systems and adapt the own setup to the desired scientific topic or questions.

2.2 Experimental Conditions

In addition to the above mentioned experimental technique and their associated dissolution mechanisms, the knowledge of experimental conditions is equally important to estimate their influences on the mineral dissolution and/or precipitation process. The following three subsections will describe the parameters temperature, CO_2 partial pressure ($p\text{CO}_2$), and the experimental run duration as conditions that influence dissolution and/or precipitation mechanisms.

2.2.1 Temperature

The parameter that will be considered first is the temperature at which mineral dissolution experiments take place. Within the 30 compared publications the experimental temperatures ranged between 3°C and 300°C , whereat a large number of experimental studies were accomplished at standard temperature (25°C). As mentioned in the first brief comparison (cf. figure 2.1B) the values of calcite dissolution rates exhibit a large spreading of up to 12 orders of magnitude. A clear temperature dependency cannot be observed. But a more precise comparison of dissolution rates at similar experimental conditions (batch reactor, pH-value: 3 – 5.5, ionic strength: $< 0.5 \text{ M}$, p : 1 bar, $p\text{CO}_2$: < 1 bar, stirring rate: $< 427 \text{ rpm}$) describes a slight temperature dependency (c.f. figure 2.9): with increasing temperature the calcite dissolution rate increases. The maximum change in dissolution rates between the lowest and the highest employed temperature is about two orders of magnitude.

When compared to calcite, feldspar dissolution rates show an already obvious temperature dependency with increasing dissolution rate at higher temperatures (c.f. figure 2.10), although other experimental parameters (e.g. pH-value, ionic strength, mineral composition) are not yet similar and still influence the temperature dependence. For example even at a single temperature of 25°C the dissolution rates varies by five orders of magnitude. A fur-

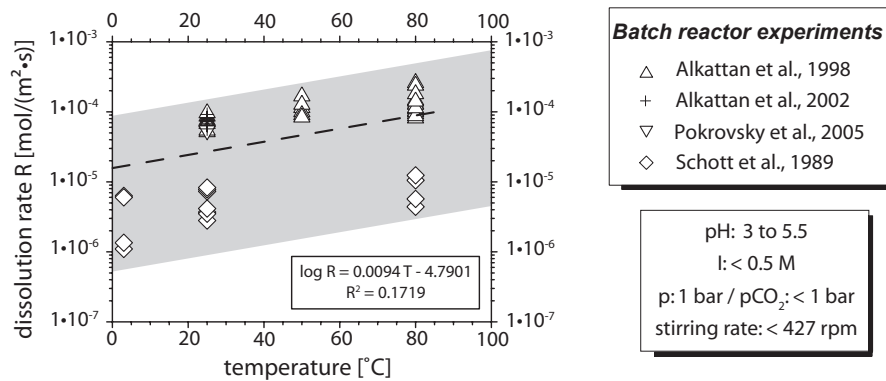


Figure 2.9: Temperature as influencing parameter for calcite dissolution rates: all data describe batch reactor experiments at low acid pH-values (3 to 5.5), low ionic strength (< 0.5 M), atmospheric pressure and stirring rates < 427 rpm.

ther more precise comparison (flow through reactor, pH-value: 3 – 5.5, ionic strength: < 0.1 M, p: <90 bar, pCO_2 : <1 bar, fluid flow rate: <9 ml/min) affirms the observation of increasing dissolution rates with increasing temperature (c.f. figure 2.11). These two literature compilation show different mineral behaviors in regard to temperature variations: dissolution rates of carbonates exhibit in general a faster kinetic, but the influence of the temperature is not clearly pronounced, feldspar dissolution has a comparatively slow kinetic, but a clear temperature dependency.

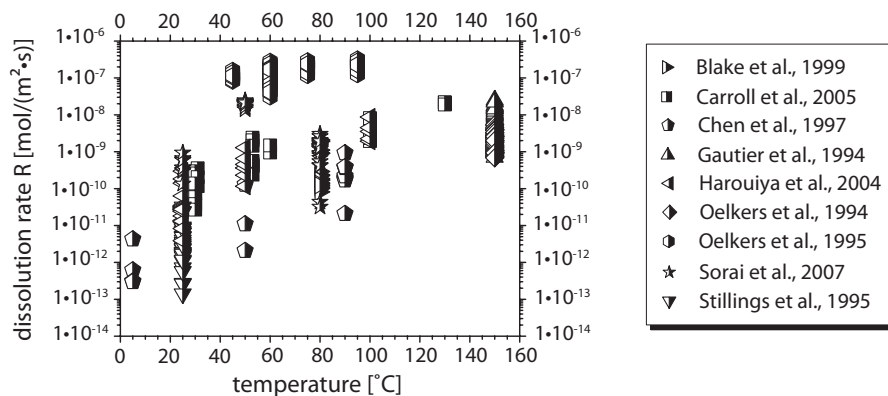


Figure 2.10: Temperature as influencing parameter for feldspar dissolution rates. Data represent all considered publications of feldspar experiments regardless of other influencing parameters like pH-value, ionic strength or mineral composition.

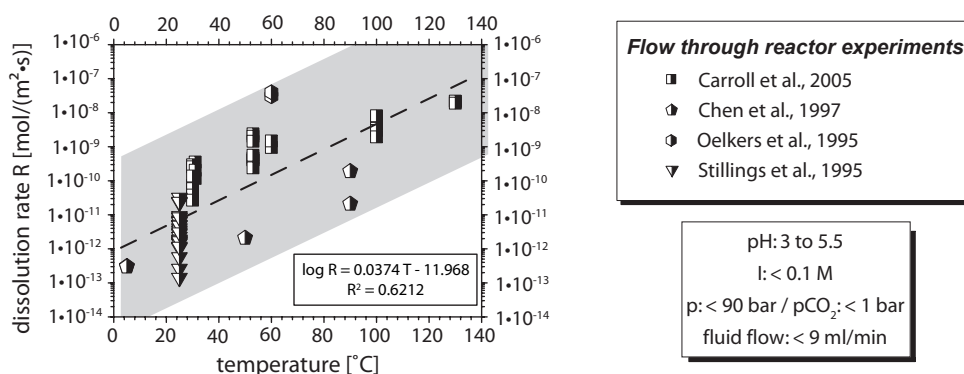


Figure 2.11: Detailed description of the temperature dependency on feldspar dissolution rates: all data describe flow through reactor experiments at low acid pH-values (3 to 5.5), low ionic strength (< 0.1 M), total pressures up to 90 bar and flow rates < 9 ml/min.

Regardless of the used materials various authors (Casey and Sposito (1992), Gautelier et al. (1999), Gledhill and Morse (2006a), Finneran and Morse (2009), Lasaga and Lüttge (2004), Lund et al. (1973), Morse and Arvidson (2002) or Raines and Dewers (1997)) describe similar changes of the minerals' reaction behavior with increasing temperature: whereas at low temperatures surface controlled processes dominate the mineral dissolution, at high temperatures a change into transport controlled processes can be observed. For example Gautelier et al. (1999) and Lund et al. (1973) describe transport controlled processes at temperatures of 100 °C as dominant reaction behavior. In connection with these observations Lund et al. (1973) noted that an increasing temperature results also in an increasing influence of the stirring rate implying that at low temperatures the dissolution of minerals is limited by chemical reactions on the mineral surface, whereas at high temperatures the transport of reactants/reaction products is the limiting factor. Furthermore the temperature not only influences the transport and surface controlled dissolution mechanisms, but also influences the dissolution of complex minerals regarding their incongruent or congruent dissolution behavior. Experiments with kaolinite (Carroll and Walther (1990)) as well as labradorite (Carroll and Knauss (2005)) show a change of incongruent dissolution behaviors at low temperatures to congruent dissolution behaviors with increasing temperatures. Although at experiments with kaolinite the effect is not so clearly pronounced: aluminum dissolution rates are slower than silicon dissolution rates at pH-values of two to nine and a temperature of 25 °C (Carroll and Walther (1990)). The incongruent dissolution behavior of labradorite can be observed at temperatures up to 60 °C where an earlier

and faster release of sodium, calcium and aluminum takes place compared to the silicon release. Temperatures higher than 100 °C represent congruent dissolution mechanisms (Carroll and Knauss (2005)). However, in contrast to these two experimental studies, Zhang et al. (2007) describe incongruent dissolution behavior above temperatures of 100 °C for dolomite dissolution experiments.

In general, the derivation of activation energy values is possible based on experiments with varying temperatures. After Lasaga and Lüttge (2004) minerals with perfect surface areas exhibit the highest activation energies. With increasing surface defects like steps, kinks or holes the activation energy decreases. Furthermore the complexity of the mineral composition influences the value of the activation energy. The more complex a mineral composition is, the higher is the activation energy because of higher amounts of bonds that have to be broken (Lasaga and Lüttge (2004)). As mentioned above the extent of temperature gives information about the dissolution process. Equally, the activation energy can also give information about dissolution processes. Low activation energies up to 10 kJ/mol (in some cases 20 kJ/mol) argue for transport controlled processes. In contrast activation energies higher than 10 kJ/mol (or 20 kJ/mol) represent surface controlled dissolution rates (described by Carroll and Walther (1990), Casey and Sposito (1992), Finneran and Morse (2009), Gledhill and Morse (2006a)).

Various authors describe the influence of the temperature in combination with other experimental parameters. The most common combination is the correlation between temperature and pH-value. While Casey and Sposito (1992) and Gautelier et al. (1999) only mentioned this correlation, Carroll and Walther (1990) and Chen and Brantley (1997) even describe an increasing influence of the pH-value on the dissolution process with increasing temperature. But there are also authors like Oelkers and Schott (1995) who observed no pH-value dependency with varying temperatures. A further combination of parameters were described by Zhang et al. (2007), who proposed a correlation between temperature and mineral grain size. Experiments with dolomite and de-ionized water show a maximum dissolution rate at 200 °C for grain size fractions between 20 μm and 40 μm . In contrast the maximum dissolution rate for experiments with larger grain size fractions (40 – 60 μm /60 – 80 μm) is observed at temperatures from 100 °C to 150 °C. The dissolution rates decreases again at temperatures higher than 150 °C. A third combination of parameters is described by Finneran and Morse (2009), who described a decreasing temperature influence with increasing ionic strength of the fluid used in the experiments.

In conclusion the parameter temperature has a positive effect on the mineral dissolution process. With increasing temperature the dissolution process will be intensified. Furthermore correlations exist between temperature and parameters like pH-value, grain size and ionic strength. With regard to possible numerical modeling scenarios it has to be noted that increasing temperatures influence the dissolution mechanisms. At low temperatures incongruent and surface controlled mechanisms dominate. In contrast high temperature milieus cause congruent and transport controlled mechanisms. Raines and Dewers (1997) for example explicitly pointed out that numerical models which were developed for low temperatures cannot easily be extrapolated to higher temperatures with the help of the Arrhenius relation because of the changing dissolution mechanisms with increasing temperatures. Also Casey and Sposito (1992) describe incorrect results of modeled activation energies related to neglected influences of varying dissolution mechanisms.

2.2.2 Pressure

A second influencing – and in terms of CO₂ sequestration fundamental – parameter is the CO₂ partial pressure (pCO₂). The data base regarding pCO₂ and total pressure within the 30 compared publications is not as abundant as in the case of the temperature. Within eight publications neither pCO₂ data nor total pressure data are described, thus a detailed comparison is not possible. It is striking that this lack of data is generally observed at feldspar, olivine or pyroxene experiments, indicating that the influence of pressure is either negligible for these minerals or not well investigated until now. In contrast 12 publications include both pCO₂ data and total pressure data, whereat the majority of authors accomplished experiments with carbonates (e.g. calcite, dolomite, magnesite or siderite) at atmospheric pressure and associated pCO₂. Altogether the total pressure ranges between atmospheric pressure and 124 bar whereas the pCO₂ ranges between zero and 100 bar. Figure 2.12 represents a detailed comparison of calcite dissolution rates as function of pCO₂. The comparison includes all publications that describe batch reactor experiments on calcite at 25 °C, acid pH-values (3 – 5.5), low ionic strengths (<0.5 M) and stirring rates up to 2000 rpm. It can be observed that the change of dissolution rate with pCO₂ is more pronounced at lower pCO₂ than at higher pCO₂: the dissolution rate increases by two orders of magnitude within the first ten bar, but only by 0.5 orders of magnitude within a range from ten to 50 bar.

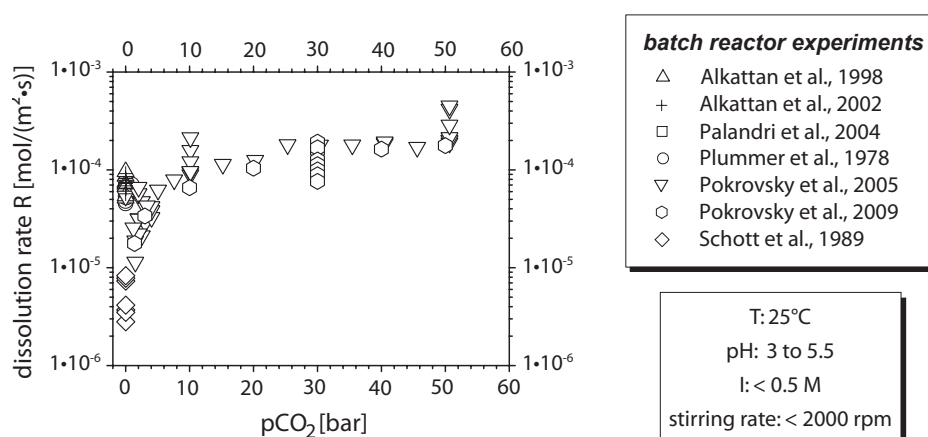


Figure 2.12: Partial CO_2 pressure as influencing parameter for calcite dissolution rates: all data describe batch reactor experiments at room temperature (25°C), low acid pH-values (3 to 5.5), low ionic strengths ($< 0.5 \text{ M}$) and stirring rates below 2000 rpm.

Different observations in connection with a CO_2 atmosphere and/or $p\text{CO}_2$ are described in the literature, whereat a well-defined, distinctive $p\text{CO}_2$ dependency is not affirmed in the most of cases.

A more or less increasing dissolution rate with increasing $p\text{CO}_2$ is described for carbonate experiments (e.g. Gledhill and Morse (2006a), Golubev et al. (2009), Finneran and Morse (2009), Pokrovsky et al. (2005) or Pokrovsky et al. (2009)). The greatest change in dissolution rates regarding $p\text{CO}_2$ is observed at calcite experiments. For example Finneran and Morse (2009) as well as Gledhill and Morse (2006a) describe similar dissolution behaviors: for increasing $p\text{CO}_2$ values from 0.1 to 1 bar a three to four fold (Finneran and Morse (2009)) and a five fold (Gledhill and Morse (2006a)) increase in dissolution rates is observed. The research group of Pokrovsky (Toulouse, France) even describes a five to ten fold as well as an eight fold increase in dissolution rates during an increase of $p\text{CO}_2$ from one to 50 bar and one to 25 bar, respectively. In comparison with the results of calcite experiments dolomite and magnesite dissolution reactions are less affected by $p\text{CO}_2$. Up to values of 10 bar the dissolution rates for dolomite and magnesite are increased by a factor of 2 to 3 (Pokrovsky et al. (2009), Pokrovsky et al. (2005)). In contrast to these three mentioned carbonates (calcite, dolomite, magnesite) siderite exhibits no influence of $p\text{CO}_2$ on its dissolution rate (Golubev et al. (2009)). All above mentioned authors describe supplemental changes of the $p\text{CO}_2$ effect in connection with other parameters, whereat the most important observation is made at varying pH-values. The research group of Pokrovsky

(Pokrovsky et al. (2009), Pokrovsky et al. (2005)) as well as Golubev et al. (2009) and Gledhill and Morse (2006a) state that at low pH-values the effect of $p\text{CO}_2$ is overlapped by the pH effect. The addition of CO_2 triggers a pH decrease caused by the dissolution of CO_2 in the fluid. At neutral to basic pH-values another process influences the $p\text{CO}_2$ effect: within these pH milieus the addition of CO_2 triggers a carbonate and bicarbonate development (Gledhill and Morse (2006a), Pokrovsky et al. (2009)). As a consequence the change in the dissolution rate is therefore not caused by $p\text{CO}_2$ per se but caused by the decreasing pH-value (acid pH: advanced dissolution) and the formation of carbonate complexes (neutral/basic pH: inhibited dissolution), respectively. Recalculations for experiments at $\text{pH} < 4$ to disentangle the connection of pH and $p\text{CO}_2$ show an increase of dissolution rates only by a factor of three instead of a factor of eight (Pokrovsky et al. (2005)). A further parameter that influences the $p\text{CO}_2$ effect is the temperature. With increasing temperature the $p\text{CO}_2$ effect decreases. Both Pokrovsky et al. (2009) and Golubev et al. (2009) describe negligible $p\text{CO}_2$ effects at 60 to 100 °C and 80 to 100 °C, respectively. In addition to the influence of the pH-value and the temperature on the $p\text{CO}_2$ effect Finneran and Morse (2009) and Gledhill and Morse (2006a) describe also changes of the $p\text{CO}_2$ effect by varying ionic strengths as well as varying chemical compositions of the used fluid. However at low $p\text{CO}_2$ values the influence of the ionic strength and the chemical composition of the fluid on the $p\text{CO}_2$ effect of the dissolution rate is smaller than at high $p\text{CO}_2$ values.

In comparison experiments with feldspar, olivine or pyroxene minerals show much smaller changes in dissolution rates regarding the $p\text{CO}_2$ than carbonate experiments. The primary effect of $p\text{CO}_2$ is either very small (e.g. Hänchen et al. (2006): fosteritic olivine) or even negligible in the range of the measurement error (Brady and Carroll (1994): augite, anorthite; Berg and Banwart (2000): anorthite; Carroll and Knauss (2005): labradorite; Golubev et al. (2005): fosterite, diopside, wollastonite, hornblende). The majority of the authors state that the addition of CO_2 triggers a pH decrease caused by the dissolution of CO_2 in the fluid. Consequently, the pH effect has a far stronger influence on the dissolution rate than the $p\text{CO}_2$ effect. Furthermore the authors describe an insufficient disentanglement of both effects during the experiment. A clear statement about a $p\text{CO}_2$ dependency is therefore not possible. Other influencing parameters regarding the $p\text{CO}_2$ effect e.g. temperature or ionic strength are not described in detail.

In conclusion a well-defined, distinctive dissolution rate dependency regarding CO_2 partial pressures cannot be observed. Experiments with carbonates show a slight increase in the dissolution rates with increasing $p\text{CO}_2$ values.

In contrast most of the feldspar or olivine experiments show only negligible changes of dissolution rates. The majority of authors point out that at low pH-values the $p\text{CO}_2$ effect is overlapped by the pH effect as a consequence of CO_2 dissolution processes in the fluid. Furthermore in connection with parameters like temperature and ionic strength carbonate experiments show changes in the $p\text{CO}_2$ effect on the dissolution rate. In conclusion the effect of $p\text{CO}_2$ has a second order influence regarding the pH and/or the ionic strength effect and can be neglected in most of cases. At temperatures, that occur in possible CO_2 reservoir horizons, the effect of $p\text{CO}_2$ is also of no significance. The calcite dissolution behavior of increasing dissolution rate with higher $p\text{CO}_2$ (see figure 2.12) could be confirmed by the detailed literature survey. Furthermore the lack of information about the $p\text{CO}_2$ influence on the feldspar, olivine or pyroxene dissolution is most likely caused by the negligible $p\text{CO}_2$ effect on these mineral groups.

2.3 Material Properties

Just as important as choosing the right experimental setup and experimental conditions described within the previous chapters, the choice of appropriate materials (solids and fluids) is also significant.

The choice of solid materials on its own results in a high variability of dissolution behaviors and consequently kinetic data due to differences in the chemical composition or the crystal structure of the used minerals. Furthermore the treatment of solid materials plays an important role within dissolution experiments. How the materials were prepared: were they polished or mechanically fractured and subsequently washed with different fluids? Which grain size fractions were used in the experiments? Are the fractionated grains pressed into tablets or are the grains available as unconsolidated components within a fluid? A third non-negligible fact is the choice of a monomineralic sample or a mineral association. Varying reaction agents enable to influence the reaction behavior of identical mineral phases in different ways.

But not only solid materials have an influence, also the used fluid affects the dissolution process. Within the literature a wide range of fluids were described: for example deionized water, varying organic and inorganic acids and bases or brines of different composition and ionic strength. For dissolution processes the bulk concentration as well as the percentages of single components within the fluids are important and dictate the reaction progress in different ways. In addition buffered fluids exhibit other effects on the mineral dissolution than non-buffered fluids.

Looking at both solid and fluid phases the ratio of solid to fluid also influ-

ences the dissolution behavior of the studied minerals.

The following subsections describe three material properties – the pH-value and the ionic strength of the fluid as well as the reactive surface of minerals – as significant examples for the influencing parameters mentioned above.

2.3.1 pH - value

The first and supposable most important material property is the pH-value of the employed fluid. Numerous authors describe strong dependencies of mineral dissolution rates regarding the pH-value, whereat the characteristics of dependencies vary between different mineral phases. Carbonates, for example, exhibit a clear linear dependency between dissolution rate and pH-value. Within the 30 compared publications an increasing pH-value results in a decreasing dissolution rate. Even without the limitation of other parameters such as temperature or ionic strength, the significant pH-value dependence is already seen. A briefly description was already given at the beginning of this chapter as well as in figure 2.1A. The figure shows that the dissolution rate varies about 12 orders of magnitude between the lowest and the highest pH-value. Furthermore it becomes apparent that most of the experiments were accomplished at low acidic pH-values ($3 \leq \text{pH} \leq 6$). The restriction of data ($T = 25^\circ\text{C}$, $I = \leq 5.6 \text{ M}$, $p_{\text{total}}/p_{\text{CO}_2} \leq 1 \text{ bar}$, stirring rate $< 2000 \text{ rpm}$) clearly illustrates the linear dependency between pH-value and dissolution rate (cf. figure 2.13). Within this dataset the dissolution rates vary about 7 orders of magnitude between the lowest and the highest pH-value. In contrast to this clear linear dependency the mineral group of feldspars shows an u-shaped curve progression with a minimum of dissolution rates at neutral pH-values (compare Chen and Brantley (1997) for example).

The reason for the linear dissolution rate dependency for carbonate experiments regarding the pH-value is basically described similar within the literature. Thus, the dissolution of carbonates is induced by the adsorption of hydrogen ions (H^+) on the mineral surface (Alkattan et al. (1998), Gautelier et al. (1999), Golubev et al. (2009), Sjöberg and Rickard (1984a), Sjöberg and Rickard (1984b)). However, the effect of H^+ adsorption is not similar at all pH-values. The effect is most pronounced at pH-values between two and five (Golubev et al. (2009)), whereat the controlled mechanisms are described differently within the literature. Earlier studies (e.g Sjöberg and Rickard (1984a), Sjöberg and Rickard (1984b) or Berner and Morse (1974)) describe transport controlled mechanisms, where the diffusion of H^+ through the diffusion boundary layer limits the overall dissolution process. In contrast recent authors like Gautelier et al. (1999) state that the dissolution processes of carbonates are governed by surface controlled mechanisms. The

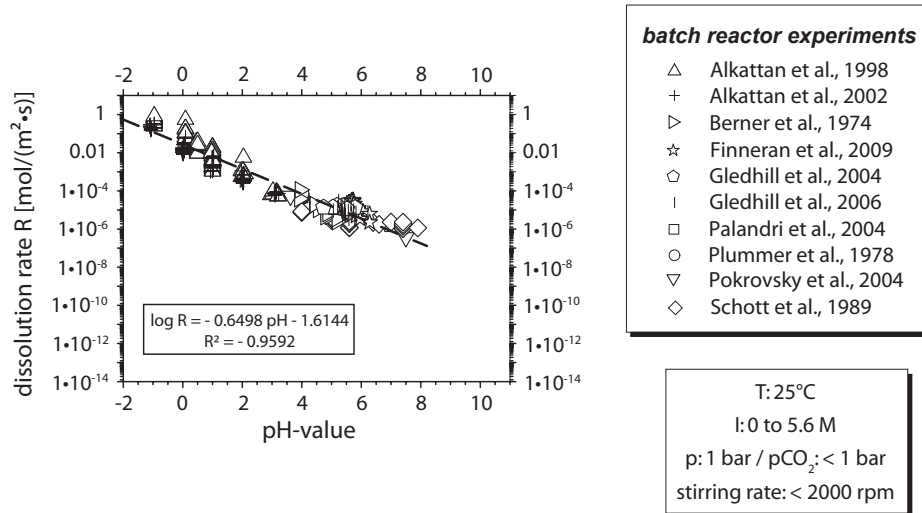


Figure 2.13: pH-value as influencing parameter for calcite dissolution rates: all data describe batch reactor experiments at room temperature (25 °C), ionic strengths up to 5.6 M, atmospheric pressure and stirring rates < 2000 rpm.

authors justify their statements with different rates of H^+ diffusion and reaction progresses on the mineral surface. Whereas the diffusional transport of H^+ increases proportional with increasing concentration, the adsorption of H^+ on the mineral surface increases by a fractional power of the activity of H^+ (a_{H^+}). Therefore surface controlled mechanisms are induced. Morse and Arvidson (2002) partly confirmed this observation and stated that the diffusion coefficient of H^+ is about three times faster than that of other diffusion species. As a consequence surface controlled mechanisms as well as transport controlled mechanisms could be assumed: the fast diffusion of H^+ will be limited by H^+ adsorptions on the mineral surface (surface controlled mechanisms). The slower diffusion coefficients of other species (fluid reactants or released ions from the mineral surface) limited also the reaction progress (transport controlled mechanisms). Beyond the above mentioned pH-range of two to five the dissolution behavior of carbonates changes. With decreasing pH-values ($pH < 2$) a decrease in dissolution rates can be observed. Within this pH-range all lattice sites of the mineral surface (where H^+ is able to adsorb) are occupied and consequently the dissolution rates decrease (Gautelier et al. (1999), Golubev et al. (2009)). At neutral to alkaline pH-environments ($pH > 5$) the dissolution rates also decrease. Kehew (2001) described decreasing H^+ activities as one reason for slower dissolu-

tion kinetics. Furthermore various authors described changing dissolution mechanisms. Gautelier et al. (1999), for example, observed increasing transport controlled mechanisms with increasing pH-values. However, Sjöberg and Rickard (1984a) distinguished between a transitional regime and neutral to alkaline regimes: within the transitional regime H^+ -dependent reactions with not entire transport controlled mechanisms become more negligible and change to H^+ -independent reactions with mixed kinetics at neutral to alkaline regimes.

The influence of other parameters like temperature or pCO_2 on the pH-effect is addressed to some extent in the literature. In general this observation is caused by the dominant pH-effect during carbonate experiments. Nevertheless Pokrovsky et al. (2005), Pokrovsky et al. (2009) and Gautelier et al. (1999) described a more pronounced pH-dependency of carbonate dissolution rates at low temperatures ($25^\circ C$) than at high temperatures ($150^\circ C$), whereat changing dissolution mechanisms with increasing temperature have to be kept in mind. The influence of the pCO_2 on the pH-effect is already described in more detail above (cf. chapter 2.2.2).

The pH-dependency of aluminosilicates is caused by adsorption processes of protons or hydroxyl ions on Al^{3+} or Si^{4+} lattice sites, whereat the dissolution process at acid pH-values ($pH < 5$) is proton-promoted and the dissolution process at alkaline pH-values ($pH > 8$) is hydroxyl-promoted. The intermediate pH-range is described as region where a third mechanism operates. The changes of dissolution mechanisms are reflected by a typical u-shaped dependence of the dissolution rate on the pH-value with a minimal dissolution rate at neutral pH-regimes. The faster dissolution rates at acidic and alkaline pH-values are induced by congruent dissolution behavior with surface controlled mechanisms (Chen and Brantley (1997), Carroll and Walther (1990)). The influence of other parameters like temperature is controversially discussed in the literature. Whereas Chen and Brantley (1997) and Carroll and Walther (1990) observed no temperature effect on the pH-dependency, Brady and Walther (1992) and Hellmann (1994) predicted a temperature effect on the pH-dependency.

In summary the majority of mineral dissolution processes are significantly influenced by the pH-value of the fluid and are induced generally by first order reactions. However, the characteristics of pH-dependencies differ for various minerals. Explicit declarations about dissolution mechanisms within different pH-values are not possible and are controversially discussed in literature for several years. Furthermore the influence of other parameters on the pH-effect like the temperature still remains vague. In regard to the CO_2 sequestration the pH-value in connection with the pCO_2 plays a superior

role. During the CO₂ injection the pCO₂ increases close to the injection point and therefore results in a decreasing pH-value within the reservoir. In the case of carbon bonded sandstones the brine is buffered by the dissolution of the carbonate components at the beginning of the injection. After the complete dissolution of the carbonatic components the pH-value decreases. Consequently the pH-decrease could trigger additional dissolution processes of the other non-carbonate components (Knauss et al. (2005)). At non carbon bonded sandstones the buffering impact is missing and the dissolution processes are therefore advanced.

2.3.2 Ionic Strength

In terms of CO₂ sequestration processes within deep saline aquifers the knowledge of interactions between injected CO₂ and fluids with high salt contents and therefore high ionic strengths is of great importance. The variability of fluids regarding their origin as well as their compositions is clearly pronounced in the literature. Thus, both synthetic and natural fluids were adopted. Deionized water as the simplest and at the same time most unnatural fluid was mentioned by Eisenlohr et al. (1999) or Zhang et al. (2007). In relation to the composition of more complex fluids experiments with organic components as well as inorganic components were accomplished. Authors like Yadav et al. (2008) or Blake and Walter (1999) for example used acidic acid or organic ions like oxalate and citrate in their experiments. Furthermore numerous experiments with different brines were conducted. These experiments differed in terms of the components themselves, the amount of each component within the overall fluid as well as the total salt content. Commonly used components were NaCl, KCl, MgCl₂ or CaCl₂ and were employed for example by Dove and Crerar (1990), Finneran and Morse (2009), Gautelier et al. (2007), Gledhill and Morse (2006a), Golubev et al. (2006), Liteanu and Spiers (2009) or Pokrovsky et al. (2009). In some cases components like NaPO₃, NaHCO₃, AlCl₃ or H₄SiO₄ were also used by Alkattan et al. (2002), Carroll and Knauss (2005), Gautelier et al. (2007), Gautier et al. (1994) or Pokrovsky et al. (2009). In addition many experiments run with acids or bases to keep the solution at constant pH-values. Furthermore several experiments with pure acids and bases – for example HCl, KCl, NaOH or succinic acid – were accomplished by Alkattan et al. (1998), Carroll and Walther (1990), Chou et al. (1989) or Cubillas et al. (2005). The overall range of ionic strengths used in the literature varied between 0 and 5.57 M. All these variabilities of ionic strength and resulting dissolution rates were briefly described for carbonate experiments at the beginning of the chapter and are illustrated in figure 2.1C. Without the limitation of other parameters like pH-value, pres-

sure or temperature a dependency between ionic strength and dissolution rate cannot be observed. The overall range of dissolution rates varies by about 12 orders of magnitude, whereat most experiments were accomplished at ionic strengths between zero and 0.1 M. Stronger solutions up to an ionic strength of 5.5 M were used considerably less. However, the restriction of the parameters temperature ($T = 25\text{ }^\circ\text{C}$), pH-value ($3 \leq \text{pH} \leq 5.5$), pressure (atmospheric pressure) and stirring rate ($< 2000\text{ rpm}$) also describes no clear dependence of the dissolution rate with respect to the ionic strength (cf. figure 2.14). The majority of experiments were also accomplished at low ionic strengths ($0 - 0.7\text{ M}$), whereat the determined dissolution rates vary about two orders of magnitude. This suggests that not only the ionic strength per se influences the mineral dissolution process, but also the single components and their amount within the overall fluid.

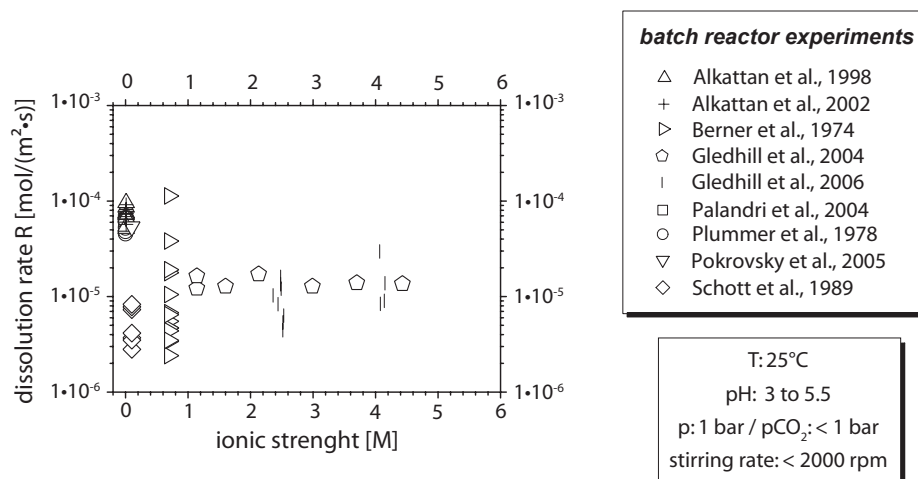


Figure 2.14: Ionic strength as influencing parameter for calcite dissolution rates: all data describe batch reactor experiments at room temperature ($25\text{ }^\circ\text{C}$), low acid pH-values (3 to 5.5), atmospheric pressure and stirring rates $< 2000\text{ rpm}$.

Even though the depicted literature data do not show an clearly pronounced decrease in dissolution rate with increasing ionic strengths several authors describe an inhibitory effect of the ionic strength on the dissolution processes of minerals. For example, Finneran and Morse (2009), Gledhill and Morse (2006a) and Raines and Dewers (1997) justify this statement with the change of the water activity coefficient (a_{H_2O}) in high concentrated fluids, whereat the decrease in dissolution rates is not proportional to the decrease of a_{H_2O} and is effected by different dissolved components. The authors describe a

three times faster decrease in dissolution rates compared to the decrease of a_{H_2O} . Furthermore, the authors describe a stronger influence on the dissolution behavior by doubly charged ions (e.g. Mg^{2+} , Ca^{2+}) compared to the influence of singly charged ions (e.g. K^+ , Na^+). In addition to the activity coefficient of water Finneran and Morse (2009) or Gledhill and Morse (2006a) describe changes in the mineral dissolution behavior as a result of different hydration processes on the mineral surfaces.

In combination with other experimental conditions the ionic strength also influence the dissolution behavior of minerals. As mentioned in chapter 2.1 different flow regimes cause different dissolution mechanisms. These mechanisms are additionally influenced by the saturation state of the used fluid phase. Morse and Arvidson (2002) describe transport controlled dissolution behaviors in undersaturated fluids. In approximation to the chemical equilibrium and hence, with ongoing run duration the transport controlled processes change in surface controlled mechanisms. After reaching the chemical equilibrium solely surface controlled reactions take place. Other authors describe ionic strength dependent effects in combination with the CO_2 partial pressure. For example, Gledhill and Morse (2006a) observed ionic strength independent calcite dissolution behaviors for experiments performed at low CO_2 partial pressures (0.1 bar). Similar observations are made by Pokrovsky et al. (2005), who describe ionic strength independent calcite dissolution rates for experiments performed at CO_2 partial pressures of 2 to 4 bar.

Even though the mentioned observations describe various mineral dissolution behaviors as an effect of the ionic strength itself as well as an effect of combined experimental parameters the influence of the ionic strength is minor pronounced in comparison to other parameters like temperature, pH-value or CO_2 partial pressures. In the case of CO_2 sequestration processes the chemical composition of the prevailing formation water has to be taken into account but is not the dominating factor which influence chemical processes within the respective CO_2 storing reservoir. Nevertheless, the influence of the formation water composition and hence, the ionic strength is not to be underestimated because the high variability of formation water compositions in combination with the injected gas-phase mixture result in a large number of chemical reactions which have to be taken into account.

Chapter 3

Experimental Techniques and Materials

Subject of chapter 3 is the description of the experimental setups and conditions, the starting materials as well as the analysis methods of the accomplished dissolution experiments used in the present study. To perform the experiments two experimental setups were available: (i) steel autoclaves with teflon inlay (teflon reactors) and (ii) a titan reactor from PARR instruments (PARR reactor). Altogether 148 dissolution experiments with calcite, dolomite, anorthite and orthoclase were accomplished. As solvent a synthetic model brine was used. The brine composition was similar to a formation water of a theoretical storage horizon within the Northern German Basin. As pressurizing medium as well as CO₂-source dry ice and CO₂ gas, respectively, were used in most cases. A few reference experiments were also accomplished with N₂ gas to estimate the influence of CO₂. Based on different analysis methods the fluid as well as the solid materials were analyzed before and after each experiment concerning their chemical composition and their surface properties.

3.1 Experimental Technique

As mentioned above two different experimental setups were used within the present study. Both reactor types simulate closed, static systems and are able to reconstruct reservoir behaviors far from the injection site (cf. chapter 2.1/figure 2.2). The most important differences are characterized by the possibility of pressure control as well as the possibility of fluid extraction during an ongoing experiment. While the teflon reactors do not have these facilities, both, pressure control and fluid extraction are possible by using the PARR

reactor. Furthermore the maximum capacities of pressure and temperature differ, even though the p-T conditions were chosen to be identical to compare the experimental results of both reactor types. The extraction of gas phases during an ongoing experiment was not accomplished, even though the possibility theoretically exists by using the PARR reactor.

3.1.1 Teflon Reactor Experiments

The majority of experiments were performed using teflon reactors (schematic illustration: figure 3.1/photograph: appendix A.1). This reactor type is characterized by a closed, static setup, where an exchange of fluid or solid phases do not take place during the ongoing experiment. To achieve the temperature of 150 °C and 100 °C, respectively, the reactors were placed in a Memmert - heating cabinet. It has to be noted that the used temperature conditions presented in this study were higher than the temperature conditions estimated within a potential reservoir. As listed in table 2.1 the possible reservoir temperatures vary between 25 °C and 90 °C. To perform the experiments of the present study within appropriate time and with significant results, the higher temperatures were used to accelerate the chemical reactions. The total pressure of ~ 85 bar was generated by dry ice, which is also conducted as CO₂-source. Regarding the pressures of the three exemplary reservoirs represented in table 2.1 the total pressure used in the present study was appropriate.

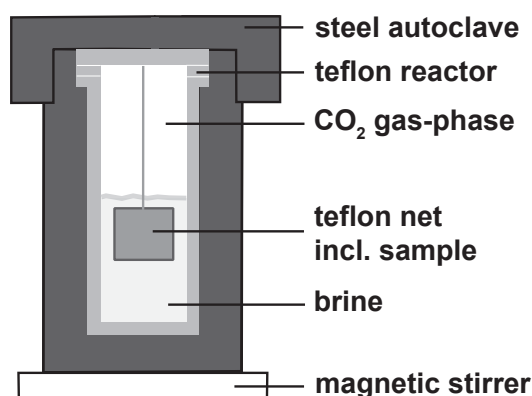


Figure 3.1: Schematic sketch of the used teflon reactors: total reactor volume: 55.75 ml

Due to the lack of pressure control during the ongoing experiments nine reference experiments were accomplished with the help of the PARR reactor

under identical run conditions. All p-T curves exhibit similar characteristics with a target pressure of ~ 85 bar (c.f appendix A.2). Differences in the amount of pressure are caused by initial weight uncertainties of the high volatile dry ice and the amount of CO_2 release during the installation process.

In order to reconstruct natural flow rates in saline, deep aquifers far from the injection site the experiments were stirred three times a day for five minutes with a teflon coated magnetic stirrer. The stirring speed was set up to 1100 rpm using combined stirring and heating plates. According to authors like Dreybrodt and Buhmann (1991), Raines and Dewers (1997) or Pokrovsky et al. (2005) the used stirring rate results in a turbulent fluid flow regime. A Reynolds number of $Re = 27465$ for experiments presented in this study affirmed the turbulent fluid flow regime and was determined after equation 3.1 for stirred vessels:

$$Re = \frac{\rho \cdot N \cdot D^2}{\eta} \quad (3.1)$$

where Re describes the Reynolds number (dimensionless), ρ is the density of the used fluid ($\rho_{brine} = 1156 \text{ kg/m}^3$), N corresponds to the rotation speed ($N = 1100 \text{ rpm}$), D describes the diameter of the magnetic stirrer ($D = 2 \text{ cm}$) and η is the kinetic viscosity ($\eta = 3.1 \cdot 10^{-4} \text{ kg/(m}\cdot\text{s)}$)¹. In table 3.1 the calculated Reynolds number is compared to literature data. Differences between Reynolds numbers are attributed to different geometries of the rotating body and different fluid properties (e.g. density, viscosity).

The solid samples were put into teflon fabric nets and were completely wetted with fluid during the entire run duration (cf. chapter 3.2).

As mentioned above an exchange or removal of fluid and solid phases during an ongoing experiment is not possible. Therefore experimental series with identical run conditions were compiled and included six experiments with varying experimental run durations (1, 2, 5, 10, 20 and 30 days). In two cases a seventh experiment with a run duration of 180 days was added. After each mentioned time step the autoclave was removed from the heating cabinet and was cooled down by an air shower for 15 minutes to permit a rapid and safe sampling of the reacted materials. Twenty ml of the homogenized fluid were removed from the reactor. Immediately after the fluid was taken the pH-value was measured with a pH-meter Typ QpH 70 (VWR International) at room temperature and atmospheric pressure. The pH-meter was

¹specified value for sea water at 100°C ; after: http://www.schweizer-fn.de/stoff/seewasser/v2_seewasser.htm (14.09.2011)

calibrated continuously with WTW - reference solutions of three pH-values (4.006, 6.865 & 9.182). Afterwards the fluid was filtered through a 0.45 μm syringe filter. To stabilize the sampled fluid chemically 14.35 M nitric acid was added. The acidulated sample was stored at 8 °C in a fridge until the fluid's chemistry got analyzed. In addition to the fluid phase the solid phase was also removed after finishing the experiment. Therefore the teflon meshes with the reacted material were rinsed with deionized water to remove residual brine and consequently inhibit salt precipitates on the mesh surface or within the reacted material. The meshes were stored at room temperature until analyzing.

Table 3.1: Comparison of Reynolds numbers described in the literature and calculated within the present study

stirring rate (rpm)	Reynolds number	flow regime	reference
900	≥ 15000	turbulent	Dreybrodt and Buhmann (1991)
	< 15000	laminar	Pokrovsky et al. (2005)
300	4000	laminar	Raines and Dewers (1997)
600	8000	laminar	
900	9000	laminar	
1200	16000	laminar	
1100	27465	turbulent	present study

3.1.2 PARR Reactor Experiments

The second experimental setup which was mainly used for reference experiments was a closed, static Ti-reactor from PARR instruments (schematic illustration: figure 3.2/photograph: appendix A.3).

Temperatures of 150 °C were adjusted by means of a temperature controller and an associated furnace (heating shoe). The pressure build-up took place either via gas bottles (CO_2 , N_2) or dry ice (CO_2) in cases of reference experiments. The gases were not only used as pressurizing medium, but also as reactants within the chemical reaction during the ongoing experiment. The maximum pressure for this assembly is 110 bar at 150 °C, however, it was not exploited. In general pressures of ~ 85 bar were employed to compare these results with results of teflon reactor experiments. A continuous pressure measurement is possible at any time by means of a mounted pressure gauge. The solid samples were put into teflon nets and were mounted on the sampling tube within the reactor. During the entire run duration the nets

were wetted with fluid (cf. chapter 3.2).

As mentioned for teflon reactor experiments a natural flow rate for saline, deep aquifers far from the injection site was realized by stirring the fluid three times a day for five minutes by using a teflon coated magnetic stirrer. Identical to the described teflon experiments turbulent fluid flow regimes existed during the time of agitating also within the PARR reactor.

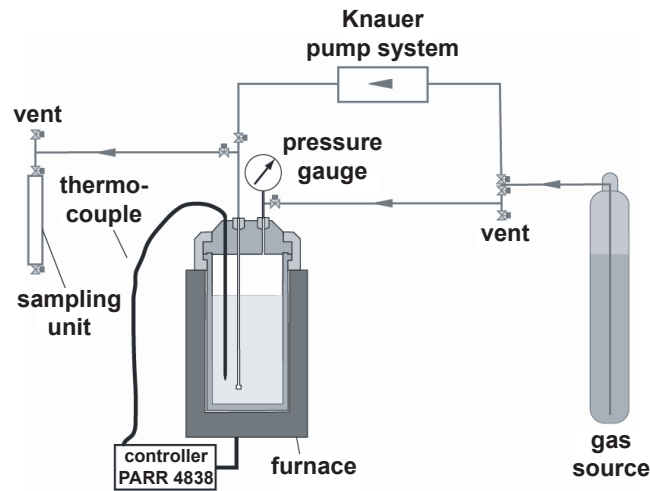


Figure 3.2: Schematical sketch of the used PARR reactor: total reactor volume: 282.74 ml (provided by W.-A. Kahl)

An exchange of fluid phases during an ongoing experiment would have theoretically been possible, but was not practiced. The sampling of fluid phases was possible at any time and was accomplished after 5, 7, 11 and 14 days. With the help of the sampling unit 12 ml fluid were removed, which corresponds to 6.1% of the entire fluid volume. After fluid sampling only the loss of pressure was compensated by the supply of gas in the reactor. A replenishment of fluid up to the initial volume did not take place, but would have been theoretically possible. The removal of solids only took place after finishing the entire experiment and opening the reactor. All sampled fluids and solids were treated like samples from the teflon reactors (pH-value measurements, acidification, cleaning and storage).

3.2 Materials

Dissolution experiments in the present study were performed on transparent crystals of calcite and anorthite as well as lacteal crystals of dolomite and orthoclase obtained from Krantz (Rheinisches Mineralien-Kontor GmbH & Co. KG). Figure 3.3 shows photo-micrographs and backscattered electron images of the starting materials.

An electron microprobe was used to analyze different grains of each monomineralic sample regarding their chemical composition (cf. appendices B.2 & B.3). For carbonatic samples the grains themselves as well as all analyzed grains exhibit nearly the same composition, which describes the homogeneity of the samples and makes a comparison of results of individual experiments possible. The same phenomena were observed at the anorthite grains, which exhibited a purity of 95%. The orthoclase samples exhibit clear features of lamellas unmixing, whereat the lamellas consists of either pure albite phases or pure orthoclase phases. The overall chemical formula of each mineral phase is listed in table 3.2.

Table 3.2: Chemical formula of the used mineral phases

mineral	chemical formula
calcite	$\text{Ca}_{0.99}\text{R}_{0.01}\text{CO}_3$
dolomite	$\text{Ca}_{0.58}\text{Mg}_{0.41}\text{R}_{0.01}\text{CO}_3$
anorthite	$\text{Ca}_{0.97}\text{Na}_{0.03}[(\text{Al},\text{Si})_4\text{O}_8]$
orthoclase	$\text{K}_{0.75}\text{Na}_{0.25}[\text{AlSi}_3\text{O}_8]$

R: sum of residual components (SiO_2 , TiO_2 , Al_2O_3 , Cr_2O_3 , FeO , MnO , Na_2O , K_2O , ZrO) measured by EMP analyses

All experiments were performed with powders. Therefore the monomineralic rock specimens were mechanically crushed with a hammer and pestled with an agate swing mill (TS 100 A). Afterwards the material was sieved into four different grain size fractions: $<63 \mu\text{m}$, $63 - 160 \mu\text{m}$, $160 - 250 \mu\text{m}$ and $250 - 500 \mu\text{m}$. To remove dust which was produced during the milling process all fractions were cleaned several times with deionized water and acetone. The cleaned starting materials were dried for ~ 3 hours under IR heat lamp.

The starting mixture consisted of with 0.18 g solid material in 37 ml brine (teflon reactor) and 1.36 g solid material in 195.14 ml brine (PARR reactor), respectively, and consequently results in a mineral-brine ratio of 1:200 by

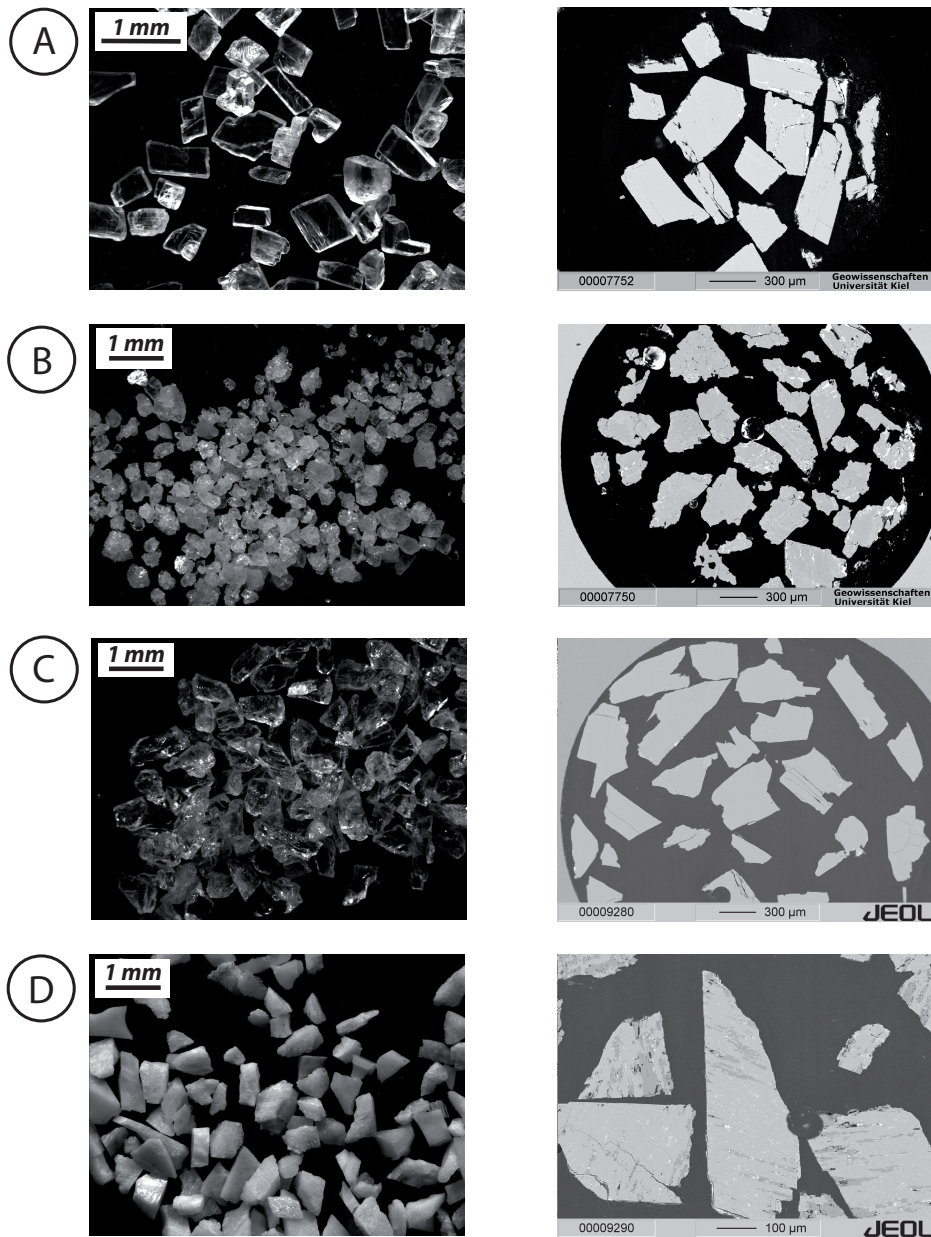


Figure 3.3: Photo-micrographs (right, stereo microscope Leica M205 C, IfG, CAU Kiel) and backscattered electron images (left, EMP laboratory, IfG, CAU Kiel) of the starting materials; grain size fraction: 250 – 500 μm ; (A) calcite, (B) dolomite, (C) anorthite, (D) orthoclase

weight. To avoid fresh splitting areas on the grain surfaces caused by clashing of the particles during the stirring process, the starting material was put

into teflon fabric nets with a mesh opening of $70\ \mu\text{m}$ (cf. appendix A.1 right; Lechleiter GmbH). These nets were completely wetted with brine and had no contact with the stirrer. Scanning electron microscopy analyses of the nets before and after the experiment featured little deformations of the fabric but no precipitates which clog the mesh openings (cf. appendix A.4). Therefore an exchange of the fluid between the teflon fabric net and the brine volume was assured during the entire run duration.

As described in chapter 2.3.2 the composition and the ionic strength of the used fluid play an important role for determining the dissolution rates. Regarding the aim of this study another literature survey was accomplished to find potential stratigraphic formations where CO_2 sequestration is theoretical possible and composition data of the formation waters are known. In Müller and Papendieck (1975) a detailed description of the Northern German Basin concerning its stratigraphy as well as the associated formation water composition is listed. For accomplished experiments within the present study a Lower Cretaceous brine was exemplary chosen. With a total dissolved solid value (TDS) of $156\ \text{g/L}$ and a ionic strength of $2.88\ \text{M}$ the brine is higher concentrated than many literature data but is nevertheless far from the saturation point. Consequently objectionable precipitations caused by a high ionized solution can be minimized. Figure 3.4 shows a comparison of the natural formation water composition (left) and the synthetic model brine composition used in the experiments (right).

To simulate natural conditions but still restrict the variability of the experiments in regard to its chemical composition the synthetic model brine only includes the 4 main cations Na^+ , Ca^{2+} , Mg^{2+} and K^+ as well as the main anion Cl^- . To prepare the model brine A.C.S. reagent grade NaCl and $\text{MgCl}_2 \cdot 6\text{H}_2\text{O}$ (Merck), as well as suprapure KCl (Merck) and extra pure $\text{CaCl}_2 \cdot 2\text{H}_2\text{O}$ (Riedel - de Haën) were used. All components were available as salts and were dissolved in deionized water. A fluid buffer to keep the pH-value constant was not used. The synthetic model brine was stored at $8\ ^\circ\text{C}$ in a fridge prior to the experiments. Each newly prepared batch of the model brine was analyzed for its chemical composition by ICP-OES measurements. Within the period of storage, the composition did not alter within the error of measurement (cf. appendix A.5). Differences between single model brine charges were caused by initial weight uncertainties of salts or deionized water.

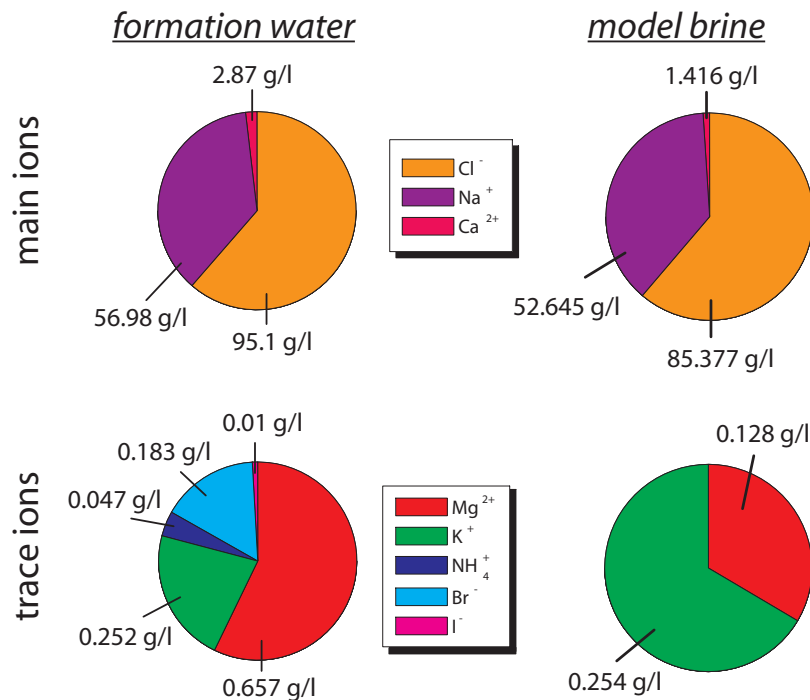


Figure 3.4: Composition of the used synthetic model brine (right, ICP-OES measurement, IfG, CAU Kiel) in comparison to a Lower Cretaceous formation water of the Northern German Basin after Müller and Papendieck (1975) (left)

3.3 Analytical Methods

To observe changes in the chemical composition of fluids and solids as well as changes on the solid surfaces different analytical methods were applied.

3.3.1 Analyses of Solid Materials

As mentioned above all starting materials as well as selected reaction products were analyzed by electron microprobe measurements (EMP, Jeol Superprobe JXA 8900R, IfG, CAU Kiel) concerning their chemical composition. All phases were analyzed with 15 kV and 15 nA. While the feldspar samples were measured with a defocused beam of 15 μm , the carbonates were measured with a focused beam. All samples were mounted in epoxy and were subsequently polished. Before measurement, the prepared samples were cleaned with petroleum ether in an ultrasonic bath to remove contaminants of the preparation process. As final step the cleaned microprobe sections were carbon coated.

With the help of scanning electron microscopy measurements the solid samples were analyzed before and after the experiment to determine dissolution or precipitation phenomena on the mineral surface. The measurements were accomplished at the SEM laboratory (IfG, CAU Kiel) using a CamScan 44/EDX. The samples were placed on a aluminum pin sample plate, which was covered with a coal tab. Afterwards the samples were sputtered with a gold-palladium alloy to achieve the required conductivity. The measurements were accomplished at an excitation voltage of 15 kV. The image magnifications ranged between 9 and 7000 depending on the respective image section.

To determine the reactive surface of the used materials gas adsorption measurements were accomplished (BEL Japan Inc. BELSORP, AC, CAU Kiel). Unfortunately, with the available method no usable results were produced. In consequence values for reactive surfaces of different mineral phases and different grain size fractions were taken from the literature.

A further method to characterize changes on the mineral surface was the X-ray micro computer tomography (μ -CT, Skyscan 1172, IfG, CAU Kiel). In addition to this surface characteristic measurements realistic estimations of grain - grain and grain - fluid contact areas should be determined. A special preparation of the studied samples was not necessary. Depending on the aim of measuring the sample position regarding the X-ray source, the used filters and the calculation methods varied.

3.3.2 Solution Analyses

One of the main tasks within the present study was the description of mineral dissolution behaviors under the influence of dense CO₂ in saline fluids. The simplest method to determine chemical changes of the reactants is the analysis of the fluid phase by ICP-OES measurements.

Multi element measurements at the ICP-OES laboratory (IfG, CAU Kiel) were accomplished at a spectrometer type Spectro Ciros CCD SOP by using a longtime applied measuring technique for seawater. Therefore the high concentrated fluid samples used in the present study were diluted in 2% nitric acid until seawater concentration was approximately reached. In addition, each sample was loaded with Yttrium as internal standard. The measurement of each single fluid sample includes five single measurements, which were automatically averaged after the analyses. The system calibration is based on different lab internal as well as commercial standards (e.g. MWSTD05 or NASS4). To obtain a measuring control of the main components (e.g. Ca, Cl, Mg or Na) the commercial standard IAPSO K15 was analyzed after every tenth measurement of the unknown samples. For trace elements

(e.g. Fe, Mn, Ni) the measuring control based on the commercial standard NIST 1643d. Between two individual samples the apparatus was rinsed with 2% nitric acid.

Multi element analyses were also accomplished at the Wietze E&P laboratory (RWE Dea AG, Wietze) by using a Spectro Ciros Vision. The applied method is for example used for concomitant waters produced during the oil production. To adopt this method the fluids used within the present study were diluted with ultrapure water (ratio 1:100). The use of an internal standard was omitted, but to improve the analytical method all fluid samples were loaded with 1 ml nitric acid. The addition of nitric acid affects the solubility of components which have to be measured and therefore provides a finer nebulization (aerosol formation) of the sample within the apparatus. In consequence the sample input into the torch is more constant and results in minor fluctuation of measuring values. The measurement of each single fluid sample includes four single measurements, which were automatically averaged after analyzing. The system calibration based on different diluted standards (Bernd Kraft GmbH). The ingredients of the used standards are conformed to samples, which are generally analyzed at this laboratory. Between two single samples the apparatus was rinsed with ultrapure water.

In terms of CO₂ sequestration processes the gas content within the fluid samples is of increased importance. To determine the content of gas within the sampled fluids gas chromatography analyses were accomplished at the hydrochemical laboratory (IfG, CAU Kiel). Caused by the employed fluid sampling process the gas disappeared from the fluid uncontrollably. In consequence a significant, realistic statement about the gas content within the fluid samples was not possible.

Chapter 4

Experimental Results and Interpretation

In this chapter all experimental results are described followed by interpretation of the findings. In appendix B.4 experiments and the corresponding experimental conditions are summarized. Details about the experimental setup, the starting materials and the analysis methods are described in chapter 3.

4.1 Teflon Reactor Experiments at Carbonatic Samples

In total 66 dissolution experiments at carbonatic samples (calcite and dolomite) were accomplished in the present study, whereat the main focus was on experiments at calcite samples.

To compare the results of different experimental series the following experimental conditions were hold constant: (i) the total pressure at a value of ~ 85 bar, (ii) the ratio between solids and fluids (1:200) and therefore the initial weight of solids and fluids, and (iii) the composition of the synthetic model brine. In contrast parameters like temperature, grain size fraction and run duration varied at different experimental series to estimate dependencies on the mineral dissolution process in regard to these parameters. Therefore two temperatures ($100^\circ\text{C}/150^\circ\text{C}$), four grain size fractions ($<63\ \mu\text{m}$, $63 - 160\ \mu\text{m}$, $160 - 250\ \mu\text{m}$, $250 - 500\ \mu\text{m}$) and run durations of 1, 2, 5, 10, 20, and 30 days (180 days in two cases) were applied. Each experiment was accomplished twice to demonstrate the reproducibility of the experiments. In the context of CO_2 sequestration processes a few experiments at calcite samples were accomplished without CO_2 to determine the influence of this

gas on the dissolution process.

4.1.1 Analyses of the Solid Samples

During the dissolution and/or precipitation process of minerals within fluid phases reaction rims may form on the solid samples. On the one hand this reaction rim may be characterized by chemical changes along the grain boundaries. Thus, for example, exchange reactions between cations of the solid phase and cations of the fluid phase take place. Furthermore the adsorption of various fluid components on the mineral surface is possible. A third possibility of chemical changes along the grain boundary is the formation of more or less stable precipitates as result of the chemical reaction between the mineral surface and the used fluid phase. In addition or instead of the chemical modifications structural changes can although occur. The development of reactions rims per se as well as the characteristics of the reaction rim formation vary for different mineral phases.

Three different analytical methods were applied to study the above mentioned chemical (EMP) and structural (SEM, μ -CT) changes on the reacted mineral surfaces as a result of occurred dissolution processes.

Electron Microprobe Analyses (EMP)

EMP measurements were accomplished to detect chemical changes on the mineral surfaces as a result of dissolution processes. Post-run *calcite* charges of experiments at 150 °C and \sim 85 bar were chosen to study these changes in more detail. Reaction products of two different fractions (250 – 500 μ m/ 160 – 250 μ m) were used to study grain size dependencies. In addition post-experimental charges of varying run durations (1, 2, 20, and 30 days) were chosen to determine time dependent chemical changes. Backscattered electron images of the analyzed grains including the points of measurement are depicted in appendix A.6. Furthermore appendix B.5 lists measured EMP data of reacted calcite grains as well as the average composition of the starting material to compare possible chemical changes.

As depicted in figure 4.1 neither a significant time dependency nor a significant grain size dependency can be observed at post-experimental calcite charges. All apparent chemical changes are within the range of measuring error and thus allow no significant statements. Within the considered literature comparable EMP measurement results of post-experimental solid materials are also not described.

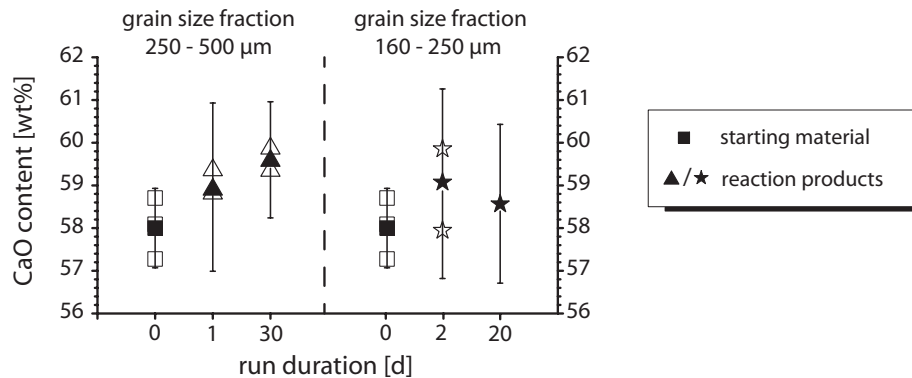


Figure 4.1: CaO content of pre- & post-experimental calcite samples as function of the experimental run duration and the applied grain size: significant alterations of the CaO content are verified. *Filled symbols:* average of all measuring points within all grains at a given time step; *open symbols:* average of all measuring points within one grain at a given time step. Measuring results are also listed in appendix B.5. (EMP laboratory, IfG, CAU Kiel)

Compared to calcite, *dolomite* exhibits similar mineralogical structures and reaction behaviors. Therefore significant chemical changes of the mineral surfaces are also not expected and thus detailed EMP measurements were not performed.

Scanning Electron Microscope Analyses (SEM)

SEM measurements were accomplished to determine structural changes on the mineral surface as consequence of dissolution processes. Post-run charges of experiments at 150 °C and ~85 bar were chosen to study these changes in more detail. To determine time dependencies reaction products of different experimental run durations were analyzed. Possible grain size as well as temperature dependencies were not taken into account.

As depicted in figure 4.2 the starting materials reflect typical crystallographic characteristics. Pre-experimental SEM images of *calcite* grains show rhombohedral shapes with kinks and steps along all crystallographic directions on the grain boundaries as well as on the mineral surfaces. However, *dolomite* samples exhibit both rhombohedral shapes and polycrystalline agglomerates. Rectangular pits on the mineral surface can be observed in addition to the also apparent kinks and steps.

Despite multiple rinsing prior to the experiments all analyzed calcite and dolomite grains exhibit ultrafine dust particles on the mineral surfaces.

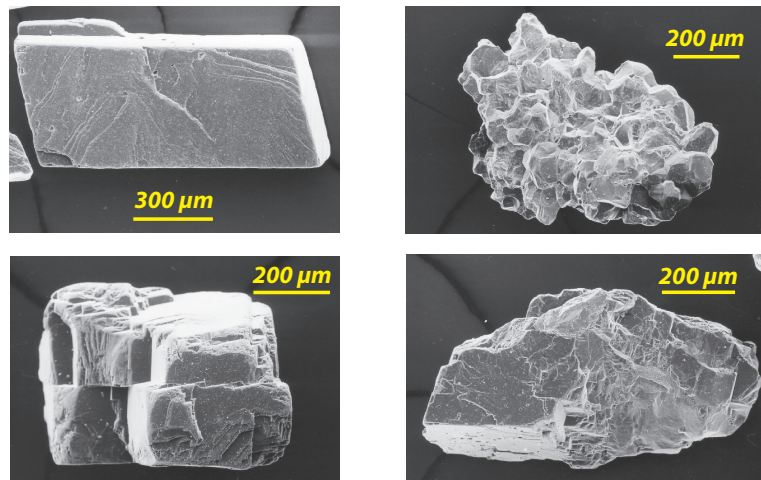


Figure 4.2: SEM photomicrographs of the starting materials: calcite (left, 250 - 500 μm); dolomite (right, 250 - 500 μm) (SEM laboratory, IfG, CAU Kiel)

At first structural surface changes on post-experimental *calcite* grains will be described. The initial rhombohedral shape of the grains is maintained after an experimental run duration of one day (cf. figure 4.3). Furthermore dissolution features along all crystallographic directions are clearly visible indicating a preferentially occurred calcite dissolution on the above mentioned kinks and steps on the mineral boundaries as well as on the mineral surfaces. In the literature kinks and steps are described as dislocation sites where atoms preferentially detach from the surface due to their lower binding energy. Yadav et al. (2008), for example, describe an increased Ca release on dislocation sites by a factor of 2.25 compared to flat smooth surfaces. A further considerable structural feature of the post-run calcite grains is the development of needles on the overall mineral surface. Within a single crystal face all needles exhibit the same orientation. This phenomena is for instance described by Pokrovsky et al. (2009), who characterize the observed needles as remnants of the initial mineral surface. At the beginning of the dissolution process the development of etch pits along the crystallographic directions can be observed. During the process of dissolution these etch pits enlarged and overlapped each other. In consequence needles remain as remnants of old etch pit walls which have overlapped with other pits (Pokrovsky et al. (2009)). During the ongoing experimental run duration the etch pit dominated mineral surface morphology convert into a needle dominated mineral surface with a significant increased reactive surface area. For example, dissolution experiments with organic/inorganic carbonatic samples and HCl-

solutions carried out by Cubillas et al. (2005) exhibit a 30% as well as a 100% increased BET surface area for calcite and aragonite samples, respectively, in comparison to their initial BET surface.

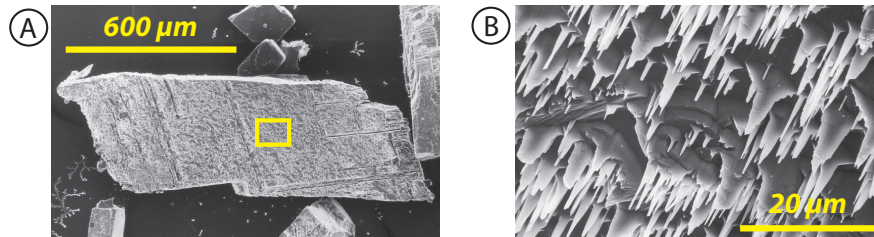


Figure 4.3: SEM images of post-experimental calcite grains after a 1-day run duration: (A) overview screen, (B) magnification of illustration A. Results: (i) preservation of the initial rhombohedral shape, (ii) development of clear dissolution features along all crystallographic directions, (iii) crystalline needles on the mineral surfaces as remnants of former etch pit walls. (SEM laboratory, IfG, CAU Kiel)

With ongoing experimental run duration an onward structural change on the mineral surfaces can be observed (cf. figure 4.4). The rhombohedral grain shape is still maintained. In contrast to short-time experiments the clear visible dissolution features as well as the needles appearance have changed during the progressional dissolution process. Dissolution features along the crystallographic directions are less developed. Furthermore the former sharp needles changed partly into blunt needles. Yadav et al. (2008) characterize the atomic structure of calcite by layers analogous to the framework structure of halite. With this assumption, the observed needle appearance of long-time experiments within the present study suggests different dissolution steps. Blunt needles characterize an almost completely dissolved calcite layer. The observed less visible dissolution features on the mineral surfaces are probably also caused by the advanced dissolution of the outermost layer. The sharp needles at long-time experiments stand either for a slower dissolution on the same calcite layer or characterize a faster dissolution, whereas a subjacent layer is etched.

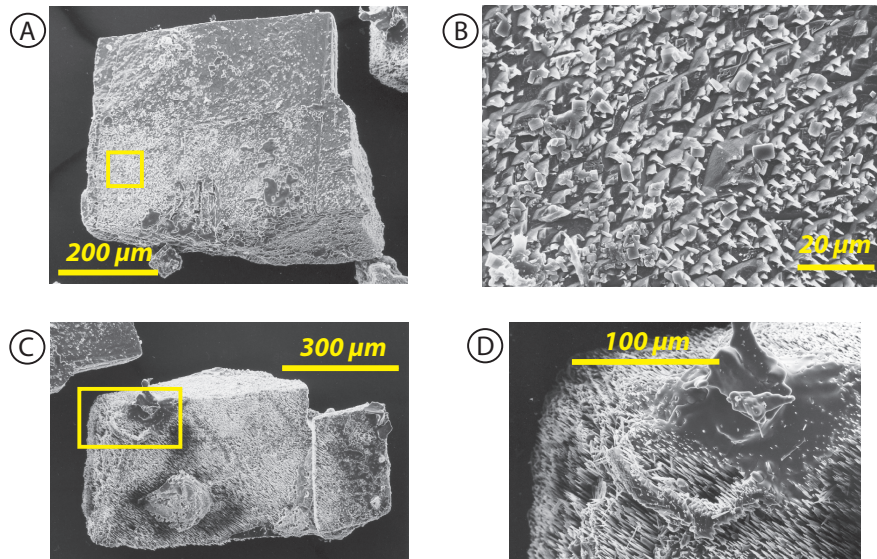


Figure 4.4: SEM images of post-experimental calcite grains after a 30-day run duration: (A, C) overview screen, (B, D) magnification of illustration A and B. Results: (i) preservation of the initial rhombohedral shape, (ii) less visible dissolution features along all crystallographic directions in contrast to short-time experiments, (iii) formation of sharp as well as blunt crystalline needles on the mineral surfaces. (SEM laboratory, IfG, CAU Kiel)

In comparison to the observed structural changes on calcite grains, post-experimental *dolomite* charges exhibit a less significant alteration (cf. figure 4.5). While the initial rhombohedral or polycrystalline shape of grains is maintained after a run duration of one day, neither clear visible dissolution features nor the development of needles can be observed on the mineral surfaces or boundaries. Furthermore the structural changes do not occur evenly on all analyzed grains. A few grains exhibit their initial appearance without any dissolution features. Other grains are characterized by an irregular etch behavior without any crystallographic orientation. But there are also grains, which include both, dissolution characteristics as well as unreacted parts.

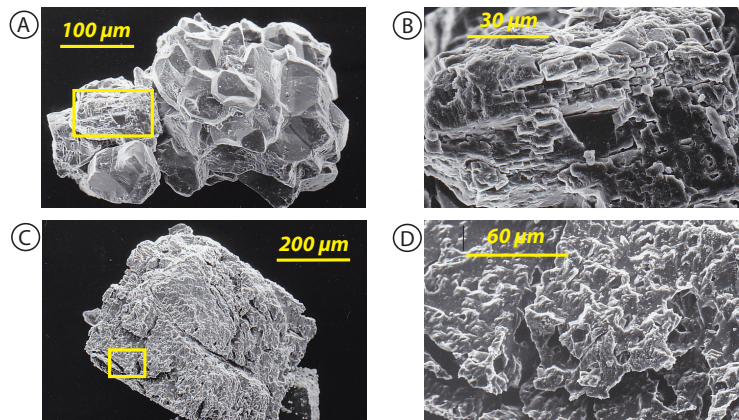


Figure 4.5: SEM images of post-experimental dolomite grains after a 1-day run duration: (A, C) overview screen, (B, D) magnification of illustration A and B. Results: (i) preservation of the initial rhombohedral or polycrystalline shape, (ii) irregular dissolution features on the mineral surfaces. (SEM laboratory, IfG, CAU Kiel)

With increasing run duration the initial shape of dolomite grains still maintains (cf. figure 4.6). The irregular etch behavior observed at short-time experiments changes into a preferentially stepped dissolution along the crystallographic directions at long-time experiments. The development of crystalline needles is still not observed. These dissolution behaviors are caused by the atomic structure of dolomite, whereat Ca^{2+} and Mg^{2+} ions are arranged in alternate layers (Yadav et al. (2008)). Due to the dense atomic packing a destruction of framework bonds and therefore the dissolution of these alternate layers do not take place. Rather, Ca^{2+} and Mg^{2+} ions are detached from the mineral surface resulting in other structural changes compared to calcite samples.

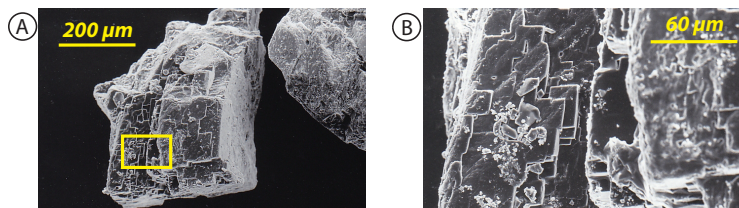


Figure 4.6: SEM images of post-experimental dolomite grains after a 30-day run duration: (A) overview screen, (B) magnification of illustration A. Results: (i) preservation of the initial rhombohedral shape, (ii) stepped dissolution features along the crystallographic directions. (SEM laboratory, IfG, CAU Kiel)

In conclusion the SEM analyses of pre- and post-experimental calcite and dolomite charges show time dependent structural changes on the mineral surfaces, whereas the development of dissolution features (e.g. etch pits, needles or irregular shapes) is differentially pronounced with increasing run duration and is related to the employed starting material. Despite of the same crystal system and similar crystal shapes calcite and dolomite samples exhibit different dissolution behaviors. Reasons for these differences are described in more detail by Yadav et al. (2008): (i) The calcite dissolution is characterized by the destruction of framework bonds, whereat Ca^{2+} ions are released. In contrast the dissolution of dolomite is described by the detachment of Ca^{2+} and Mg^{2+} ions from the crystal surface. (ii) The atomic structure of calcite is arranged in layers, whereas within the dolomite the Ca^{2+} and Mg^{2+} ions are segregated in alternate layers and thus results in a denser atomic packing. In consequence the observed varying structural changes are based on the differences in the atomic configuration of the mineral framework structure. All observed structural changes mentioned in the present study can be compared to SEM analyses results of Cubillas et al. (2005), Pokrovsky et al. (2005), Pokrovsky et al. (2009) and Yadav et al. (2008).

Micro Computertomography Analyses (μ -CT)

In addition to the above mentioned SEM analyses structural changes on the mineral surfaces can also be determined by micro computertomography analyses (μ -CT). The carbonatic samples analyzed in the present study do not represent a sufficient data base to determine significant structural changes on the mineral surfaces. Thus, an interpretation of analyzed data does not occur in the present study.

4.1.2 Analyses of the Fluid Samples (ICP-OES Analyses)

In addition to structural changes on the mineral surfaces, dissolution and/or precipitation processes can also be determined by the alteration of the used fluid phase. During dissolution processes various components (e.g. ions or complexes) release from the mineral surface and thus enhance the concentration of these components within the fluid phase. In contrast precipitation processes result in the removal of different components out of the fluid and cause the enrichment of these components within secondary minerals. A third process is the cation exchange process between fluid and solid, which also results in the chemical alteration of the fluid phase. The degree of fluid alteration varies for different mineral phases.

In the present study the determination of fluid alterations was accomplished by ICP-OES measurements on pre- and post-experimental fluid charges. The fluid samples were taken after each single experiment and were prepared as described in chapter 3.1.1. The analyses of the fluid samples were proceeded after the method described in chapter 3.3.2.

Following sub-chapters include descriptions of temperature dependent, grain size dependent and gas-phase dependent alterations of the post-experimental fluid charges in regard to the temporal progression of dissolution processes. To ensure each single parameter dependency all further experimental conditions were held constant within the respective experiments. Therefore, temperature dependent experiments were accomplished at 100 °C and 150 °C by using solid phases with a grain size of 250 – 500 μm . In contrast grain size dependent experiments were accomplished at 150 °C by using solid phases of four grain size fractions (< 63 μm , 63 – 160 μm , 160 – 250 μm , 250 – 500 μm). All these experiments run under a total pressure of 85 bar. The influence of the gas phase was determined by experiments without CO_2 and experiments with CO_2 (total pressure: 85 bar), whereat the parameters temperature and grain size were held constant at 150 °C and 250 – 500 μm , respectively.

All experiments described in the present study were performed twice at identical run conditions to demonstrate the reproducibility of experimental results. In the following descriptions the experiments are distinguished in V-I and V-II. To identify the reproducibility of the experimental results both experiments are compared to each other. At first the five analyses of each individual fluid sample are averaged after equation 4.1. Subsequent the determined average of experiment V-II is related to the determined average of experiment V-I.

$$\bar{x}_{arithm} = \frac{1}{n} \sum_{i=1}^n x_i = \frac{x_1 + x_2 + \dots + x_n}{n} \quad (4.1)$$

To compare the determined analytical results of the respective experimental series all values are conformed to each other in the following manner.

First of all the analyzed composition of the used standard (IAPSO K15) is compared to the theoretical composition given by the manufacturer. The determined differences are added to the measuring values of the unknown samples. For example, the Ca-concentration in one complete ICP-OES measurement exceeds the theoretical value by an average of 5 mg/L. In consequence these 5 mg/L Ca are added to the determined Ca values of the unknown samples.

Furthermore the determined analytical results have to be conformed to the

used model brines. As mentioned in chapter 3.2 the total number of experiments could not be accomplished with one charge of model brine. Therefore several charges with theoretical the same composition have been prepared. However, due to possible initial weight inaccuracies minor differences in the composition of the model brine charges are not ruled out. All initial model brine charges are normalized in the following manner to distinguish chemical changes which are caused by different concentrated initial model brines and "real" chemical changes which are caused by dissolution and/or precipitation processes during the ongoing experiments. Those initial model brine which exhibit the best fit to the theoretical model brine composition is fixed. All other model brine charges are normalized to this fixed model brine composition. The resulting differences are added to the respectively determined values of the unknown samples. For example, the Ca-concentration in the model brine charge "B" exceeds the Ca-concentration of the fixed model brine charge "A" by a value of 5 mg/L. In consequence, this 5 mg/L Ca are added to the determined Ca values of all unknown samples which are based on the initial model brine charge "B".

All measuring results of experiments with calcite and dolomite are adjusted with the above mentioned methods and form the data base for the following considerations.

Temperature Dependent Alterations

When considering the dissolution behavior of carbonates the variable temperature exhibits an influence on the reaction's progression, even though the influence is not so clearly pronounced as known from feldspar dissolution processes (c.f. chapter 4.2.2). For example, Alkattan et al. (1998) and Schott et al. (1989) describe slightly increasing dissolution rates with increasing temperature. These assumptions are to be verified by experiments accomplished in the present study. As mentioned above two temperatures – 100 °C and 150 °C – were used. It has to be noted that these chosen temperatures are higher compared to assumed temperatures in potential reservoir horizons. However, to perform the experiments within appropriate time and with significant changes, the higher temperatures were used to accelerate the chemical reactions.

All following descriptions are based on analyses of post-experimental fluid samples of 24 teflon experiments with calcite. Therefore, each temperature is represented by 12 experiments with run durations of 1, 2, 5, 10, 20 and 30 days. The reproducibility of experimental results was realized by the accomplishment of two experiments (V-I & V-II) with identical run conditions at

every time step. Three of the 24 mentioned experiments have to be excluded from the following considerations – the 1-day and 30-day experiment of series V-I at 150 °C as well as the 10-day experiment of series V-II at 100 °C. The measuring results of these samples exhibit in large parts lower concentrations than the other analyzed samples. It is to be assumed that these low concentrations are caused by a faulty dilution during the sample preparation. All analytical results of the measured fluid components are summarized in appendices B.6 and B.8.

At first the *reproducibility of experimental results* will be considered. The differences between experimental series V-I and V-II are listed in appendices B.7 and B.9.

In regard to the main components Cl and Na the reproducibility of experimental results is clearly apparent. For both temperatures the differences between the experimental series range between 0.27% and 5.54%. In contrast the minor components Ca and Mg exhibit larger differences up to 16.82% (Ca) and 1.88% to 14.43% (Mg). It is to be observed that the smaller the total concentration of compound the larger the differences between experiment V-I and V-II. Since the measured values of the component K are below the detection limit all following descriptions exclude this component.

In general it can be assumed that the experimental results are reproducible. Hence, all following descriptions are based on a combination of both experiments (V-I and V-II), wherein the differences are taken into account. In consequence each time step is represented by the average (after equation 4.1) of ten single analyses. The denoted deviations are calculated after equation 4.2 and include these ten individual measuring points.

$$SD = \sqrt{\frac{\sum(x - \bar{x})^2}{(n - 1)}} \quad (4.2)$$

When considering the measuring results in regard to the *geochemical behavior* of the included components with increasing run duration, three main observations can be made:

1. in relation to the components Cl, Na and Mg the pre- and post- experimental fluid samples do not exhibit significant differences within the determined standard deviation
2. fluid samples of experiments performed at 150 °C exhibit an detectable increase in Ca-concentrations with increasing run duration, whereas

3. fluid samples of experiments performed at 100 °C show no significant Ca-concentration changes during the entire run duration.

As already listed above Cl-, Na- and Mg-concentration changes between pre- and post-experimental fluid samples are not detected. The progression of all curves – independent of the applied experimental temperature – is similar with increasing run duration (c.f. appendix A.8). All concentration changes ranged within the calculated errors. Based on the initial model brine composition and the solid phase an alteration of the fluid composition in regard to the elements Cl, Na and Mg is not expected during the ongoing reaction. Minor deviations in regard to the initial model brine are possible caused by faulty sampling, storing and/or preparation of the fluid samples.

As known from the measurements of the solid samples (c.f. chapter 4.1.1) the dissolution of calcite during the ongoing experiment can be assumed. In consequence a time dependent Ca release should to be observed within the taken fluid samples. This statement is partly affirmed by the measuring results. For experiments performed at 150 °C a significant increase in the Ca-concentration in regard to the Ca-concentration within the initial model brine is observed. Already after a 2-days run duration the Ca-concentration is increased by ~ 200 mg/L (c.f. figure 4.7 left, diamonds). In contrast, the Ca-concentration changes in fluid samples of experiments performed at 100 °C ranged within the calculated errors and are not significantly increased in regard to the Ca-concentration within the initial model brine (c.f. figure 4.7 left, pentagons).

Based on these measuring results the derivation of the *dissolution rate* R is possible after following equation:

$$R = \frac{\Delta c_{Ca}}{RS \cdot t} \quad (4.3)$$

where Δc_{Ca} describes the Ca-concentration change (mol) between pre- and post-experimental fluid samples, RS is the reactive surface (m^2) of the used solid phase and t describes the experimental run duration (s). In the present study Δc_{Ca} and t result from the ICP-OES measurements and the experimental conditions, respectively. In contrast, the reactive surface values used for the calculations are based on experimental data after Eisenlohr et al. (1999), who determine reactive surfaces of $0.0116 m^2/g$ and $0.0082 m^2/g$ (BET measurements) for limestone samples with a grain size of $250 - 350 \mu m$ and $350 - 500 \mu m$, respectively. Since the grain size fraction used in the present study comprises both grain size fractions of the mentioned literature data an average of both reactive surface values is used to calculate the

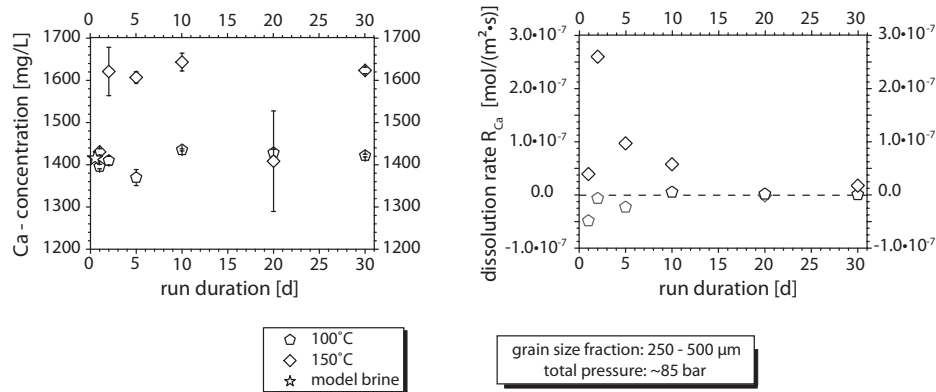


Figure 4.7: Temperature dependent alteration of the model brine in regard to the Ca-concentration (*left*) and corresponding calcite dissolution rates calculated after equation 4.3 (*right*): starting material calcite (250 – 500 μm); detailed information about the used data set see text; **Results:** (i) an increasing experimental temperature results in an increasing Ca release out of the solid and hence an increasing Ca-concentration within the fluid phase; (ii) lower Ca release at experiments with lower temperatures results in lower dissolution rates (ICP-OES laboratory, IfG, CAU Kiel)

dissolution rates in the present study. Appendix B.15 summarizes the used parameters as well as the calculated calcite dissolution rates.

The right graph in figure 4.7 depicts the calculated dissolution rates with increasing run duration. As expected from the ICP-OES measurements the dissolution rates for experiments at 100 °C are negligible small ($R: 5.71 \cdot 10^{-10}$ mol/(m²·s) to $5.15 \cdot 10^{-9}$ mol/(m²·s)). In contrast, the determined dissolution rates for experiments at 150 °C are more significant and are caused by the increased Ca-release during the ongoing experimental run duration. It has to be noted that during the first and the second day the clearest dissolution rate increase can be observed and is caused by the most significant Ca-release of ~ 200 mg/L during this time step. After reaching this concentration level the amount of Ca within the fluid does not change significantly with increasing run duration. In consequence, the determined dissolution rates for experiments longer than 2 days decrease and converge to zero. The observed negative dissolution rates (c.f. figure 4.7 right, gray symbols) for experiments at both temperatures might be caused by the precipitation of Ca-bearing secondary minerals during the ongoing experiment or during the cooling process after the experiment. However, SEM analyses of the reacted solids could not exactly affirm this assumption.

The comparison of calculated dissolution rates and literature data is in prin-

principle possible and is depicted in figure 4.8. However, the following constraints have to be noted. Although all mentioned experiments are carried out in closed batch reactor systems different stirring rates influence the flow regimes within the used reactors. As known from chapter 2.1 the parameters "experimental setup" and "flow regime" are probably the parameters with the largest influence regarding the considered comparison of literature data. Various authors like Alkattan et al. (1998) or Plummer et al. (1978) describe increasing dissolution rates with increasing stirring rates. However, the lower stirring rates (< 425 rpm) for experiments described in the literature cause faster dissolution rates compared to the calculated dissolution rates within the present study where the stirring rate achieves a value of 1100 rpm. The determined differences in dissolution rates are between two and five orders of magnitude.

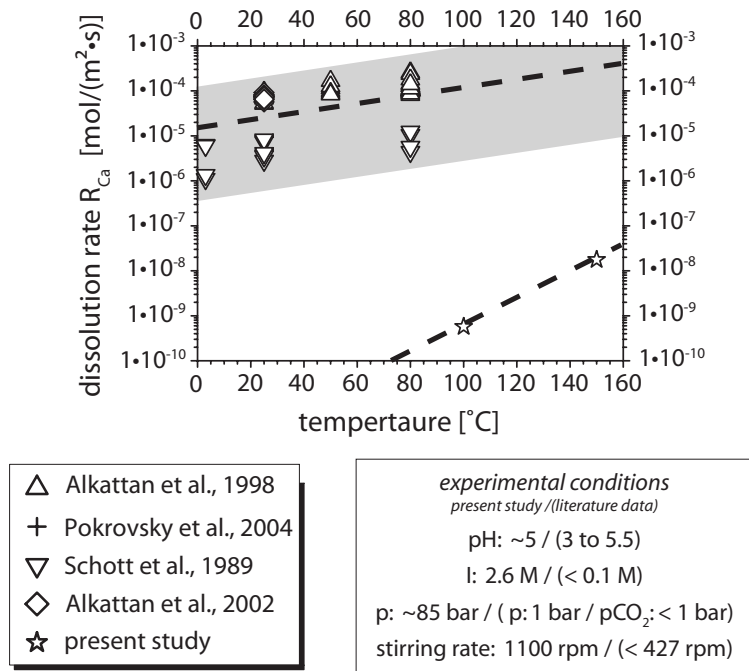


Figure 4.8: Comparison of calculated dissolution rates and literature data (temperature dependent)

These observations are based on the continuousness of the stirring process. While the stirring process is permanent for experiments described in the literature the stirring process in the present study is limited to 3 times a day. Thus, in general the experiments of the present study are run under static conditions without any fluid flow and consequently result in slower dissolution rates. Even the increased experimental temperature does not

significantly accelerates the calcite dissolution rates compared to the literature data. However, the combination of experimental setup and temperature seems to have an influence on the calcite dissolution behavior. The dissolution rates described in the literature based on rotating disk experiments with a continuous stirring and might reflect potential CO_2 reservoirs close to the injection site. In this case the influence of the stirring process overlaps the influence of the temperature, what results in a minor slope of dissolution rates with increasing temperature. In contrast, the calculated dissolution rates described in the present study based on static experimental conditions with a temporal fluid flow and represent potential CO_2 reservoirs far from the injection site. Taking the steeper slope of the dissolution rate into account it has to be assumed that in the present study the influence of the temperature is more pronounced than the influence of stirring rate. These mentioned observations about different dissolution rates at different flow regimes are crucial and might influence the numerical simulations of various sequestration scenarios significantly. Chemical reactions which are taking place close to the injection sites exhibit faster dissolution rates than chemical reactions far from the injection site.

The ionic strength of the used model brine also influences the dissolution behavior of calcite. While the shown literature data are based on ionic strength smaller than 0.1 M, the model brine used within the present study exhibits an ionic strength of 2.6 M. In regard to the fluid composition different chemical interactions take place. Due to the high variability of fluid compositions within the literature a well-defined statement about the influence of the parameter "ionic strength" is not possible.

A further parameter, which varies between the compared data is the grain size fraction. Whereas Alkattan et al. (1998, 2002) and Pokrovsky et al. (2005) accomplished the experiments with grain size fractions of $< 125 \mu\text{m}$ and $100 - 200 \mu\text{m}$, respectively, the used calcite grains in the present study exhibit sizes between $250 - 500 \mu\text{m}$. As known from the literature smaller grain size fractions exhibit a larger reactive surface. In consequence, the Ca release out of larger reactive surfaces is increased in regard to smaller reactive surfaces and hence, results in increased dissolution rates. Detailed descriptions of grain size dependent calcite dissolution processes are explained in the following sub-chapter.

In addition to the dissolution rate R the *activation energy* E_A is derived. To calculate the activation energy with the help of the Arrhenius equation the rate constant k needs to be known. As deduced from descriptions of Lasaga and Kirkpatrick (1981) the dissolution of calcite is a pseudo first-order reac-

tion, where the rate constant is described by following equation:

$$-\frac{dC_A}{dt} = kC_A \quad (4.4)$$

Transferred to the present study, where a Ca release out of solid phase into the fluid phase is described, equation 4.4 has to be rewritten in the following manner:

$$-\frac{dc_{sol}}{dt} = k(c_{sat} - c_{sol}) \quad (4.5)$$

where c_{sol} describes the Ca-concentration (mg/L) in a post-experimental fluid at a defined point of time t (s) and c_{sat} describes the saturation concentration of Ca (mg/L). By integrating this equation the following exponential function is obtained:

$$\frac{c_{sat} - c_{sol}}{c_{sat} - c_0} = e^{-kt} \quad (4.6)$$

or

$$c_{sol} = c_{sat} - (c_{sat} - c_0) \cdot e^{-kt} \quad (4.7)$$

where c_{sol} describes the Ca-concentration (mg/L) in a post-experimental fluid at a defined point of time t (s), c_{sat} describes the saturation concentration of Ca (mg/L) and c_0 stands for the Ca-concentration of the initial model brine (mg/L). In the present study both, c_{sol} and c_0 , are known from the accomplished ICP-OES measurements. Hence, the saturation concentrations and the rate constants for both temperatures (T: 100 °C & 150 °C) have to be determined by the following mathematical algorithm:

$$y = A_1 - A_2 \cdot e^{-kx} \quad (4.8)$$

The analyzed ICP-OES data are fitted in 30 iterations steps and result in the values listed in table 4.1. Figure 4.9 (left) depicts the mathematical fit of data. It has to be noted that the customization of the function on analytical results of experiments performed at 150 °C is better than the fit of analytical results of experiments performed at 100 °C. This phenomena is caused by the different Ca release out of the solid phase into the fluid phase. Due to the insignificant Ca-concentration changes within the fluid samples of experiments performed at 100 °C the customization of the exponential function on the analytical results is improper. In contrast, the more significant

Ca-concentration changes within the fluid samples of experiments performed at 150 °C exhibit a better customization of the exponential function on the analytical results.

Table 4.1: Determined parameters as basis of activation energy calculations

	c_{sat} [mg/L]	$(c_{sat}-c_0)$ [mg/L]	k [1/d]	R^2
100 °C	1415.83 ± 17.79	10	0.11094 ± 0.8805	0.13027
150 °C	1628.71 ± 26.78	300	0.72669 ± 0.2845	0.86867

To analyze the influence of the temperature on the chemical reaction of the calcite dissolution the Arrhenius plot is used (c.f. figure 4.9 right). This plot displays the logarithm of rate constants ($\ln(k)$) plotted against the inverse temperature ($1/T$). By including the above determined rate constants for both temperatures into the plot a linear equation can be fitted. Transferred to the present study and according to the Arrhenius equation the linear equation can be described as followed:

$$\ln k = \ln A - \frac{E_A}{R} \cdot \frac{1}{T} \quad (4.9)$$

where k describes the rate constants (1/d), A is the pre-exponential factor (or prefactor, dimensionless), E_A describes the activation energy (J/mol), R stands for the universal gas constant (J/mol·K), and T describes the absolute temperature (K).

Using this mathematical derivation the determination of the activation energy is now possible. Experiments described in the present study exhibit an activation energy of 10.646 kJ/mol (equals 2.54 kcal/mol). Even though experiments of only two temperatures were accomplished in the present study, the determined value is in good agreement with literature data of Plummer et al. (1978) and Salem et al. (1994) who determine activation energies of about 10 kJ/mol. These relative small activation energies indicate diffusion controlled reactions and thus strengthens the assumption mentioned in chapter 2.1 that mineral dissolution behaviors of experiments with slow or without any fluid flow are affected by diffusion controlled processes. Due to the experimental setup used in the present study the calculated activation energy is plausible. In comparison to determined activation energies described by Alkattan et al. (1998) (19 kJ/mol), Finneran and Morse (2009) (20 kJ/mol) or Gledhill and Morse (2006a) (21 kJ/mol) the calculated activation energy in the present study is up to two times lower. Again, these observations are

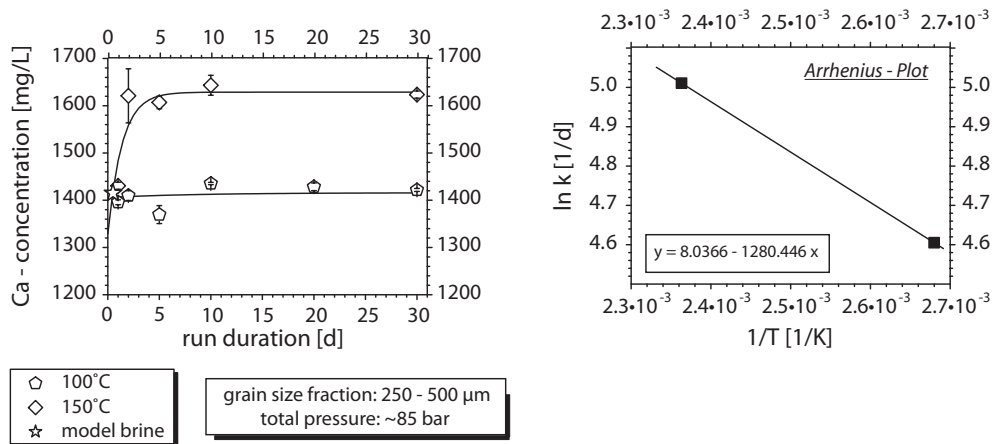


Figure 4.9: Derivation of the activation energy of calcite: *left*: determination of the saturation concentration (c_{sat}) and the rate constant (k) after equation 4.7; *right*: illustration of the Arrhenius plot to deviate the activation energy

caused by the application of different experimental setups. The experiments accomplished in these three mentioned studies run under a permanent fluid flow. In consequence, the mineral dissolution in these experiments are not only influenced by diffusion controlled mechanisms but also influenced by hydrodynamic processes (c.f. chapter 2.1). Due to the fluid movement the mass transport of reactants/reaction products accelerates and consequently results in increasing dissolution rates as well as increasing activation energies. As already mentioned for the determined dissolution rates the flow regime impacts the activation energy in a crucial way. In consequence, these different activation energies might influence the numerical simulations of various sequestration scenarios significantly. Chemical reactions which are taking place close to the injection sites exhibit a larger activation energy than chemical reactions far from the injection site.

Grain Size Dependent Alterations

In addition to the knowledge about temperature dependent calcite dissolution behaviors the grain size of the solid samples represents a second influencing parameter on the calcite dissolution behavior. As known from the literature (e.g. Eisenlohr et al. (1999) or Zhang et al. (2007)) increasing grain sizes result in decreasing dissolution rates caused by the smaller reactive surface of larger grain size fractions. Based on this statement it can be assumed that different potential reservoir rocks exhibit various chemical reaction be-

haviors caused by their wide spread of grain size composition. To verify this assumption experiments at calcite grains of four grain size fractions were accomplished within the present study: $<63 \mu\text{m}$, $63 - 160 \mu\text{m}$, $160 - 250 \mu\text{m}$ and $250 - 500 \mu\text{m}$.

All following descriptions based on analyses of post-experimental fluid samples of 36 teflon experiments with calcite. Therefore, the two larger grain size fractions are in each case represented by 12 experiments with run durations of 1, 2, 5, 10, 20 and 30 days. To demonstrate the reproducibility of experimental results two experiments (V-I & V-II) with identical run conditions are accomplished at every time step. All experiments at the two smaller grain size fractions are only carried out once. Three of the 36 mentioned experiments have to be excluded from the following considerations – the 1-day and 30-day experiment of series V-I at a grain size of $250 - 500 \mu\text{m}$ as well as the 10-day experiment of series V-I at a grain size of $160 - 250 \mu\text{m}$. The measuring results of these samples exhibit in large parts lower or higher concentrations than the other analyzed samples. It is to be assumed that these low/high concentrations are caused by a faulty dilution during the sample preparation or by an evaporation process and consequently a saturation of the dissolved components during the storage of the fluid samples. All analytical results of the measured fluid components are summarized in appendices B.8 ($250 - 500 \mu\text{m}$), B.10 ($160 - 250 \mu\text{m}$), B.12 ($63 - 160 \mu\text{m}$) and B.13 ($<63 \mu\text{m}$).

The identification of the *reproducibility of experimental data* is identical to the above mentioned procedure for experiments at different temperatures. Appendices B.9 and B.11 list the determined results.

The geochemical behavior of the main components Cl and Na in post-experimental fluids of experiments at different grain size fractions is similar to the experiments performed at different temperatures. The differences between the series V-I and V-II of experiments performed at the larger grain sizes range between 0.46% and 5.54%. Also the minor components Ca and Mg exhibit a similar geochemical behavior compared to experiments at different temperatures. It is to be observed that the smaller the total concentration of compound the larger the differences between experiment V-I and V-II. Hence, the differences range between 1.72% and 25.85% for Ca and 3.2% and 61.31% for Mg. Since the measured values of the component K are below the detection limit all following descriptions exclude this component.

Despite the partly significant differences between both experimental series all following descriptions are based on a combination of experiment V-I and V-II. In consequence each time step is represented by the average (after equation 4.1) of ten single analyses. The denoted deviations are calculated after

equation 4.2 and include these ten individual measuring points.

Based on the measuring results three main observations can be made in regard to the *geochemical behavior* of the included fluid components with increasing run duration:

1. in relation to the main components Cl and Na the post-experimental fluid samples exhibit slightly increased concentrations in regard to the initial model brine
2. in relation to the minor component Mg significant differences between pre- and post-experimental fluid samples can be observed, whereat the measuring results suggest neither clearly increased nor clearly decreased concentrations
3. with increasing run duration as well as decreasing grain size of the solid samples a significantly increased Ca release can be observed

As depicted in Appendix A.9 the geochemical behavior of Cl and Na is similar with increasing run duration. It strikes that especially the fluid samples of experiments performed at the smaller grain size fractions exhibit slightly increased Cl- and Na-concentrations in regard to the concentrations in the initial model brine. Furthermore it is to be noted that these increased concentrations are only observed in fluid samples of short run durations. However, due to the initial model brine composition and the used starting material, respectively, an alteration of the fluid samples in regard to the components Cl and Na is not expected during the ongoing dissolution process. A possible reason for the observed concentration changes can be described by evaporation processes during the sample's storage, which result in a saturation of fluid compounds. The Cl- and Na-concentration changes within the fluid samples of experiments performed at larger grain size fractions are negligible and range between the error of measurements.

As already mentioned above significant Mg-concentration changes can be observed between pre- and post-experimental fluid samples. Based on the measuring results a clear tendency of increasing or decreasing Mg-concentrations is not determined. This suggests, that the concentration changes with increasing run duration are not caused by dissolution and/or precipitation processes. One possible explanation for the observed concentration changes might be the adjacency to the detection limit of Mg during the ICP-OES analyses. However, a definite explanation cannot be given.

In contrast to the main components Cl and Na as well as the minor component Mg the amount of Ca in the post-experimental fluid samples changes significant with increasing run duration as well as with increasing grain size.

As depicted in figure 4.10 (left) the most important Ca release with increasing run duration can be observed in post-experimental fluid samples of experiments performed at a grain size of $<63 \mu\text{m}$. In regard to the used initial model brine the Ca-concentration is increased by a value of about 700 mg/L. Furthermore it can be observed that increasing grain sizes result in decreasing Ca releases. Therefore, post-experimental fluid samples of experiments performed at a grain size of $250 - 500 \mu\text{m}$ exhibit a maximum Ca release of 200 mg/L. The only exception is given by experiments performed at a grain size of $160 - 250 \mu\text{m}$. Within the error of measurements the Ca-concentrations of these post-experimental fluid samples are similar to the Ca-concentration of the initial model brine. The observed grain size dependent Ca release is comparable with experimental result described in the literature. For example, Eisenlohr et al. (1999) describe increasing Ca releases with decreasing grain sizes as a result of the increased reactive mineral surfaces with decreasing grain sizes.

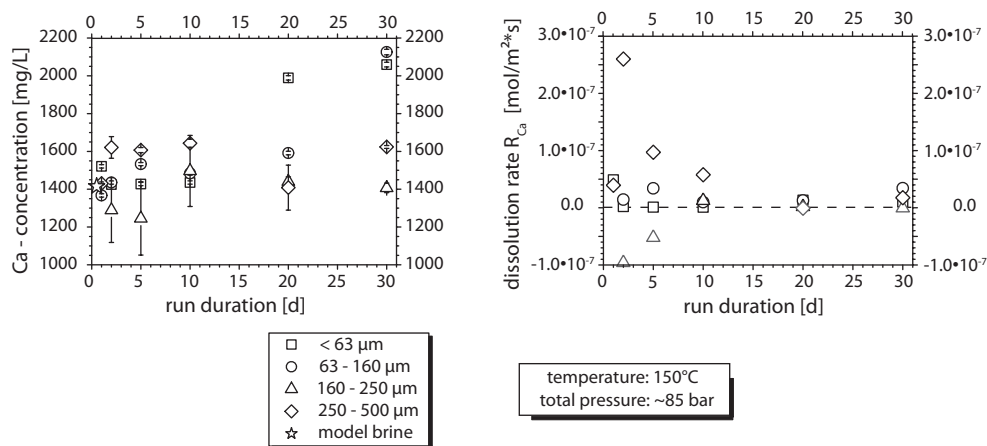


Figure 4.10: Grain size dependent alteration of the model brine in regard to the Ca-concentration (*left*) and corresponding calcite dissolution rates (*right*) calculated after equation 4.3: detailed information about the used data set see text; **Results:** (i) increasing grain size results in lower Ca-concentrations within the fluid phase; (ii) in relation to the available reactive surface samples with smaller grain sizes exhibit a lower Ca-release and consequently result in smaller dissolution rates (ICP-OES laboratory, IfG, CAU Kiel)

In general the above mentioned Ca release variations correspond to experiments longer than 10 days. In contrast, the Ca-concentration changes between larger and smaller grain size fractions are not so clearly pronounced for experiments with a short run duration (<10 days). This observation is

attributed to the chemical disequilibrium, which prevails in the used experimental setup at short run durations.

Based on the mentioned measuring results the *dissolution rate* R is derived after equation 4.3. In the present study Δc_{Ca} and t result from the ICP-OES measurements and the experimental run conditions, respectively. In contrast the reactive surface values used for the calculations are based on experimental data after Gledhill and Morse (2006b), Finneran and Morse (2009) and Eisenlohr et al. (1999), who determine following reactive surfaces:

Table 4.2: Determined reactive surfaces for calcite as well as limestone described in the literature

material	grain size [μm]	reactive surface ^a [m^2/g]	reference
calcite	32 – 63	0.0500	Gledhill and Morse (2006b)
calcite	63 – 125	0.0160	Finneran and Morse (2009)
limestone	180 – 250	0.0163	Eisenlohr et al. (1999)
limestone	250 – 350	0.0116	Eisenlohr et al. (1999)
limestone	350 – 350	0.0082	Eisenlohr et al. (1999)

^a BET measurements

Even though the listed grain size fractions do not exactly reflect the grain size fractions used in the present study, the determined reactive surface values are nevertheless used to calculate the dissolution rates. Furthermore it has to note that the largest grain size fraction used in the present study comprises two grain size fractions which are described in Eisenlohr et al. (1999). In consequence, the average of both reacted surface values is used to calculate the dissolution rate for these experiments. Appendix B.15 summarize the used parameters as well as the calculated calcite dissolution rates.

The right graph in figure 4.10 depicts the calculated dissolution rates with increasing run duration. Based on the above mentioned observations about the grain size dependent Ca release the determined dissolution rates are also grain size dependent. However, in contrast to the most significant Ca release at experiments with the smallest grain size, the fastest dissolution rate is calculated for experiments with the largest grain size. Between the largest and the smallest grain size fraction differences of about $2 \cdot 10^{-8} \text{ mol}/(\text{m}^2 \cdot \text{s})$ are determined. It is noticeable (especially for experiments at a grain size of 250 – 500 μm) that during the first and the second day the dissolution rates exhibit the clearest increase. It means that in regard to the elapsed run duration and the available reactive surface the highest absolute Ca release out of the solid sample takes place. In contrast, with increasing run duration the

absolute Ca release over the available reactive surface decreases from time step to time step and consequently results in decreasing dissolution rates, which converge to zero. The observed negative dissolution rates (c.f. figure 4.10 right, gray symbols) might be caused by a chemical disequilibrium at short time experiments. Furthermore the precipitation of Ca-bearing secondary minerals during the ongoing experiment or during the cooling process after the experiment is a possible reason for the observed negative dissolution rates. However, SEM analyses of the reacted solids could not affirm this assumption (c.f. chapter 4.1.1).

As already known from literature data decreasing dissolution rates are caused by increasing grain sizes and hence, decreasing reactive surfaces. However, this assumption is not affirmed by the determined dissolution rates in the present study, where the observations are contrary. It means that the largest grain size results in the fastest dissolution rates. In turn, this statement seems not plausible considered to the observed minor Ca release out of solids with larger grain sizes compared to the increased Ca release out of smaller grains. The reason for this observation is amongst others caused by the calculation itself, whereat a concentration change between two time steps is related to a defined reactive surface. In the case of the present study the absolute Ca release out of the solid phase in regard to the available reactive surface is exceeded for experiments performed at larger calcite grains compared to experiments performed at smaller calcite grains. This indicates that the larger grain size fraction exhibits a larger available reactive surface as explained as followed. Due to the denser packing of smaller grain size fractions within the applied teflon meshes used in the present study it is assumed that the available reactive surface is smaller in regard to larger grain size fractions. In turn, this is caused by a certain amount of surfaces, which contact each other and are consequently not available for fluid-solid interactions. All these observations result in the contrary calcite dissolution behavior compared to the described dissolution behavior of decreasing dissolution rates with increasing grain sizes in the literature.

The comparison of determined dissolution rates with literature data is very difficult in regard to grain size dependent data. Even though experiments with varying grain size fractions are described in the literature further experimental conditions like the reactor type, the temperature, the ionic strength or the pH-values are differ too much to compare the data reasonably.

Based on the above mentioned observations it is assumed that the grain size and therefore the reactive surface plays an important role for CO₂ sequestration processes. Within a potential CO₂-storing reservoir the grain bond is consolidated and cemented. In consequence mineral surfaces contacting each

other are not available for fluid-solid interactions. Furthermore, some pore spaces can be separated from the usable pore space by the cementation of the connections. Hence, these pore spaces are also not available for fluid-solid interactions. Consequently the application of the "real" reactive surface is crucial for the numerical simulations of various sequestration scenarios. In general the reactive surfaces currently used for numerical simulations based on the BET method (c.f. Gunter et al. (1997) or Morse and Arvidson (2002)), whereat the solid surface is determined by the amount of gas adsorbed on the free accessible surface. Therefore, the analyzed grains are placed unconsolidated within the apparatus resulting in "ideal" reactive surfaces, whereat the whole surface is included. However, the above mentioned observations exhibit the strong influence of the reactive surface on the dissolution rate and show the exigency of using realistic values to represent natural conditions.

In addition to the determination of the "real" reactive surface the structural change of the reactive surface during the ongoing dissolution and/or precipitation process is necessary to know. For example, the SEM analyses of post-experimental calcite grains exhibit different structural changes in regard to the accomplished experimental run duration. This procedure is also transferable to CO₂ sequestration processes. During the injection of CO₂ as well as during the storage of CO₂ various mechanical and/or chemical reaction processes may result in the alteration of the mineral surfaces. Due to these processes the available reactive surfaces of minerals and therefore the dissolution behavior of the considered materials are crucial influenced. In consequence, the fact of the structural alteration of the reservoir components have to integrate in the numerical simulations.

Possible methods to describe and determine such realistic surfaces as well as structural changes of the mineral surfaces are given by μ -CT analyses (e.g. Kahl and Holzheid (2010)).

Gas-phase Dependent Alterations

When considering CO₂ sequestration processes the influence of the gas-phase on the geochemical behavior of different materials has to taken into account. As known from the literature and described in chapter 2.3.1 gas-phases like CO₂ cause pH-value variations in the fluid phases. However, dissolution and/or precipitation processes occur differently depending on the respective materials. While the calcite dissolution process accelerates with increasing pH-values the fastest feldspar dissolution processes take place at both, acid and alkaline pH-values. Although many literature data describe pH-dependent experiments on various materials the accomplishment of further experiments is necessary. Especially earlier studies exhibit experimental con-

ditions far from natural conditions as they occur in potential CO₂ reservoir rocks. For example the pH-value of experiments described in earlier studies is adjusted by acids or bases. In contrast, the pH-value within a potential reservoir is adjusted by the injected gas-phase and the associated chemical reactions with the formation water. In the present study the influence of gas-phases is rudimentally described by the accomplishment of a few experiments with and without CO₂. To ensure this gas-phase dependent influence all further experimental conditions were held constant: T = 150 °C, calcite grain size = 250 – 500 μm, solid-fluid ratio = 1:200. The total pressure of the experiments is related to the temperature-induced expansion of the gaseous and the fluid phases as well as the solution of gas in the fluid phase. Therefore the total pressure in a system without CO₂ is lower compared to a system with CO₂.

All following descriptions are based on 16 teflon reactor experiments, whereat the experiments with CO₂ are represented by 12 experiments. Three of the 16 mentioned experiments have to be excluded from the following considerations — the 1-day and 30-day experiment (series V-I) performed with CO₂ as well as the 2-day experiment performed without CO₂. The measuring results of these samples exhibit lower concentrations than the other analyzed samples. It is to be assumed that these low concentrations are caused by a faulty dilution during the sample preparation. Appendices B.8 and B.14 summarize the analytical results of all measured fluid components.

When considering the measuring results in regard to the *geochemical behavior* of Ca with increasing run duration different amounts of Ca are released from the solid phases (c.f. figure 4.11, left). Only experiments with CO₂ exhibit significant increasing Ca-concentrations of about 200 mg/L with increasing run duration. The Ca-concentrations for experiments without CO₂ are similar to the Ca-concentration of the initial model brine and seems to decrease with increasing run duration. The main reason for this observation is the pH-value of the fluid phase. Due to the use of dry ice as CO₂-source the chemical milieu changes, whereat the solution of CO₂ in the fluid phase results in a decrease of the pH-value. In contrast, the pH-values of fluid samples removed from experiments without CO₂ keep constant with increasing run duration. This observed geochemical behavior affirms the assumptions described in the literature and mentioned in chapter 2.3.1, whereat the dissolution of carbonates is induced by the adsorption of hydrogen ions (H⁺) on the mineral surface (Alkattan et al. (1998), Gautelier et al. (1999), Golubev et al. (2009), Sjöberg and Rickard (1984a), Sjöberg and Rickard (1984b)). In conclusion, the dissolution of CO₂ in the model brine enhances the amount of free H⁺ and consequently, accelerates the dissolution of calcite at experi-

ments with CO_2 .

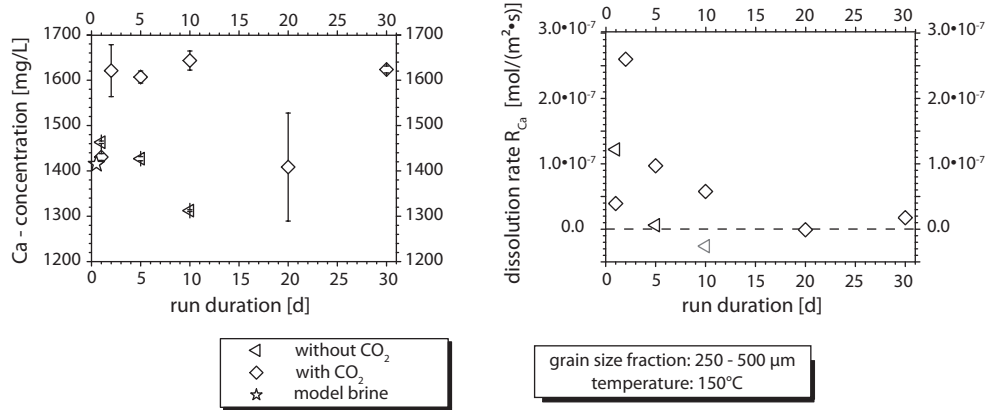


Figure 4.11: Gas-phase dependent alteration of the model brine in regard to the Ca-concentration (*left*) and corresponding calcite dissolution rates (*right*) calculated after equation 4.3: starting material: calcite (250 – 500 μm): detailed information about the used data set see text; **Results:** (i) the used dry ice as CO_2 -source causes a decreasing pH-value of the fluid phase and consequently results in an enhanced Ca-release out of the solid; (ii) lower Ca release in experiments without CO_2 results in lower dissolution rates (ICP-OES laboratory, IfG, CAU Kiel)

The observed Ca-release differences are also reflected in the determined *dissolution rates* calculated after equation 4.3. The parameters Δc_{Ca} and t result from the ICP-OES measurements and the experimental conditions, respectively. In contrast, the reactive surface values used for the calculations are based on experimental data after Eisenlohr et al. (1999), who determine reactive surfaces of 0.0116 m²/g and 0.0082 m²/g (BET measurements) for limestone samples with a grain size of 250 – 350 μm and 350 – 500 μm , respectively. The grain size fraction used in the present study comprises both grain size fractions of the mentioned literature data. In consequence, an average of both reactive surface values is used to calculate the dissolution rates in the present study. Appendix B.15 summarized the used parameters as well as the calculated calcite dissolution rates.

As depicted in figure 4.11 (right) experiments performed with CO_2 exhibit significant larger dissolution rates compared to experiments without CO_2 . The differences between the dissolution rates range up to one order of magnitude. In comparison with dissolution rates described in the literature the dissolution rates calculated in the present study adapt to the tendency of decreasing dissolution rates with increasing pH-value (c.f. figure 4.12). Furthermore figure 4.12 depicts the significant influence of the pH-value on the

calcite dissolution rate. Despite the large variations of other experimental conditions like ionic strength, total pressure or stirring rate (c.f. 4.12 right box) the pH-value dependency is still clearly pronounced. This observation confirms the assumption compiled at the beginning of the monograph: the pH-value of the used fluid is the most important influencing parameter for dissolution and/or precipitation processes.

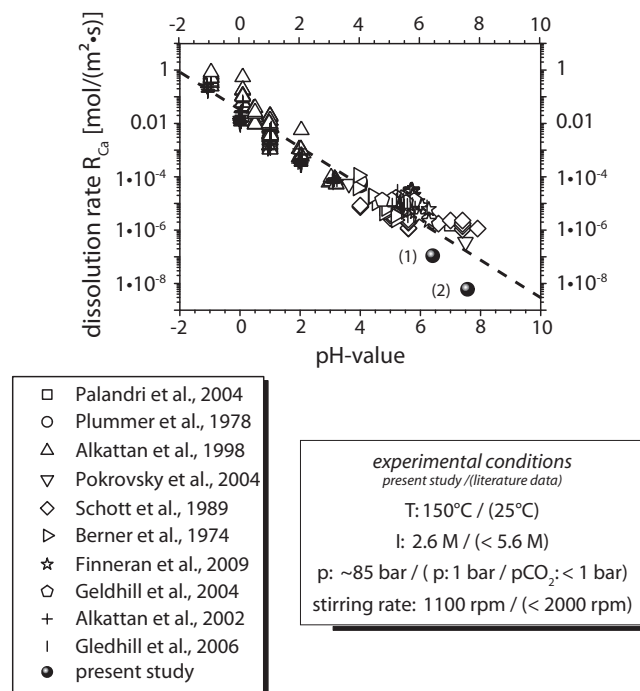


Figure 4.12: Comparison of calculated dissolution rates and literature data (pH-value dependent): point (1) illustrates the dissolution rate of the 5-day experiment performed with CO₂; point (2) illustrates the dissolution rate of the 5-day experiment performed without CO₂

Indeed it is to be noted that the above mentioned experiments pursue the tendency described in the literature. However, the data base is too small to describe gas-phase dependent alteration processes. In the case of CO₂ sequestration processes it is known that the separation of CO₂ from combustion gases of fossil fuel burning power plants does not result in pure CO₂. A certain admixture of other combustion gases (e.g. SO_x or NO_x) will always be present in trace amounts. Therefore, a detailed study including various gases is absolutely necessary to describe gas-phase dependent geochemical behaviors within potential CO₂ storing reservoirs.

Geochemical Behavior of Dolomite Compared to Calcite

In addition to the numerous calcite dissolution experiments dolomite dissolution experiments were also accomplished in the present study to compare the geochemical behavior of carbonates with different chemical compositions. In spite of already described dissolution experiments at various carbonates in the literature (e.g. Chou et al. (1989), Eisenlohr et al. (1999) Pokrovsky et al. (2009) or Yadav et al. (2008)) the present study includes such experiments due to the more realistic conditions according to the used model brine or the used gas-phases.

All following descriptions based on analyses of post-experimental fluid samples of 24 teflon reactor experiments with calcite as well as dolomite. Therefore, each mineral phase is represented by 12 experiments with run durations of 1, 2, 5, 10, 20 and 30 days. The reproducibility of experimental results was realized by the accomplishment of two experiments (V-I & V-II) with identical run conditions ($T = 150\text{ }^{\circ}\text{C}$, grain size = $250 - 500\text{ }\mu\text{m}$, total pressure = 85 bar, solid-fluid ratio = 1:200) at every time step. Two of the 24 mentioned experiments have to be excluded from the following considerations – the 1-day and 30-day experiment of series V-I with calcite. The measuring results of these samples exhibit lower concentrations than the other analyzed samples. It is to be assumed that these low concentrations are caused by a faulty dilution during the sample preparation. All analytical results of the measured fluid components are summarized in appendices B.8 and B.16.

As listed in B.9 and B.17 the *reproducibility of experimental results* is given for all considered experiments. In regard to the main components Cl and Na the differences between the experimental series V-I and V-II range between 0.19% and 6.16%. In contrast the minor components Ca and Mg exhibit larger differences of 0.27% to 16.82% (Ca) and 0.41% to 19.90% (Mg). The increasing differences between series V-I and V-II are caused by the decreasing total concentrations of Ca and Mg compared to the total concentrations of Cl and Na. Since the measured values of the component K are below the detection limit all following descriptions exclude this component.

As consequence of the above mentioned observations all following descriptions are based on a combination of both experiments – V-I and V-II. Therefore, each time step is represented by the average of ten single analyses and is calculated after equation 4.1. The denoted deviations are calculated after equation 4.2 and include these ten individual measuring points.

As depicted in figure 4.13 the *geochemical behavior* of calcite and dolomite differs with increasing run duration. While the Ca-concentrations in post-experimental fluids of calcite experiments increase with increasing run du-

ration the Ca-concentrations in post-experimental fluids of dolomite experiments are similar to the Ca-concentration in the initial model brine. The maximum Ca-concentration change between both starting materials range about 200 mg/L. In regard to the component Mg the alteration of the model brine is similar for both carbonates: with increasing run duration a Mg-concentration increase seems to occur.

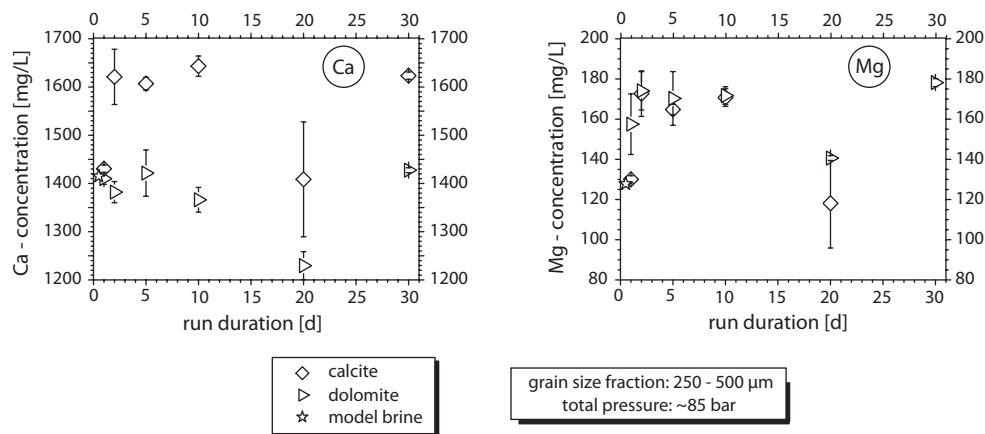


Figure 4.13: Material dependent alteration of the model brine in regard to the Ca- and Mg-concentration: detailed information about the used data set see text; **Results:** (i) dolomite and calcite samples used in the present study exhibit different dissolution behaviors; (ii) compared to the Ca release from calcite the Ca release from the used dolomite is negligible; (ii) the apparent increasing Mg-concentration for both starting materials can be negligible (ICP-OES laboratory, IfG, CAU Kiel)

As know from the literature the observed differences in the dissolution behavior are plausible. For example, Yadav et al. (2008) describe minor Ca^{2+} and Mg^{2+} releases for dolomite samples compared to the Ca^{2+} release for calcite samples. The authors explain this observation by different dissolution mechanisms. While the calcite dissolution is based on the destruction of framework bonds and hence, the release of Ca^{2+} , the dissolution of dolomite is based on the detachment of Ca^{2+} and Mg^{2+} from the crystal surface. Furthermore the authors explain the different dissolution behaviors of calcite and dolomite as a result of the atomic structure of the several minerals. In spite of the same crystal system dolomite exhibits a denser atomic packing than calcite and therefore, results in different dissolution behaviors.

In the case of the present study detectable dissolution processes are only observed for calcite experiments. The ongoing dissolution mechanisms for this starting material are described in the above mentioned sub-chapters. The

apparent Mg-concentration increase in the analyzed fluid samples can be neglected because the combination of the initial model brine and calcite does not allow alteration processes of the fluid samples in regard to this component during the ongoing reaction. In regard to experiments with dolomite dissolution processes are not clearly pronounced. The Ca-concentrations in the analyzed post-experimental fluids are similar to the Ca-concentration in the initial model brine. In contrast, with increasing run duration a Mg-concentration increase seems to occur. Assuming a stoichiometric dissolution of dolomite the release of both components have to be similar. Compared to the analyzed amount of Ca and the associated measuring errors of Ca the Mg-concentrations in the post-experimental fluid samples of dolomite experiments do not increase but rather range within the Ca-concentration changes. Hence, in regard to the error of measurements the apparent Mg-concentration increase is a result of the used measuring technique as well as the depicted axis scale and can be neglected.

Based on the mentioned measuring results the *dissolution rate* R can be derived after equation 4.3. The parameters Δc_{Ca} , Δc_{Mg} and t result from the ICP-OES measurements and the experimental run conditions, respectively. As known from the literature reactive surfaces of dolomite and calcite exhibit different values even though both materials have similar grain sizes (c.f. Finneran and Morse (2009), Gautelier et al. (2007), Yadav et al. (2008)). Due to missing literature data of reactive surfaces for dolomite and calcite samples with a grain size of 250 – 500 μm , the reactive surface values determined by Eisenlohr et al. (1999) are used to calculate the calcite and dolomite dissolution rates in the present study. The authors determine reactive surfaces of 0.0116 m^2/g and 0.0082 m^2/g (BET measurements) for limestone samples with a grain size of 250 – 350 μm and 350 - 500 μm , respectively. Since the grain size fraction used in the present study comprises both grain size fractions of the mentioned literature data an average of both reactive surface values is used to calculate the dissolution rates in the present study. Appendix B.15 and B.18 summarize the used parameters as well as the calculated dissolution rates.

Based on the above mentioned observations about the Ca and Mg release, respectively, the determined dissolution rates affirm the different dissolution behaviors of calcite and dolomite. Compared to calcite dissolution rates the dolomite dissolution rates are up to two orders of magnitude smaller. These observed dissolution behavior variations are comparable with observations in the literature and are caused as mentioned above by different dissolution mechanisms and differences in the atomic packing of both starting materials (c.f. Yadav et al. (2008)).

Conclusion of Measuring Results of ICP-OES Analyses (Carbonatic Samples)

To conclude all observations mentioned in this chapter the following statements can be made. In general the reproducibility of experimental results is given. Due to the high amounts of Cl and Na in the used model brine and consequently, the well detectable concentrations the reproducibility of experimental results is clearly verified. In contrast, differences between both experimental series are more pronounced for the minor components Ca and Mg because of the lower concentrations of these components in the fluid samples. Furthermore alteration processes of the fluid samples are not detected in regard to the components Cl and Na as well as Mg (in the case of calcite experiments). Due to the combination of the initial model brine and the used solid phases an alteration of the initial model brine in regard to these components is not expected during the ongoing dissolution process. The only significant detectable concentration changes between pre- and post-experimental fluids are measured in regard to the component Ca. Based on the accomplished experiments temperature dependent, grain size dependent, gas-phase dependent as well as material dependent dissolution mechanisms are observed and are comparable in the most cases with experimental results mentioned in the literature. For calcite dissolution experiments the parameter pH-value as a result of the used gas-phase is the most important parameter influencing the geochemical behavior. Both, dissolution rates as well as activation energies are calculated and are generally comparable with literature data. However, it has to be noted that varying experimental setups and conditions can cause slight differences in the compared dissolution rates. Nevertheless, in regard to the scientific question of geochemical behaviors at CO₂ sequestration processes the experimental results are plausible and describe mechanism far from the injection site.

4.2 Teflon Reactor Experiments at Feldsparic Samples

In total 72 dissolution experiments with two different feldspar varieties were accomplished in the present study, whereat anorthite samples typify Ca-bearing feldspars and orthoclase samples represent K-bearing feldspars.

Similar to experiments with carbonatic samples different experimental series were carried out to determine grain size fraction as well as temperature dependencies on the mineral dissolution process. Therefore the following ex-

perimental parameters were hold constant: (i) the total pressure at a value of ~ 85 bar, (ii) the ratio between solids and fluids (1:200) and therefore the initial weight of solids and fluids, and (iii) the composition of the synthetic model brine. But the parameters temperature, grain size fraction and run duration varied at different experimental series to estimate the dependencies of these parameters: $T = 100^\circ\text{C}$ or 150°C , grain size = $160 - 250 \mu\text{m}$ or $250 - 500 \mu\text{m}$, $t = 1, 2, 5, 10, 20$ or 30 days. Each single experiment was accomplished twice at identical run conditions to demonstrate the reproducibility of the experimental results. In contrast to the accomplished experiments with carbonatic samples all feldspar experiments were carried out at a constant CO_2 partial pressure.

4.2.1 Analyses of the Solid Samples

During the dissolution and/or precipitation process of minerals within fluid phases reaction rims may form on the solid samples. On the one hand these reaction rims may be characterized by chemical changes along the grain boundaries. Thus, for example, exchange reactions between cations of the solid phase and cations of the fluid phase take place. Furthermore the adsorption of various fluid components on the mineral surface is possible. A third possibility of chemical changes along the grain boundary is the formation of more or less stable precipitates as result of the chemical reaction between the mineral surface and the used fluid phase. In addition or instead of the chemical modifications structural changes can although occur. The development of reactions rims per se as well as the characteristics of the reaction rim formation vary for different mineral phases.

Three different analytical methods were applied to study the above mentioned chemical (EMP) and structural (SEM, μ -CT) changes on the reacted mineral surfaces as a result of occurred dissolution processes.

Electron Microprobe Analyses (EMP)

To detect chemical changes of the feldspar grains as a result of dissolution processes EMP measurements provide an opportunity.

As known from soil sciences feldspar alteration processes take place during the weathering process, whereat ion exchange processes as well as the release of different ions cause chemical changes of the mineral surfaces or result in the development of reaction rims on the edge of the mineral grains. It is to be assumed that these alteration processes might also observe at the feldspar grains which are used in the present study. As described in the following sub-section (SEM analyses) structural changes on the analyzed

post-experimental mineral grains are clearly visible. Based on this observation chemical changes and thus, the development of reaction rims on the edges of the mineral grains are possible. However, the SEM analyses also show that the structural changes on the post-experimental mineral surfaces are within the range of nanometers, what makes a preparation of EMP-thin sections very difficult. Therefore, in the present study EMP-Analyses were refrained.

Nevertheless, in order to confirm or to disprove the above mentioned assumption of chemical changes in form of reaction rims EMP analyses of the post-experimental feldspar grains are necessary and should be accomplished in further studies.

Scanning Electron Microscope Analyses (SEM)

To determine structural changes of the mineral surfaces of both feldspars (anorthite, orthoclase) SEM analyses were accomplished. Different post-run charges of experiments at 150 °C and ~85 bar were chosen to study these changes. First significant chemical changes within the reacted model brine occurred after 10 days due to the slower dissolution rate of feldspars compared to carbonates (see chapter 4.1.2 & 4.2.2). Therefore, only 30-day post-run solid charges were analyzed by SEM measurements as structural changes also occurred probably delayed. Possible grain size as well as temperature dependencies related to structural changes were not studied.

Figure 4.14 depicts photo-micrographs of the starting materials. In the minority of cases the studied feldspar grains exhibit euhedral crystallographic shapes due to the pre-experimental mechanical crushing of the monomineralic rock specimens. For *anorthite* the less developed cleavage along two crystallographic directions ($\langle 010 \rangle$, $\langle 110 \rangle$) results in conchoidal to uneven mineral surfaces (c.f. figure 4.14A). These mineral surfaces dominate the studied grains. Furthermore a few grains exhibit even mineral surfaces which represent the perfect cleavage parallel to the crystallographic direction $\langle 001 \rangle$ (c.f. figure 4.14B). In contrast *orthoclase* samples exhibit more regular shapes due to their perfect as well as good developed cleavage into two crystallographic directions ($\langle 001 \rangle$, $\langle 010 \rangle$) (c.f. figure 4.14C). Due to the exsolution behavior of alkali feldspars the orthoclase surfaces seem to be fibrous (c.f. figure 4.14D). Despite multiple rinsing prior to the experiments ultrafine dust particles were still present on the mineral surfaces.

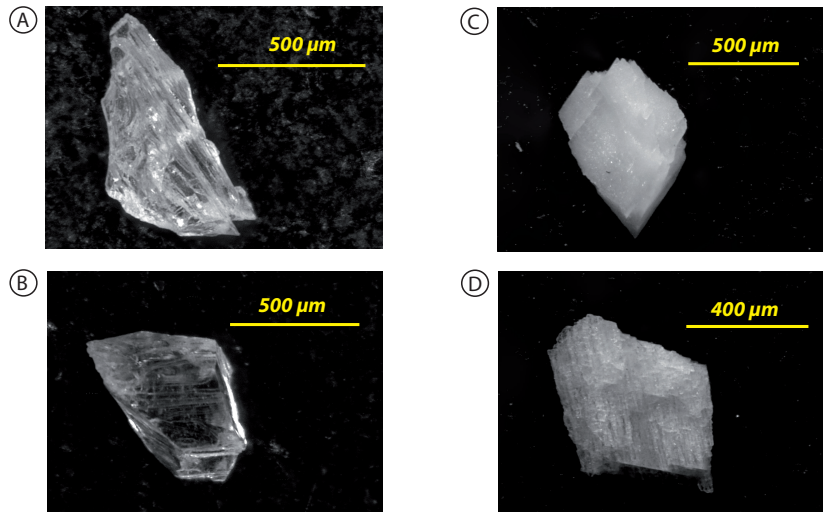


Figure 4.14: Photo-micrographs of the starting materials: (A, B) anorthite: 250 – 500 μm ; (C, D) orthoclase: 250 – 500 μm (stereo microscope, IfG, CAU Kiel)

At first structural surface changes on post-experimental *anorthite* grains will be described. The initial irregular shape with even as well as conchoidal/uneven surfaces is maintained after an experimental run duration of 30 days (cf. figure 4.15). All studied grains exhibit a complete coating with secondary mineral phases. At smaller magnifications the development of these mineral phases seems to be pseudomorph related to the initial feldspar (cf. figure 4.15 B and C). However, larger magnifications clearly show small platy/planar and in some cases radiating rose-like aggregates of grain sizes $\leq 1 \mu\text{m}$ (cf. figure 4.15 D). This structure is typical for many phyllosilicates like clay minerals or mica.

The results of the present study are very well comparable with results described by Hangx and Spiers (2009). The authors describe their post-experimental charges as minerals with widespread shaped surface precipitations like fine, platy, lath-like, honeycomb-like, rose-like particles or as "booklets" of hexagonal shaped plates. In general the observed secondary mineral phases described by Hangx and Spiers (2009) are smaller than 1 μm in size. While the grains of the present study are completely coated with secondary mineral phases, Hangx and Spiers (2009) describe thin, discontinuous porous layers, which occupy the surface by only 10% to 40%. The authors assume that the observed precipitations represent phyllosilicates like illite, smectite or kaolinite due to their typical crysyallographic shapes. In addition to the clear visible precipitation of secondary minerals Hangx and Spiers (2009) describe

the development of occasionally observed etch pits. This dissolution feature is also described by Hodson (2006) and Oelkers and Schott (1995), whereat these authors describe no secondary mineral phases. In contrast to the mentioned literature data the development of etch pits on post-run charges is not observed in the present study.

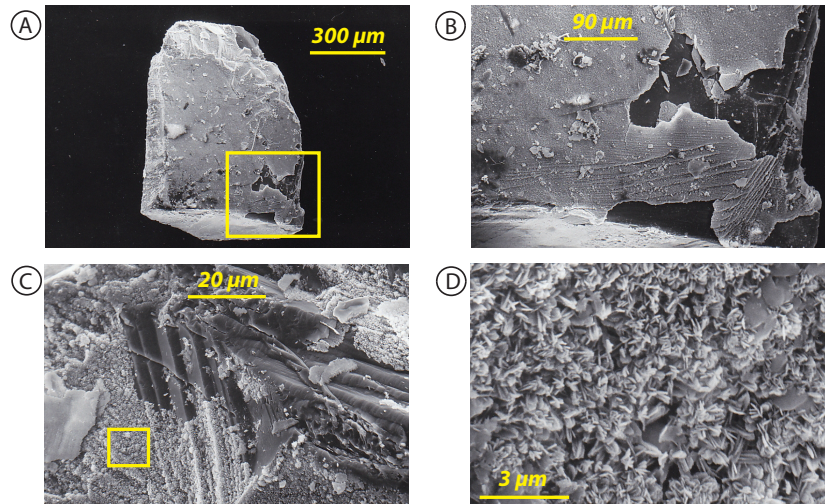


Figure 4.15: SEM images of post-experimental anorthite grains after a 30-day run duration: (A, C) overview screen, (B, D) magnification of A and C. **Results:** (i) preservation of the initial irregular shape, (ii) complete coating of all grains with secondary mineral phases like clay minerals. (SEM laboratory, IfG, CAU Kiel)

In contrast to the observed structural changes on anorthite grains, post-experimental *orthoclase* charges exhibit other dissolution features (cf. figure 4.16). However, the initial shape of grains is also maintained after a 30-day run duration. A comprehensive precipitation of secondary minerals is not observed. Only selective areas with star-like mineral phases are found (cf. figure 4.16 A). In the literature precipitation of secondary minerals is also not well documented. For example, Blake and Walter (1999) observe Al-containing precipitations and interpret this mineral phases as smectites. However, Gautier et al. (1994) observe no precipitates at all.

The much more significant structural changes on the orthoclase surfaces are the extensive development of etch pits and steps. The etch pits exhibit irregular shapes and are cord-like placed (cf. figure 4.16 B). These phenomena are also described by Gautier et al. (1994), who combine the location of etch pits with the presence of feldspar exsolution features. Furthermore Harouiya and Oelkers (2004), describe etch pits as indicator for heterogeneous disso-

lution processes. In the present study the observed steps are oriented along the crystallographic directions and are visible according to their observed crystal face (cf. figure 4.16 C and D). Furthermore it can be noted that different crystallographic directions exhibit different dissolution features as well as dissolution progressions. Thus, it is uncommon that etch pits and dissolution steps appear corporately on the same single crystal face.

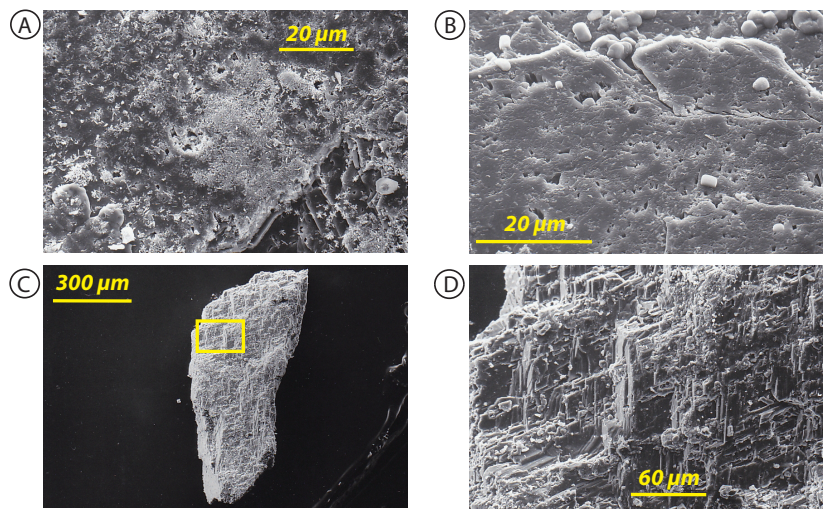


Figure 4.16: SEM images of post-experimental orthoclase grains after a 30-day run duration: (A, B) formation of etch pits and precipitations, (C) overview screen, (D) magnification of box within C. **Results:** (i) preservation of the initial shape, (ii) development of etch pits and steps more or less along the crystallographic directions, (iii) local precipitation of star-like secondary mineral phases. (SEM laboratory, IfG, CAU Kiel)

In conclusion SEM analyses of pre- and post-experimental anorthite and orthoclase charges show different dissolution features on the mineral surfaces after run durations of 30 days. Anorthite samples exhibit completely coated mineral surface, whereat the secondary mineral phases can be characterized as clay minerals. The development of etch pits is not proven. In contrast post-experimental orthoclase charges exhibit both, secondary mineral precipitations and etch pits. Furthermore the development of dissolution steps is observed. It has to be noted that the etch pits occur along feldspar exsolution features and the steps are oriented along the crystallographic directions. In addition it is uncommon that these two dissolution features appear corporately on the same single crystal face.

All observed structural changes mentioned in the present study are more or less confirmed with literature data. However, the statement of Hangx and

Spiers (2009) that anorthite samples as Ca-bearing feldspars exhibit more extensive structural changes on the mineral surface than orthoclase samples as K-bearing feldspars cannot be affirmed in the present study. The overall alteration of both feldspar samples is similar. But the dissolution features are differently developed on the individual feldspars.

Micro Computertomography Analyses (μ -CT)

In addition to the above mentioned SEM analyses structural changes of the solid phases can also be determined by μ -CT analyses. For example, the observation of volume changes caused by precipitation or dissolution processes is one possibility. Therefore each sample is X-rayed before and after the experiment creating a set of different X-ray projections (c.f. appendix A.7A). Based on the image information of all these X-ray projections a reconstruction of the sample is calculated with the help of mathematical algorithms and includes a stack of 2D sections, whose distances to each other are equal to the pixel size (c.f. appendix A.7B). In consequence isometric voxels are created. The individual mineral phases within the solid samples are defined by different gray values, whereat the gray value is associated with the density of the respective material. Dense materials are not as well penetrated by X-rays as less dense materials resulting in the reduction of signals on the detector. Thus, the higher the density of the mineral phase the lower the grey value. Ore minerals, for example, are not well penetrated by X-rays and cause low grey values. In contrast carbonates or feldspars exhibit much higher grey values caused by the significant lower mineral density. Due to the complete radiation of the pore space these parts of the sample are reconstructed as black areas (highest grey value: 255). To determine a realistic image of the solid sample the detected grey values must be assigned to individual mineral phases. Mineral phases with significant different densities can be separated well from each other (e.g. ore minerals vs. carbonates). However, the distinction between mineral phases of similar densities (e.g. feldspar vs. quartz) is more difficult because the reconstruction results in overlapped grey values. Furthermore it has to be noted that grain boundaries cannot definitely assigned to one grey value. The so called "partial volume" effect appears. That means one voxel can include both, pore space and solid phase. The partial empty voxels exhibit lower grey values compared to well-defined mineral phases. Thus, grain boundaries possess a range of several shades of grey. In consequence a geometrically correct threshold detection has to be performed to binarize the grey values and thus to distinguish various mineral phases from each other as well as mineral phases from the pore space (c.f. appendix A.7C). This threshold detection can be accomplished either

automatically or manually. The following examples describe results of both methods, automatic and manual threshold detections.

To determine volume changes between starting material and reaction product μ -CT analyses on orthoclase samples of six experiments at different conditions were accomplished. The analyses include both, samples with different grain sizes and samples of experiments at different temperatures. All considered samples originate from 30-day experiments. To ensure the reproducibility of experiments each single experiment was accomplished twice at identical experimental conditions. Table 4.3 summarizes the analyzed samples and the associated experimental conditions.

Table 4.3: Experimental conditions of experiments at orthoclase samples analyzed by μ -CT measurements

sample	grain size [μm]	temperature [$^{\circ}\text{C}$]	run duration [d]	series ^a
OR 001	250 – 500	150	30	V-I
OR 002	250 – 500	150	30	V-II
OR 003	160 – 250	150	30	V-I
OR 004	160 – 250	150	30	V-II
OR 005	250 – 500	100	30	V-I
OR 006	250 – 500	100	30	V-II

^aseries V-I & V-II were performed at identical experimental run conditions to demonstrate the reproducibility of reaction products.
(see chapter 4.2 and table B.4 for more details)

At first results based on *automatic threshold detections* will be discussed. The lowest grey value is set to 76 and the highest grey value to 255. Figure 4.17 depicts the grain volume distribution compared to the grain size before and after the experiments. Each data set represents the mean of the single μ -CT analyses of two related experiments with identical experimental conditions and are calculated after equation 4.10:

$$\bar{x}_{arithm} = \frac{1}{n} \sum_{i=1}^n x_i = \frac{x_1 + x_2 + \dots + x_n}{n} \quad (4.10)$$

The denoted error bars arise from the calculation of the standard deviation (c.f. equation 4.11) of the single μ -CT analyses of two related experiments:

$$SD = \sqrt{\frac{\sum(x - \bar{x})^2}{(n - 1)}} \quad (4.11)$$

The left graph shows results of experiments with mineral samples of the larger grain size (250 – 500 μm) at temperatures of 100 °C as well as 150 °C. The right graph depicts results of experiments with mineral samples of the smaller grain size (160 – 250 μm) at 150 °C.

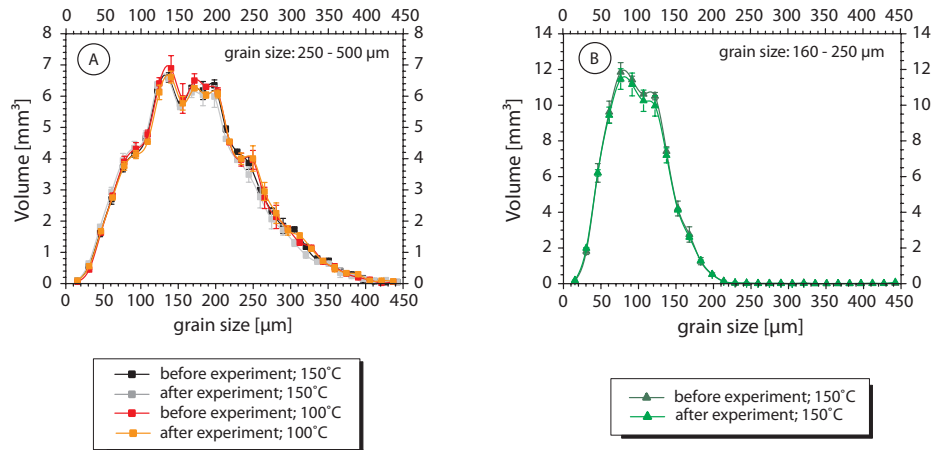


Figure 4.17: Grain volume distribution compared to the grain size before and after the experiment: grey thresholds remain constant (76 – 255). (A) grain size: 250 – 500 μm , T: 100 °C/150 °C; (B) grain size: 160 – 250 μm , T: 150 °C (μ -CT laboratory, IfG, CAU Kiel)

Within each single grain size fraction the progression of all depicted data sets is almost identical. Based on these results neither significant temperature dependent nor significant grain size dependent differences are detected. The progression of curves of pre- and post-experimental samples is nearly the same. All observed deviations range within the calculated standard deviation. In conclusion structural changes in the form of volume variations of the solid phases cannot be determined by using the automatic threshold detection.

Another method to interpret results of μ -CT analyses is based on the *manual threshold detection*. While the highest grey value is also set constant to 255 the lowest grey value is chosen manually and ranges between 66 and 80 (c.f. table 4.4). It has to be noted that samples of experiments with identical experimental conditions exhibit more or less similar grey values, whereat the grey values determined for the samples before and after the experiment can differ to some extent significantly.

Table 4.4: Determined grey values after the manual threshold detection for all considered samples before and after the experiment

sample ^a	grey value	
	pre-experimental	post-experimental
OR 001	70	66
OR 002	71	65
OR 003	76	78
OR 004	71	80
OR 005	69	76
OR 006	73	73

^aexperimental conditions see table 4.3

Figure 4.18 depicts the grain volume distribution compared to the grain size before and after the experiments. Each data set represents the mean of the single μ -CT analyses of two related experiments with identical experimental conditions and are calculated after equation 4.10. The denoted error bars arise from the calculation of the standard deviation (c.f. equation 4.11) of these single μ -CT analyses.

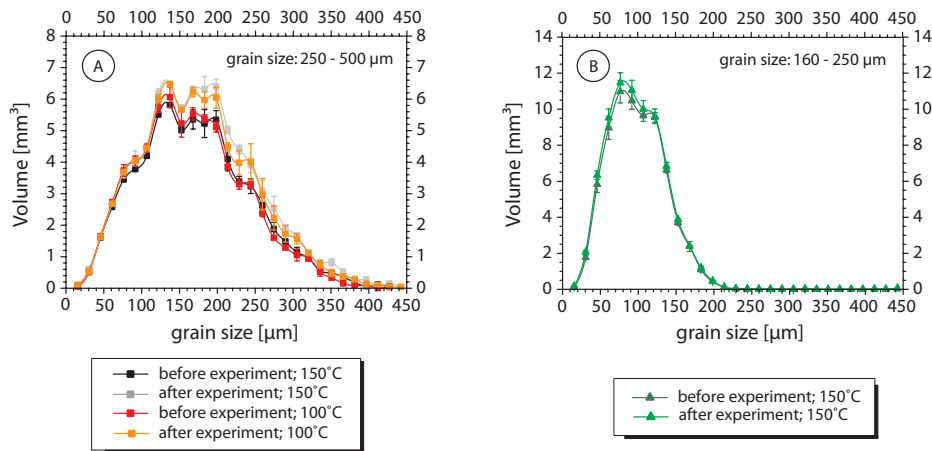


Figure 4.18: Grain volume distribution compared to the grain size before and after the experiment: manual adjustment of the lower grey threshold (66 – 80), upper grey threshold remains constant (255). (A) fraction: 250 – 500 μm , T: 100 $^{\circ}\text{C}$ /150 $^{\circ}\text{C}$; (B) fraction: 160 – 250 μm , T: 150 $^{\circ}\text{C}$ (μ -CT laboratory, IfG, CAU Kiel)

Within each single grain size fraction the progression of all depicted data sets is nearly the same. Even by using this method neither significant temperature dependent nor significant grain size dependent differences are de-

terminated. All observed deviations range within the calculated standard deviation. In contrast to results based on automatic threshold detections the differences between pre- and post-experimental solid phase volumes are more pronounced, even though the deviations are within the calculated error in most of the cases. In conclusion the method of manual threshold detection can also not determine significant structural changes in the form of volume variations of the solid phases.

In addition to the non-detectable volume changes it has to be noted that the average grain size detected by μ -CT analyses is smaller than the real average grain size detected by granulometric analyses. In the grain size fraction of 250 – 500 μm the largest volumetric content is taken by grains of 110 – 230 μm in size. The largest volumetric content for the grain size fraction 160 – 250 μm is taken by grains of 60 – 130 μm in size. These differences are caused by the analytical method to determine the grain sizes. All grains within a sample are represented by fictive spheres. Based on the diameter of these fictive spheres the grain sizes are derived. For grains with similar expansions in all crystallographic directions this method is able to estimate almost realistic grain sizes (c.f. figure 4.19A). However, grains with irregular columnar or platy shapes are misrepresented by the described analytical method, because the diameter of the fictive sphere does not reflect the real grain shape (c.f. figure 4.19B). As known from SEM analyses the feldspar samples exhibit clear rectangular grain shapes. These mineral shapes cannot be reflected by the fictive spheres resulting in the shift of natural average grain sizes to smaller calculated grain sizes.

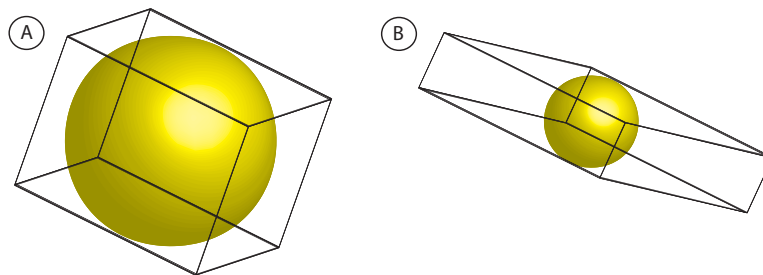


Figure 4.19: Schematical illustration of the grain size determination by μ -CT analyses

In conclusion the results of μ -CT analyses determined in the present study vary in regard to the used grey value threshold detection. The observed volume changes for both methods (automatic and manual threshold detection) are identical within the calculated experimental error. Thus, a robust

statement about volume changes between pre- and post-experimental mineral phases is not possible. It can be assumed that possible structural changes in the form of grain phase volume variations are not enough pronounced to get detected by the applied measuring technique. Furthermore it has to be noted that the real grain sizes of the rectangular shaped feldspar minerals are not reproduced by the accomplished analytical method. The average grain size of both used grain size fractions is shifted to smaller average grain sizes caused by the above mentioned method of using fictive spheres to describe the grain shape.

4.2.2 Analyses of the Fluid Samples (ICP-OES Analyses)

In addition to structural changes on the mineral surfaces, dissolution and/or precipitation processes can also be determined by chemical changes of the used fluid phase. During dissolution processes various components (e.g. ions or complexes) are released from the mineral surface and thus enhance the concentration of these components within the fluid phase. In contrast precipitation processes result in the removal of different components out of the fluid and cause an enrichment of these components in secondary minerals (precipitates). A third process is the cation exchange process between fluid and solid, which also results in the chemical alteration of the fluid phase. The degree of fluid alteration varies for different mineral phases.

In the present study the determination of fluid alteration was accomplished by ICP-OES measurements on pre- and post-experimental fluid charges. The fluid was sampled after each single experiment and was prepared for analysis as described in chapter 3.1. Following explanations are based on ICP-OES measurements of post-experimental fluid charges of experiments with orthoclase. Using these measurements temperature dependent as well as grain size dependent alterations of the fluid phases can be detected in regard to the temporal progression of the dissolution process. Furthermore the calculation of kinetic data like dissolution rates and activation energies are based on these measuring results.

Temperature Dependent Alterations

As known from the literature (e.g. Carroll and Knauss (2005); Chen and Brantley (1997); Harouiya and Oelkers (2004)) feldsparic samples exhibit temperature dependent dissolution behaviors. To verify these statements in relation to the aim of CO₂ sequestration processes various experiments at temperatures of 100 °C as well as 150 °C were accomplished in the present

study. It has to be noted that these chosen temperatures are higher compared to assumed temperatures in potential reservoir horizons. To clearly ensure the temperature dependent feldspar dissolution all further experimental conditions were held constant: grain size = 250 – 500 μm , total pressure = 85 bar and solid-fluid ratio = 1:200. All following descriptions are based on analyses of post-experimental fluid samples of 24 teflon experiments with orthoclase. Thus, each temperature is represented by two experimental series (V-I & V-II) of 6 experiments with a 1-, 2-, 5-, 10-, 20- and 30-day run duration. It has to be noted that experimental series V-I & V-II were performed at identical run conditions to demonstrate the reproducibility of experimental results. Appendices B.19 and B.21 summarize the analytical results of all measured fluid components.

To identify the *reproducibility of the experimental results* both experimental series (V-I & V-II) are compared to each other. Therefor the four analyses of each individual fluid sample are averaged after equation 4.10. Subsequently the determined averages of series V-II are related to the determined averages of series V-I (c.f. table B.20/B.22).

In regard to the main components Ca, Cl, K, Mg, and Na the differences between the experimental series range between 0.09% – 4.91% (100 °C) and 0.05% – 3.37% (150 °C), respectively. An exception is given by the 30-day experiments performed at 150 °C. Here, the determined differences of series V-I and V-II range between 9.3% and 10.74% and might be caused by a faulty sampling, storing or preparation of the samples. Because the elements Al, Ba, and Sr are not included in the initial model brine and are not significantly dissolved out of the solid phase during the ongoing reaction, the measured values for these elements are below or near the detection limit. Thus, they are not suitable to verify the reproducibility of experimental results. The element Si describes a special case. The initial model brine does not include dissolved Si. Only due to the reaction of the initial model brine and the used solid phase the Si concentration within the fluid increases with increasing run duration. It has to be noted that an increasing run duration results in increasing Si concentration. In turn, these increasing Si concentration results in qualitative better measuring results. In consequence the differences between series V-I and V-II decrease with increasing run duration and increasing Si concentration, respectively.

Including all mentioned components it can be assumed that the experimental results are reproducible. Under this assumption all following descriptions are based on results of both series (V-I and V-II). Thus, each time step is represented by the average (after equation 4.10) of eight single analyses. The denoted deviations are calculated after equation 4.11 and include these eight

individual measuring points.

When considering the measuring results in regard to the *geochemical behavior* of the included components with increasing run duration, three main observations can be made:

1. in relation to the main components Ca, Cl, K, Mg and Na the pre- and post-experimental fluid samples do not exhibit significant differences within the determined standard deviation,
2. fluid samples of experiments performed at 150 °C exhibit detectable Si concentrations after a 10-day run duration, whereas
3. fluid samples of experiments performed at 100 °C exhibit no detectable Si concentrations over the entire run duration.

To discuss the first mentioned statement appendices A.10 and A.11 depict the analytical results, whereat appendix A.10 includes all single measuring results and appendix A.11 illustrates the determined averages and the corresponding standard deviations. First of all it has to be noted, that the progression of all curves – independent of the used experimental temperature – is similar with increasing run duration, whereat the absolute values slightly differ between both temperatures (150 °C > 100 °C). Partial minor differences in regard to the initial model brine can be observed and are possibly caused by faulty sampling, storing or preparation of the fluids samples. But in general, the deviations range within the determined errors. Based on the initial model brine composition and the used solid phase an alteration of the fluid composition in regard to the elements Ca, Mg, Na and Cl is not expected during the ongoing reaction.

In contrast the alteration of the fluid composition in regard to the elements K, Al and Si is more supposable due to the release of these elements during the ongoing dissolution of orthoclase. But, neither the measuring results of K nor the measuring results of Al exhibit significant changes between the pre- and post-experimental fluid samples with increasing run duration. In the case of the component Si, concentration changes can be observed in a few samples (c.f. figure 4.20). While the Si-concentration within samples of experiments performed at 100 °C are below the detection limit, samples of experiments performed at 150 °C exhibit detectable Si-concentrations after a 10-day run duration. These measuring results confirm the common statements of temperature dependent feldspar dissolution given in the literature, whereat the absolute measured release of Si varies between different authors. For example, Blake and Walter (1999) already observed significant changes of the Si concentration within fluid samples of experiments performed at 80 °C.

Experiments performed by Harouiya and Oelkers (2004) exhibit detectable Si-concentration changes at temperatures of 100 °C. Although the results of different studies are similar, these results cannot be easily compared to each other. As mentioned in chapter 2 different experimental conditions like the experimental setup (batch reactor vs. flow through reactor) or the initial fluid composition result in variant dissolution behaviors of one mineral phase. In the case of the present study the used experimental conditions only allow a significant detectable dissolution of orthoclase at experiments performed at 150 °C.

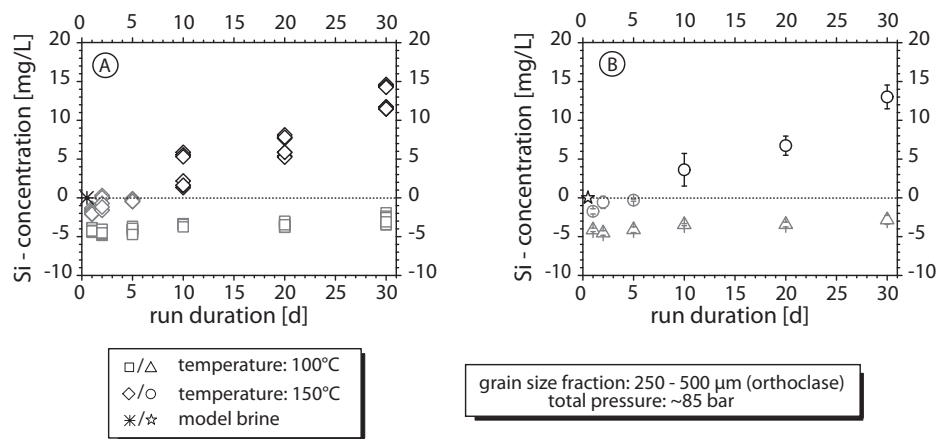
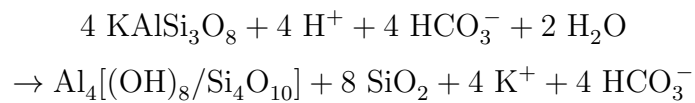


Figure 4.20: Temperature dependent alteration of the model brine in regard to the Si-concentration (starting material: orthoclase): **(A)** *single measurements* describe eight analyses of two single fluid samples at every time step; **(B)** the *average* subsumes all analyses of two single fluid samples at every time step; *grey symbols* depict values below the detection limit. **Results:** (i) all measured Si-concentrations within fluid samples of experiments at 100 °C are below the detection limit; (ii) significant increase of Si-concentrations within the fluid samples of experiments performed at 150 °C are measured at run durations longer than ten days (ICP-OES laboratory, RWE Dea, Wietze)

The reason for the non-detectable and/or the different release of K, Al and Si are caused by various, partly combined factors. First, the dissolution of orthoclase at the given experimental conditions is too slight to effect significant concentration changes between the pre- and post-experimental fluid samples. Second, the dissolution of orthoclase takes place at the given experimental conditions, but is not detectable by the used measuring technique or the changes in concentration are only within the error of measurement. The third factor for different dissolution behaviors is the precipitation of secondary minerals during the ongoing dissolution process. As mentioned in

chapter 4.2.1 local precipitations on the mineral surfaces are observed. A well-defined determination of the mineral phases is not possible due to the size of the precipitations. However, compared to literature data it has to be suggested, that these precipitations are clay minerals or mica minerals. As well known from soil weathering processes orthoclase and acid rain reacts to kaolinite. In addition, SiO_2 and K^+ are released out of the solid into the fluid phase. This reaction can be transferred to the orthoclase alteration processes observed within the present study and can be described by following equation.



If the chemical reaction completely takes place 3.5 mg K and 7.9 mg Si have to be released. In the case of the present study the release of 0.21 mg K would range within the error of measurements. Furthermore, the measured Si content within the post-experimental fluid samples would suggest a maximum orthoclase dissolution of 6% after a 30-day run duration. But, during the ongoing experiment the chemical reaction never takes place in this ideal form. Various more or less definable stable as well as meta-stable phases could develop and influence the composition of the fluid phase.

The derivation of the *activation energy* is not possible within the present study. To use the Arrhenius equation (c.f. chapter 4.1.2) rate constants of at least two temperatures are necessary. However, based on the above mentioned measuring results this condition is not given within the present study. The second kinetic data - *the dissolution rate* - is also only constricted detectable. Due to the non-measurable Si-concentrations for experiments performed at 100 °C the calculation of the dissolution rate is not possible. In contrast, the determination of dissolution rates for experiments performed at 150 °C is partly possible and will be discussed in the following sub-chapter.

Grain Size Dependent Alterations

The second influencing parameter considered within the present study is the grain size of the solid samples. As known from the literature increasing grain sizes result in decreasing dissolution rates caused by the smaller reactive surface of larger grain size fractions. This statement has to be verified within the present study by using two grain size fractions: 160 – 250 μm and 250 – 500 μm , respectively. To clearly ensure the grain size dependent feldspar dissolution all further experimental conditions were held constant:

temperature = 150 °C, total pressure = 85 bar and solid-fluid ratio = 1:200. All following descriptions are based on analyses of post-experimental fluid samples of 24 teflon experiments with orthoclase. Thus, each grain size fraction is represented by two experimental series (V-I & V-II) of 6 experiments with a 1-, 2-, 5-, 10-, 20- and 30-day run duration. It has to be noted that experimental series V-I & V-II were performed at identical run conditions to demonstrate the reproducibility of experimental results. Appendices B.21 and B.23 summarize the analytical results of all measured fluid components.

The identification of the *reproducibility of experimental data* is identical to the above mentioned procedure for experiments at different temperatures. Appendices B.22 and B.24 list the determined results.

In regard to the main components Ca, Cl, K, Mg and Na the deviation between the experimental series range from 0.06% to 6.83% (160 - 250 μm) and 0.05% to 3.37% (250 - 500 μm), respectively. The measuring results of Al, Ba and Sr are below or near the detection limit and are consequently not suitable to verify the reproducibility of experimental data. As mentioned for experiments at different temperatures the component Si is a special case. The initial model brine does not include dissolved Si. Only due to the reaction of the initial model brine and the used solid phase the Si concentration within the fluid increases with increasing run duration. Thus, with increasing run duration as well as increasing Si concentration the measuring results are qualitatively better and exhibit smaller differences between experimental series V-I and V-II.

Including all mentioned components it can be assumed that the experimental results are reproducible. Under this assumption all following descriptions are based on a consumption of series V-I and series V-II. Thus, each time step is represented by the average (see equation 4.10) of eight single measuring points. The denoted deviations are calculated after equation 4.11 and include the eight individual measuring points.

When considering the measuring results in regard to the *geochemical behavior* of the included components with increasing run duration, similar observations as mentioned for experiments performed at different temperatures can be made:

1. in relation to the main components Ca, Cl, K, Mg and Na the pre- and post-experimental fluid samples do not exhibit significant differences within the determined standard deviation,
2. fluid samples of experiments performed with both grain size fractions exhibit detectable Si-concentrations after a 10-day run duration, and

3. both grain size fractions exhibit nearly the same Si-release.

As depicted in appendices A.12 and A.13 the geochemical behavior of the main components Ca, Cl, K, Mg and Na is comparable with the observations made for experiments at different temperatures. The progression of all curves – independent of the used grain size fraction – is similar with increasing run duration. Minor deviations in regard to the initial model brine are possibly caused by faulty sampling, storing and/or preparation of the fluid samples. Due to the initial model brine composition and the used starting material, respectively, an alteration of the initial model brine in regard to the components Ca, Mg, Na and Cl is not expected during the ongoing dissolution process.

However, based on the dissolution process of orthoclase within the synthetic model brine the release of K, Al and Si and therefore the alteration of the initial model brine in regard to these components is more supposable. Similar to the observations of temperature dependent dissolution processes on orthoclase, neither Al nor K exhibit significant changes between pre- and post-experimental fluid samples. Only the amount of Si within the post-experimental fluids increases with increasing run duration (c.f. figure 4.21). For both grain size fractions the release of Si is nearly the same with increasing run duration, whereat first significant measurable Si-concentrations are detected after ten days.

The reasons for non-detectable and/or different releases of K, Al and Si are also similar to the above mentioned statements for temperature dependent dissolution processes. First, the model brine alteration in regard to the components Al and K is not detectable by the used measuring technique or the changes in concentration are only within the error of measurement. Secondly, the dissolution of orthoclase at the given experimental conditions only allows a release of Si after a 10-day run duration. Third, detectable secondary minerals developed on the mineral surfaces include different amounts of K, Al and Si into their crystal lattice and consequently cause different concentration changes within the fluid phases. In the case of the present study the measuring results suggested a placement of K, Al and partly Si within secondary minerals (e.g. clay minerals and/or mica) and a release of Si out of the orthoclase into the fluid phase.

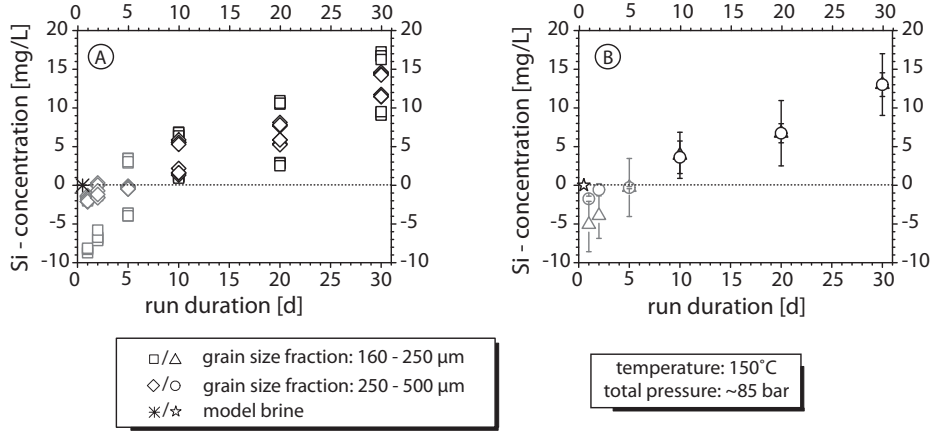


Figure 4.21: Grain size dependent alteration of the model brine in regard to the Si-concentration (starting material: orthoclase): **(A)** *single measurements* describe eight analyses of two single fluid samples at every time step; **(B)** the *average* subsumes all analyses of two single fluid samples at every time step; *grey symbols* depict values below the detection limit. **Results:** (i) no significant differences in concentration between both grain size fractions (ii) significant, measurable Si-concentrations within the fluid samples are detected at run durations ≥ 10 days (ICP-OES laboratory, RWE Dea, Wietze)

Based on the above mentioned measuring results the derivation of the *dissolution rate* (R) is possible after following equation:

$$R = \frac{\Delta c_{Si}}{RS \cdot t} \quad (4.12)$$

where Δc_{Si} describes the Si-concentration change (mol) between pre- and post-experimental fluid samples, RS is the reactive surface (m^2) of the used solid phase and t describes the experimental run duration (s). In the present study Δc_{Si} and t result from the ICP-OES measurements and the experimental conditions, respectively. In contrast, the reactive surface values used for the calculations are based on experimental data after Welch and Ullman (1996), who determine a reactive surface of $0.053 m^2/g$ (BET measurements) for albite samples with a grain size of $125 - 250 \mu m$. It has to be noted, that this literature data only reflects the reactive surface of the smaller grain size fraction ($160 - 250 \mu m$) used in the present study. But, due to the lack of literature data regarding the larger grain size fraction ($250 - 500 \mu m$), the determined reactive surface after Welch and Ullman (1996) is also used for this larger grain size fraction. Appendix B.25 summarizes the used parame-

ters as well as the calculated orthoclase dissolution rates.

Figure 4.22 depicts the determined dissolution rates with increasing run duration. In case of the present study the negative dissolution rates for experiments with run durations of 1, 2 and 5 days do not reflect precipitation effects. Due to the non-detectable Si-concentrations in the form of negative values the calculation of the dissolution rate results also in negative values. Therefore, the results of these experiments can be neglected. In contrast the increasing Si-concentrations of fluids of experiments with run durations ≥ 10 days result in more or less increasing dissolution rates with increasing run duration.

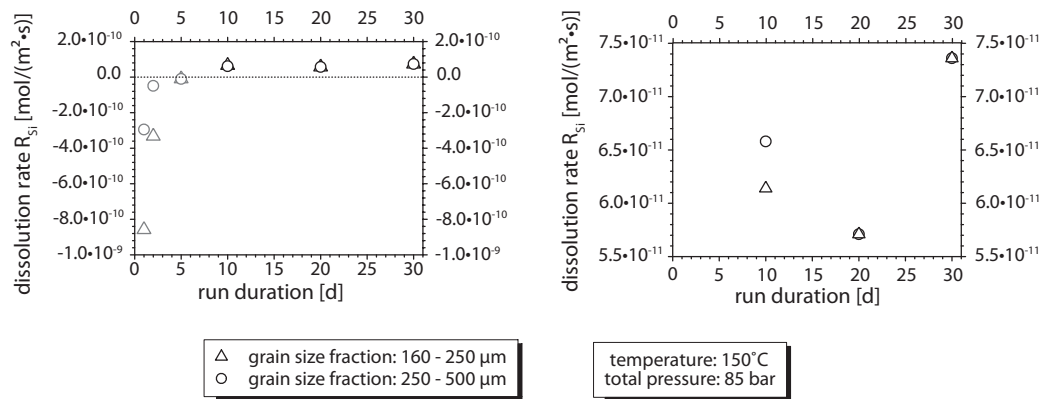


Figure 4.22: Grain size dependent development of orthoclase dissolution rates calculated after equation 4.12: *left*: calculated dissolution rates for all measured fluid samples; *right*: detailed view of the calculated dissolution rates for fluid samples with significant detectable Si-concentrations.

The comparison of calculated dissolution rates and literature data is in principle possible and is depicted in figure 4.23. However following constraints have to be noted. Most of literature data considered in the present study is based on flow through reactor experiments. As mentioned in chapter 2.1 different reactor types and hence, the associated varying flow regimes result in different mineral dissolution behaviors. Therefore, with increasing fluid flow and/or stirring rate the dissolution rate increases. Lower dissolution rates calculated in the present study are hence caused by other flow regimes within the used reactors. The parameters "experimental setup" and "flow regime" are probably the parameters with the largest influence regarding the considered comparison of literature data.

The ionic strength of the used model brine also influences the dissolution behavior of orthoclase. While the shown literature data are based on ionic strength smaller than 0.1 M, the model brine used within the present study

exhibits an ionic strength of 2.6 M. In regard to the fluid composition different chemical interactions take place. Due to the high variability of fluid compositions within the literature a well-defined statement about the influence of the parameter "ionic strength" is not possible.

Further experimental conditions like the total pressure and the pH-value are similar to the considered literature data and do not significantly influence the differences of the detected dissolution rates.

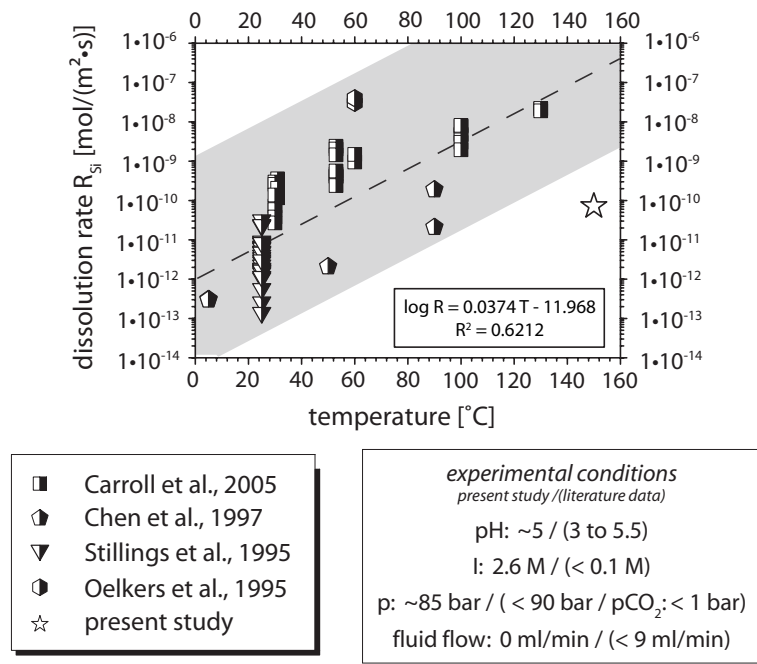


Figure 4.23: Comparison of calculated dissolution rates and literature data

As mentioned above the reactive surface value used in the present study does not reflect the real reactive surface of the used orthoclase samples. First, it is assumed that the reactive surface of albite and orthoclase differs due to different fracture behaviors of each mineral. For example, Harouiya and Oelkers (2004) detected reactive surface values of 0.0955 m²/g for orthoclase samples and 0.0846 m²/g for albite samples with identical grain size fraction (50 – 100 μm). Furthermore, the same reactive surface value is used for both grain size fractions. However, this assumption is not justified because the general scientific opinion states a decreasing dissolution rate with increasing reactive surface. In consequence dissolution rates based on Si-concentration changes within fluid samples of experiments with the larger grain size have to result in smaller values. This assumption is schematically depicted in figure 4.24 by the green curve. It has to be noted, that most of reactive surface values

described in the literature are based on the BET method, whereat the solid surface is determined by the amount of gas adsorbed on the free accessible surface. In general the analyzed grains are placed unconsolidated within the apparatus resulting in "ideal" reactive surfaces, whereat the whole surface is included (c.f. figure 4.25 left). However, within potential CO₂-storing reservoirs the grain bond is consolidated and cemented. In consequence surfaces contacting each other are not available for fluid-solid interactions. Furthermore, some pore spaces can be differentiated from the usable pore space by the cementation of the connections. Therefore, these pore spaces are also not available for fluid-solid interactions.

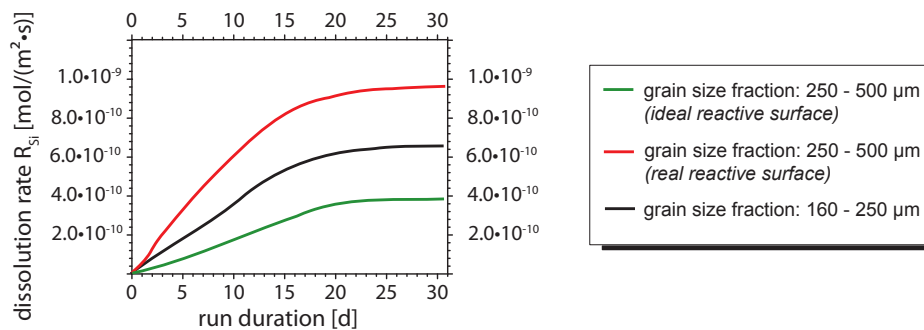


Figure 4.24: Theoretical development of dissolution rates by using different values for the reactive surface

As also known from literature data smaller grains can be packed more densely than larger grains (c.f. figure 4.25 right). This results in more grain-grain contacts and perhaps in more closed pore spaces. Consequently the usable reactive surface decreases. It has to be assumed that reservoirs including a higher amount of larger grain size fractions exhibit larger reactive surfaces than reservoirs including a higher amount of smaller grain sizes. In consequence calculations with "realistic" reactive surfaces result in higher dissolution rates for larger grain size fractions (c.f. figure 4.24 red curve). These observations exhibit the strong influence of the reactive surface on the dissolution rate and show the exigency of using realistic values to represent natural conditions. Possible methods to describe and determine such realistic surfaces are given by μ -CT analyses.

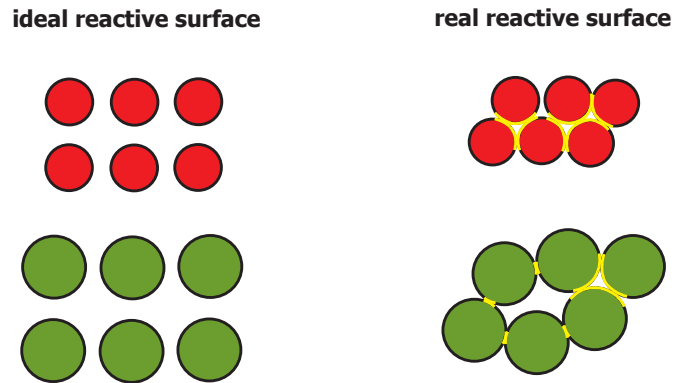


Figure 4.25: Schematic illustration of reactive surfaces: (*left*) ideal reactive surfaces without the consideration of possible grain interfaces; (*right*) real reactive surfaces including possible grain-grain contacts as well as closed pore spaces.

Conclusion of Measuring Results of ICP-OES Analyses (Feldsparic Samples)

To conclude all observations mentioned in this chapter the following statements can be made. The reproducibility of experimental data is given for temperature dependent as well as grain size dependent experiments. In regard to the main components Ca, Cl, Mg and Na concentration changes between pre- and post-experimental fluid samples of all accomplished experiments are not detected. Due to the initial model brine composition and the used starting material an alteration of the initial model brine regarding these components is not expected during the ongoing dissolution process. Furthermore, the non-detectable and/or different release of K, Al and Si within all fluid samples is caused by: (i) non detectable concentration changes and/or concentration changes that ranged only within the errors of measurements, and (ii) different inclusions of K, Al and Si into the crystal lattice of newly developed secondary minerals (clay minerals and/or mica). The only significant detectable concentration changes between pre- and post-experimental fluids are measured in samples of experiments performed at 150 °C. Based on these measuring results the derivation of the activation energy is not possible. In contrast, the orthoclase dissolution rate can be calculated. A direct comparison with literature data is not possible, due to multitude varying experimental conditions described in the literature. In the context of the present study literature data based on similar experimental conditions are not found. However, in consideration of the effects of varying experimental setups, ionic strengths and grain sizes an approximated comparison with lit-

erature data is possible. To determine the dissolution rate a special attention has to be turned on the used reactive surface of the solid samples. In most of the cases reactive surfaces based on BET measurements are used in the literature. However these values do not reflect natural conditions. Revised methods (e.g. μ -CT analyses) have to be applied to determine realistic reactive surfaces including grain-grain interfaces and closed pore spaces, which do not take part in fluid-solid interactions.

Chapter 5

Summary and Outlook

For several years scientists as well as the energy producing industry develop new technologies and methods to minimize the CO₂ emissions that are directly related to fossil fuel burning power plants. The increasing global energy consumption and the associated increasing CO₂ emission necessitate these new technologies to reduce the effects of the climate change. To realize the minimization of CO₂ emissions processes like the separation of CO₂ from power plants, the transport and the storage of CO₂ in capable reservoirs are explored and are combined under the topic of CO₂ sequestration. To make the storage technique as safe as possible amongst others it is important to study the geochemical processes in the reservoir and the surrounding rock formations in detail. Therefore, this work describes experimental studies about geochemical interaction processes between injected CO₂, saline fluids and potential reservoir materials. As mentioned in the "Introduction" (c.f. chapter 1) the answers of following questions are aimed with this work:

- Which experimental setups and/or conditions describe geochemical reaction behaviors in potential CO₂ reservoirs?
- Which parameters influence structural and/or geochemical changes of the reacting agents and how strong are these effects related to the kinetic data?
- Which literature data are suitable to compare to own data?

In the past numerous dissolution experiments on natural monomineralic materials were accomplished by different research groups. However, a closer look to the experimental setups and run conditions show high variabilities in the experimental results. The aim of earlier studies was to understand fundamental mineral dissolution processes at simplified experimental conditions.

In contrast, the number of experimental studies with more realistic conditions that prevail during the CO₂ sequestration increased during the last few years. In the case of the present study the used experimental setup (closed, static teflon autoclaves, c.f. chapter 3.1.1) is chosen to describe both, reservoir conditions far from the injection site and reservoir conditions after finishing the CO₂ injection. Natural reservoir conditions within a depth of 600 – 700 m are reflected by a dry ice induced total pressure of 85 bar. In addition to the usage as pressurizing medium dry ice also acts as CO₂ source. A further adaption to reflect more natural conditions is achieved by using a synthetic model brine (2.6 M) whereat the chemical composition is chosen according to a natural formation water of a Lower Cretaceous sandstone in the Northern German Basin. The reservoir itself is represented by monomineralic starting materials (calcite, dolomite, anorthite, orthoclase) which characterize possible constituents of potential reservoirs. Only the temperature of 100 °C and 150 °C, respectively, is increased in regard to the temperature of the prevailing reservoir depth to accelerate the kinetic of the ongoing geochemical reactions. In order to answer the first question the monitored position within the reservoir has to be taken into account. Flow through experiments are most suitable to reflect reservoir conditions close to the injection site. In contrast, closed batch reactor experiments represent reservoir conditions far from the injection site as well as reservoir conditions after finishing the CO₂ injection. Furthermore, the depth of the reservoir has to be taken into account. It is known that with increasing depth the temperature and the pressure increase. In addition to the locality and the depth of the reservoir the geochemical composition of the rock formations as well as the formation water is of crucial importance. As known from the literature numerous reservoirs at different geological locations differ significantly in their geochemical composition and consequently, also in their geochemical reaction behavior. In conclusion, the experimental setup, the experimental conditions and the starting materials have to be adapted to each individual potential CO₂ reservoir and the associated scientific question of further studies.

Directly related to the above mentioned experimental setups and conditions the second question can be answered. Within the present study temperature dependent, grain size dependent, starting material dependent and partly gas-phase dependent experiments were accomplished to determine structural and/or geochemical changes of the reacting agents and to derive related kinetic data. The determination of structural and/or geochemical changes was realized by electron microprobe (EMP), scanning electron microscopy (SEM), X-ray micro computer tomography (μ -CT) and ICP-OES analyses of pre- and post-experimental fluid and solid samples. Dissolution rates and

activation energies were calculated with different mathematical algorithms. In general it can be noted that all variable parameters influence the geochemical behavior within a potential reservoir whereat the influences are different. For example, SEM analyses of the pre- and post-experimental solid phases show time dependent structural changes on the mineral surfaces, whereas the development of dissolution features is various with increasing run duration and is related to the employed starting material. The structural change of carbonates is limited to dissolution features like etch pits and needles. In contrast, the observed structural changes of feldsparic samples are characterized by both, dissolution features like etch pits and dissolution steps and precipitation features like secondary mineral coatings. The observed dissolution and precipitation features of all analyzed post-experimental solid samples exhibit no clearly pronounced temperature and/or grain size dependencies. In addition to the mentioned SEM analyses structural changes on the starting materials can also be determined by μ -CT analyses. In the case of the present study the analyzed carbonatic samples do not represent a sufficient data base to determine significant structural changes on the mineral surfaces. The determined volume changes for experiments performed at feldsparic samples range within the error of measurements. Hence, a robust statement about volume changes between pre- and post-experimental mineral phases is not possible. It can be assumed that possible structural changes in the form of grain phase volume variations are not enough pronounced for the used starting materials at the chosen experimental run duration to get detected by the applied measuring technique.

Geochemical changes of the solid and fluid samples are determined by EMP- and ICP-OES analyses, respectively. EMP measurements of post-experimental calcite samples exhibit neither significant time dependent nor significant grain size dependent geochemical alterations. All apparent chemical changes are within the error of measurements. Due to similar mineralogical structures and reaction behaviors EMP measurements of dolomite samples are not performed in the present study. In contrast to the used carbonates the formation of reaction rims at feldsparic samples is more pronounced under the prevailing experimental conditions. Until now, EMP analyses of post-experimental feldspar samples are not carried out. However, in order to confirm or to disprove the assumption of reaction rim developments EMP analyses of the post-experimental feldspar grains are necessary and should be accomplished in further studies. The most important method to detect geochemical changes of the fluid samples is the accomplishment of ICP-OES analysis. Amongst others temperature dependent dissolution behaviors are derived from these measurements. At 150 °C feldsparic samples exhibit up to 2.5 orders of magnitude smaller dissolution rates (R_{Max} : $7.36 \cdot 10^{-11}$ mol/(m²·s)) compared to

dissolution rates of carbonatic samples (R_{Max} : $1.76 \cdot 10^{-8}$ mol/(m²·s)). With decreasing temperature the dissolution rates of all considered minerals also decrease. This observation is comparable to literature data. Furthermore the grain size influences the dissolution behavior of the used materials. Also in regard to the grain size the dissolution rates of felsparic samples (R_{Max} : $7.36 \cdot 10^{-11}$ mol/(m²·s)) are up to 2.5 orders of magnitude smaller compared to dissolution rates of carbonates (R_{Max} : $1.76 \cdot 10^{-8}$ mol/(m²·s)). Furthermore, for carbonatic samples the dissolution rates calculated for the smallest grain size fraction (R_{Max} : $1.76 \cdot 10^{-8}$ mol/(m²·s)) are about two orders of magnitude smaller compared to dissolution rates determined for the largest grain size fraction (R_{Max} : $9.93 \cdot 10^{-9}$ mol/(m²·s)). To calculate the dissolution rates in general analytical results of BET measurements are used to describe the reactive surfaces of the starting materials. Despite the usage of these reactive surface values in the literature as well as in this study the determined dissolution rates are contrary. Literature data describe increasing dissolution rates with decreasing grain size. In contrast, the calculated dissolution rates in the present study increase with increasing grain size. This contrary observation are caused by the method to determine the reactive surfaces. The applied BET measurements result in the description of "ideal" reactive surfaces whereat the entire available surface of each individual grain is considered. However, within a potential CO₂-storing reservoir the grain bond is consolidated and cemented. In consequence mineral surfaces contacting each other are not available for fluid-solid interactions. Furthermore, some pore spaces can be separated from the usable pore space by the cementation of the connections. Hence, these pore spaces are also not available for fluid-solid interactions. Consequently the application of the "real" reactive surface is crucial to calculate realistic dissolution rates. Possible methods to describe and determine such realistic surfaces are given by μ -CT analyses and have to be accomplished in further studies. As already assumed in chapter 2.3.1 the present study affirms the thesis that the pH-value is the most important influencing factor for mineral dissolution processes. In the present study even the accomplishment of a few experiments exhibits a clearly pronounced pH-value dependent dissolution behavior. For example, the decrease of only one pH unit results in a calcite dissolution rate increase of about 1.5 order of magnitudes (R_{5d} : $9.70 \cdot 10^{-8}$ mol/(m²·s) at pH 6.41; R_{5d} : $6.05 \cdot 10^{-9}$ mol/(m²·s) at pH 7.57) and therefore, confirms the tendency of increasing dissolution rates with decreasing pH-value as described in the literature. The above mentioned statement that the pH-value as most important influencing factor is also approved by the experimental results of the present study. Although other parameters like ionic strength, temperature or grain size varies for the considered literature data as well as this study's data

the pH-value dependency is still clearly pronounced. In the present study the pH-value is significantly controlled by the use of the CO₂ gas-phase whereat the dissolution of CO₂ in the model brine results in the release of H⁺ and consequently in a decreasing pH-value. In the case of CO₂ sequestration processes it is known that the separation of CO₂ from combustion gases of fossil fuel burning power plants does not result in pure CO₂. A certain admixture of other combustion gases like SO_x or NO_x will always be present in trace amounts. The knowledge of the important influence of the pH-value dependent dissolution behavior which is controlled by the dissolution of injected CO₂ into the fluid phase necessitates the accomplishment of further studies. These studies have to include other combustion gases to describe gas-phase dependent and therefore, pH-value dependent geochemical behaviors within potential CO₂ storing reservoirs in more detail.

In conclusion all described parameters – temperature, grain size, pH-value in combination with the gas-phase and the individual starting material – trigger structural and geochemical alterations of the reacting agents and consequently, change the dissolution behavior as well as the kinetic data of the starting materials. In regard to chemical processes within potential CO₂ storing reservoirs the composition of the injected gas-phase and the associated pH-value of the fluid are the most important influencing factors.

As already mentioned above determined experimental results are partly comparable with literature data. Structural changes of the used starting materials detected by SEM analyses are definitely comparable with literature data. Even earlier studies with simplified experimental conditions describe similar dissolution features compared to the results of the present study. In contrast geochemical changes of the fluid samples and associated kinetic data are not clearly comparable with literature data. The stronger the influence of a parameter the more pronounced the differences between literature data and the experimental results of the present study. Hence, in the case of similar experimental setups and run conditions as well as similar starting materials the determined data of the present study are comparable with literature data. Otherwise, the more different the experimental setups, run conditions and starting materials the more pronounced the differences between literature data and the determined data of the present study.

However, there are also experimental results which are not comparable with literature data. The application of μ -CT measurements in the geosciences is still new and result in a minor data base of experimental results in the literature.

It can be concluded that the used experimental setup is suitable to reflect geochemical behaviors of different mineral phases within a potential CO₂ storing reservoir. In the present study the used experimental setup as well as the used experimental conditions are chosen to demonstrate processes far from the injection site as well as after finishing the CO₂ injection. To investigate dissolution and precipitation processes earlier literature studies describe experiments performed at low pT-conditions. The pT-conditions in the present study are adjusted to reservoir conditions at 600 – 700 m depth. Furthermore, the used synthetic model brine is composed according to a natural formation water of a Lower Cretaceous sandstone in the Northern German Basin. In earlier studies low concentrated brines, acids and bases as well as distilled water as fluid phase are used. The evaluation of determined data and their comparison with literature data exhibit changed reaction behaviors as a result of the more natural pT-conditions and the more natural fluid phase. In regard to these natural conditions an improvement of the data's quality is therefore achieved.

Based on the obtained data even more complex natural conditions can be adjusted. For example, the determined geochemical behaviors of monomineralic solid phases are the basis to estimate geochemical behaviors of polymineralic solid phases.

In addition, the determined data can be included in data bases of numerical modeling programs. Due to the more realistic kinetic data the simulation of various sequestration scenarios can be improved.

Bibliography

- M. Alkattan, E. H. Oelkers, J.-L. Dandurand, and J. Schott. An experimental study of calcite and limestone dissolution rates as function of pH from -1 to 3 and temperature from 25 to 80 °C. *Chemical Geology*, 151:199 — 214, 1998.
- M. Alkattan, E. H. Oelkers, J.-L. Dandurand, and J. Schott. An experimental study of calcite dissolution rates at acidic conditions and 25 °C in the presence of NaPO₃ and MgCl₂. *Chemical Geology*, 190:291 — 302, 2002.
- A. Berg and S. A. Banwart. Carbon dioxide mediated dissolution of Ca-feldspar: implications for silicate weathering. *Chemical Geology*, 163:25 — 42, 2000.
- R. A. Berner and J. W. Morse. Dissolution kinetics of calcium carbonate in sea water IV. Theory of calcite dissolution. *American Journal of Science*, 274:108 – 134, 1974.
- R. E. Blake and L. M. Walter. Kinetics of feldspar and quartz dissolution at 70–80 °C and near-neutral pH: Effects of organic acids and NaCl. *Geochimica et Cosmochimica Acta*, 63(13/14):2043 — 2059, 1999.
- P. V. Brady and S. A. Carroll. Direct effects of CO₂ and temperature on silicate weathering: possible implications for climate control. *Geochimica et Cosmochimica Acta*, 58(8):1853 — 1856, 1994.
- P. V. Brady and J. V. Walther. Surface chemistry and silicate dissolution rates at elevated temperatures. *American Journal of science*, 292:639 — 658, 1992.
- Canadian International Development Agency. Development of china's coalbed methane technology/CO₂ sequestration project. Technical report, Canadian International Development Agency, Alberta Research Council, 2007. Final project report, Project No. A-030841.

- S. A. Carroll and K. G. Knauss. Dependence of labradorite dissolution kinetics on $\text{CO}_{2(\text{aq})}$, $\text{Al}_{(\text{aq})}$, and temperature. *Chemical Geology*, 217:213 — 225, 2005.
- S. A. Carroll and J. V. Walther. Kaolinite dissolution at 25 °C, 60 °C, and 80 °C. *American Journal of Science*, 290:797 — 810, 1990.
- W. H. Casey and G. Sposito. On the temperature dependence of mineral dissolution rates. *Geochimica et Cosmochimica Acta*, 56:3825 — 3830, 1992.
- Y. Chen and S. L. Brantley. Temperature- and pH-dependence of albite dissolution rate at acid pH. *Chemical Geology*, 135:275 — 290, 1997.
- L. Chou, R. M. Garrels, and R. Wollast. Comparative study of the kinetics and mechanisms of dissolution of carbonate minerals. *Chemical Geology*, 78:269 — 282, 1989.
- P. Cubillas, S. Köhler, M. Prieto, C. Chaïrat, and E. H. Oelkers. Experimental determination of dissolution rates of calcite, aragonite, and bivalves. *Chemical Geology*, 216:59 — 77, 2005.
- P. M. Dove and D. A. Crerar. Kinetics of quartz dissolution in electrolyte solutions using a hydrothermal mixed flow reactor. *Geochimica et Cosmochimica Acta*, 54:955 — 969, 1990.
- W. Dreybrodt and D. Buhmann. A mass transfer model for dissolution and precipitation of calcite from solutions in turbulent motion. *Chemical Geology*, 90(1-2):107 — 122, 1991.
- M. L. Druckenmiller, M. M. Maroto-Valer, and M. Hill. Investigation of carbon sequestration via induced calcite formation in natural gas well brine. *Energy and Fuels*, 20:172 — 179, 2006.
- L. Eisenlohr, K. Meteva, F. Gabrovšek, and W. Dreybrodt. The inhibition action of intrinsic impurities in natural calcium carbonate minerals to their dissolution kinetics in aqueous $\text{H}_2\text{O} - \text{CO}_2$ solutions. *Geochimica et Cosmochimica Acta*, 63(7/8):989 — 1002, 1999.
- D. W. Finneran and J. W. Morse. Calcite dissolution kinetics in saline waters. *Chemical Geology*, 268:137 — 146, 2009.
- M. Gautelier, E. H. Oelkers, and J. Schott. An experimental study of dolomite dissolution rates as a function of pH from -0.5 to 5 and temperature from 25 to 80 °C. *Chemical Geology*, 157:13 — 26, 1999.

- M. Gautelier, J. Schott, and E. H. Oelkers. An experimental study of dolomite dissolution rates at 80 °C as a function of chemical affinity and solution composition. *Chemical Geology*, 242:509 — 517, 2007.
- J.-M. Gautier, E. H. Oelkers, and J. Schott. Experimental study of K-feldspar dissolution rates as a function of chemical affinity at 150 °C and pH 9. *Geochimica et Cosmochimica Acta*, 58(21):4549 — 4560, 1994.
- J.-M. Gautier, E. H. Oelkers, and J. Schott. Are quartz dissolution rates proportional to B.E.T. surface areas? *Geochimica et Cosmochimica Acta*, 65(7):1059 — 1070, 2000.
- D. K. Gledhill and J. W. Morse. Dissolution kinetics of calcite in NaCl – CaCl₂ – MgCl₂ brines at 25 °C and 1 bar pCO₂. *Aquatic Geochemistry*, 10:171 — 190, 2004.
- D. K. Gledhill and J. W. Morse. Calcite dissolution kinetics in Na – Ca – Mg – Cl brines. *Geochimica et Cosmochimica Acta*, 70:5802 — 5813, 2006a.
- D. K. Gledhill and J. W. Morse. Calcite dissolution kinetics in Na – Ca – Mg – Cl brines. *Chemical Geology*, 233:249 — 256, 2006b.
- S. V. Golubev, O. S. Pokrovsky, and J. Schott. Experimental determination of the effect of dissolved CO₂ on the dissolution kinetics of Mg and Ca silicates at 25 °C. *Chemical Geology*, 217:227 — 238, 2005.
- S. V. Golubev, A. Bauer, and O. S. Pokrovsky. Effect of pH and organic ligands on the kinetics of smectite dissolution at 25 °C. *Geochimica et Cosmochimica Acta*, 70:4436 — 4451, 2006.
- S. V. Golubev, P. Bénézech, J. Schott, J. L. Dandurand, and A. Castillo. Siderite dissolution kinetics in acidic aqueous solutions from 25 °C to 100 °C and 0 to 50 atm pCO₂. *Chemical Geology*, 265:13 — 19, 2009.
- W. D. Gunter, B. Wiwchar, and E. H. Perkins. Aquifer disposal of CO₂-rich greenhouse gases: extension of the time scale of experiment for CO₂-sequestering reactions by geochemical modelling. *Mineralogy and Petrology*, 59:121 — 140, 1997.
- M. Hänchen, V. Prigiobbe, G. Storti, T. M. Seward, and M. Mazzotti. Dissolution kinetics of forsteritic olivine at 90 – 150 °C including effects of the presence of CO₂. *Geochimica et Cosmochimica Acta*, 70:4403 — 4416, 2006.

- S. J. T. Hangx and C. J. Spiers. Reaction of plagioclase feldspars with CO₂ under hydrothermal conditions. *Chemical Geology*, 265:88 — 98, 2009.
- N. Harouiya and E. H. Oelkers. An experimental study of the effect of aqueous fluoride on quartz and alkali-feldspar dissolution rates. *Chemical Geology*, 205:155 — 167, 2004.
- R. Hellmann. The albite-water system, part I. The kinetics of dissolution as a function of pH at 100, 200, and 300 °C. *Geochimica et Cosmochimica Acta*, 58:595 — 611, 1994.
- M. E. Hodson. Does reactive surface area depend on the grain size? Results from pH 3, 25 °C far-from-equilibrium flow-through dissolution experiments on anorthite and biotite. *Geochimica et Cosmochimica Acta*, 70:1655 — 1667, 2006.
- W.-A. Kahl and A. Holzheid. Estimated and "true" geometric surfaces and their possible impact on experimentally and thermodynamically derived mineral dissolution and precipitation rates in CO₂-brine-mineral reactions. DMG Tagung, Münster 20.-22.09.2010, Abstract #S04-T02, 2010.
- A. E. Kehew. *Applied Chemical Hydrogeology*. Prentice-Hall, Inc., New Jersey, 2001. 368 p.
- K. G. Knauss, J. W. Johnson, and C. I. Steefel. Evaluation of the impact of CO₂, co-contaminant gas, aqueous fluid and reservoir rock interactions on the geologic sequestration of CO₂. *Chemical Geology*, 217:339 — 350, 2005.
- A. C. Lasaga and R. J. Kirkpatrick. *Reviews in Mineralogy (Volume 8): Kinetics of Geochemical Processes*. Mineralogical Society of America, 1981. 398 p.
- A. C. Lasaga and A. Lüttge. Mineralogical approaches to fundamental crystal dissolution kinetics. *American Mineralogist*, 89:527 — 540, 2004.
- E. Liteanu and C. J. Spiers. Influence of pore fluid salt content on compaction creep of calcite aggregates in the presence of supercritical CO₂. *Chemical Geology*, 265:134 — 147, 2009.
- K. Lund, H. S. Fogler, and C. C. McCune. Acidization – II: The dissolution of dolomite in hydrochloric acid. *Chemical Engineering Science*, 28:691 — 700, 1973.

- K. Michael, A. Golab, V. Shulakova, J. Ennis-King, G. Allinson, S. Sharma, and T. Aiken. Geological storage of CO₂ in saline aquifers – A review of the experience from existing storage operations. *International Journal of Greenhouse Gas Control*, 4:659 — 667, 2010.
- J. W. Morse and R. S. Arvidson. The dissolution kinetics of major sedimentary carbonate minerals. *Earth-Science Reviews*, 58:51 — 84, 2002.
- E. P. Müller and G. Papendieck. Zur Verteilung, Genese und Dynamik von Tiefenwässern unter besonderer Berücksichtigung des Zechsteins. *Zeitschrift für geologische Wissenschaften*, 3(2):167 — 196, 1975.
- E. H. Oelkers and J. Schott. Experimental study of anorthite dissolution and the relative mechanism of feldspar hydrolysis. *Geochimica et Cosmochimica Acta*, 59(24):5039 — 5053, 1995.
- E. H. Oelkers, J. Schott, and J.-L. Devidal. The effect of aluminum, pH, and chemical affinity on the rates of aluminosilicate dissolution reactions. *Geochimica et Cosmochimica Acta*, 58(9):2011 — 2024, 1994.
- J. L. Palandri and Y. K. Kharaka. A compilation of rate parameters of water-mineral interaction kinetics for application to geochemical modeling. Technical report, U.S. Geological survey, 2004. Open File Report 2004-1068.
- L. N. Plummer and E. Busenberg. The solubilities of calcite, aragonite and vaterite in CO₂ – H₂O solutions between 0 and 90 °C, and an evaluation of the aqueous model for the system CaCO₃ – CO₂ – H₂O. *Geochimica et Cosmochimica Acta*, 46:1011 — 1040, 1982.
- L. N. Plummer, T. M. L. Wigley, and D. L. Parkhurst. The kinetics of calcite dissolution in CO₂-water systems at 5° to 60 °C and 0.0 to 1.0 atm CO₂. *American Journal of Science*, 278:179 — 216, 1978.
- O. S. Pokrovsky, S. V. Golubev, and J. Schott. Dissolution kinetics of calcite, dolomite and magnesite at 25 °C and 0 to 50 atm pCO₂. *Chemical Geology*, 217:239 — 255, 2005.
- O. S. Pokrovsky, S. V. Golubev, and G. Jordan. Effect of organic and inorganic ligands on calcite and magnesite dissolution rates at 60 °C and 30 atm pCO₂. *Chemical Geology*, 265:33 — 43, 2009.
- M. Raines and T. Dewers. "Mixed" kinetics control of fluid rock interaction in reservoir production scenarios. *Journal of Petroleum Science and Engineering*, 17(1-2):139 — 155, 1997.

- M. R. Salem, A. H. Mangood, and S. K. Hamdona. Dissolution of calcite crystals in the presence of some metal ions. *Journal of Materials Science*, 29(24):6463 — 6467, 1994.
- J. Schott, S. L. Brantley, D. Crerar, C. Guy, M. Borcsik, and C. Willaime. Dissolution kinetics of strained calcite. *Geochimica et Cosmochimica Acta*, 53:373 — 382, 1989.
- E. L. Sjöberg and D.T. Rickard. Calcite dissolution kinetics: surface speciation and the origin of the variable pH dependence. *Chemical Geology*, 42: 119 — 136, 1984a.
- E. L. Sjöberg and D.T. Rickard. Temperature dependence of calcite dissolution kinetics between 1 and 62 °C at pH 2.7 to 8.4 in aqueous solutions. *Geochimica et Cosmochimica Acta*, 48:485 — 493, 1984b.
- M. Sorai, T. Ohsumi, M. Ishikawa, and K. Tsukamoto. Feldspar dissolution rates measured using phase-shift interferometry: Implications to CO₂ underground sequestration. *Applied Geochemistry*, 22:2795 — 2809, 2007.
- L. L. Stillings and S. L. Brantley. Feldspar dissolution at 25 °C and pH 3: Reaction stoichiometry and the effect of cations. *Geochimica et Cosmochimica Acta*, 59(8):1483 — 1496, 1995.
- S. A. Welch and W. J. Ullman. Feldspar dissolution in acidic and organic solution: Compositional and pH dependence of dissolution rate. *Geochimica et Cosmochimica Acta*, 60(16):2939 — 2948, 1996.
- S. K. Yadav, G. J. Chakrapani, and M. K. Gupta. An experimental study of dissolution kinetics of calcite, dolomite, leucogranite and gneiss in buffered solutions at temperature 25 and 5 °C. *Environmental Geology*, 53:1683 — 1694, 2008.
- R. Zhang, S. Hu, X. Zhang, and W. Yu. Dissolution kinetics of dolomite in water at elevated temperatures. *Aquatic Geochemistry*, 13:309 — 338, 2007.

Appendix A

Figures

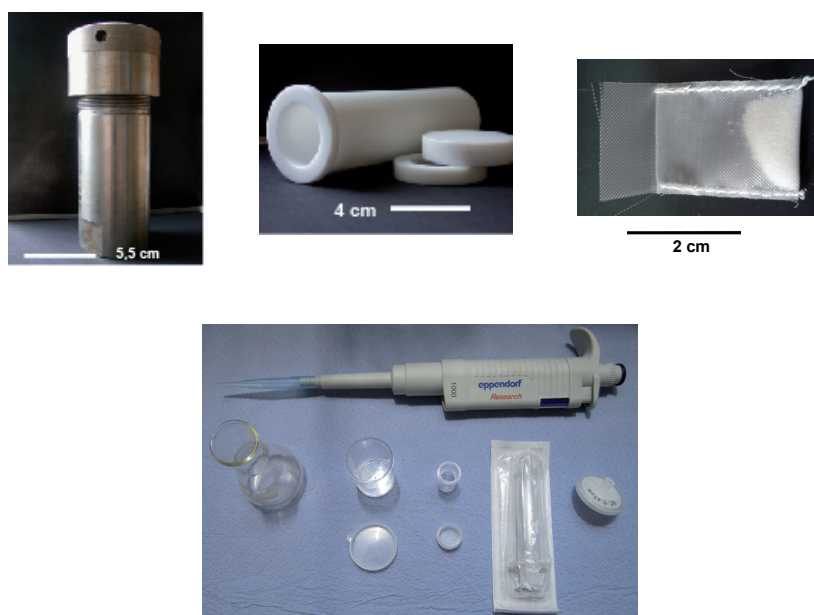


Figure A.1: Various construction elements of the used teflon reactor as well as preparation equipments: steel autoclave (top left), teflon inlay (top middle), teflon net including a solid sample (top right), preparation equipments (bottom)

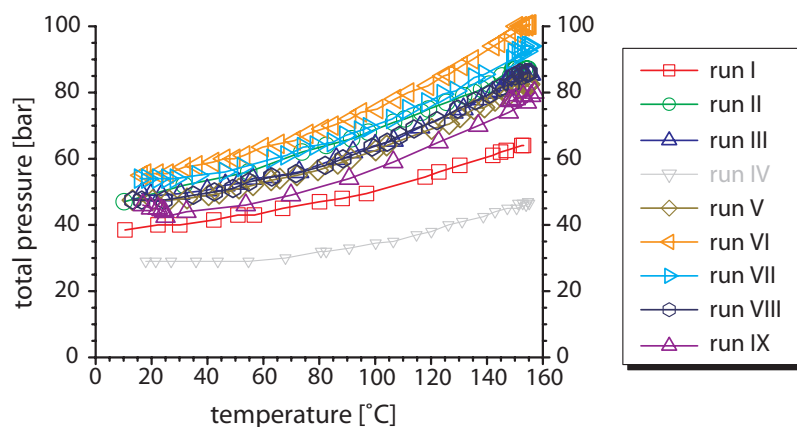


Figure A.2: p-T characteristics of nine reference experiments accomplished with the help of the PARR reactor: run conditions identical to teflon experiments result in similar curve characteristics; CO₂ source: dry ice; target temperature: 150 °C; average target pressure: 85 bar; gray data set represents a failed experiment due to an increased CO₂ release during the experimental installation



Figure A.3: Experimental setup of the used PARR reactor with heating control (top left), reactor with furnace and pressure control (top middle), Knauer pump system and gas bottle (top right) as well as the sampling system (bottom)

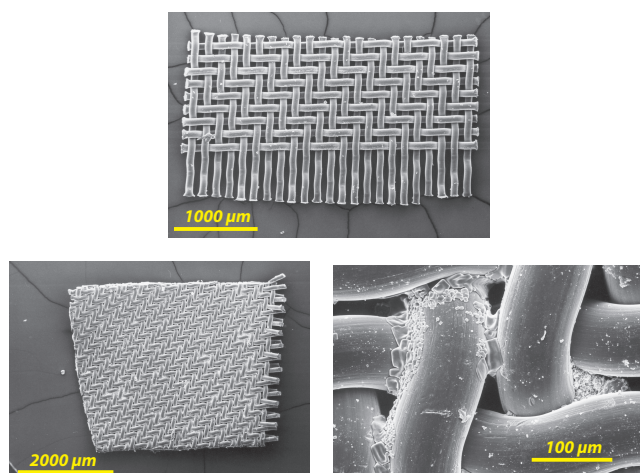


Figure A.4: SEM analyses of the used teflon meshes before (top) and after (bottom) a teflon reactor experiment (SEM laboratory, IfG, CAU Kiel)

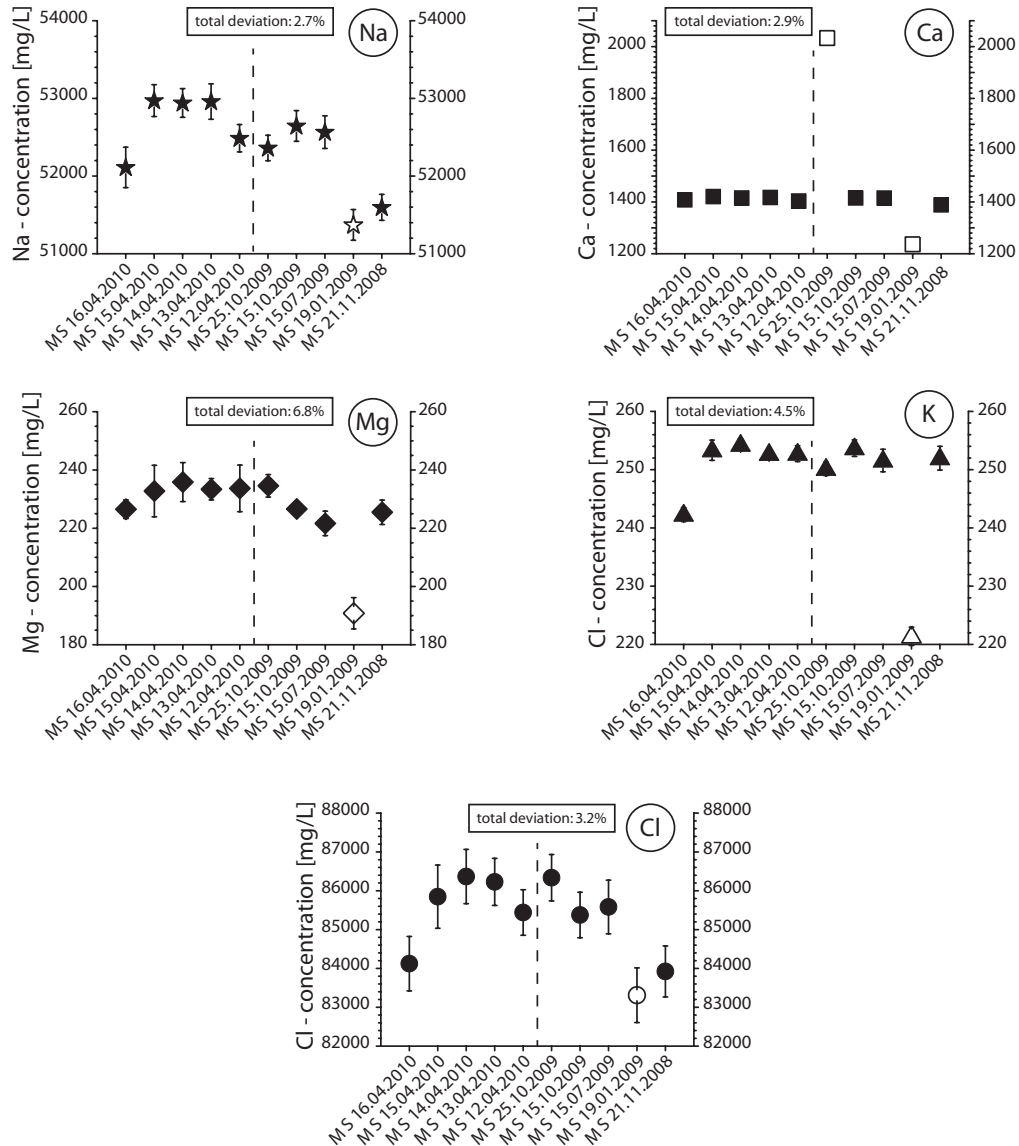


Figure A.5: Chemical composition of the initial model brine and their endurance over the period of storage: (i) data set on the left of the dashed line: five samples of the same single model brine at five time steps within the period of storage; (ii) data set on the right of the dashed line: different model brine charges. Unfilled data points describe outliers caused by initial weight uncertainties of salts or deionized water and are not used to calculate the total derivation of the entire data set. (ICP-OES laboratory, IfG, CAU Kiel)

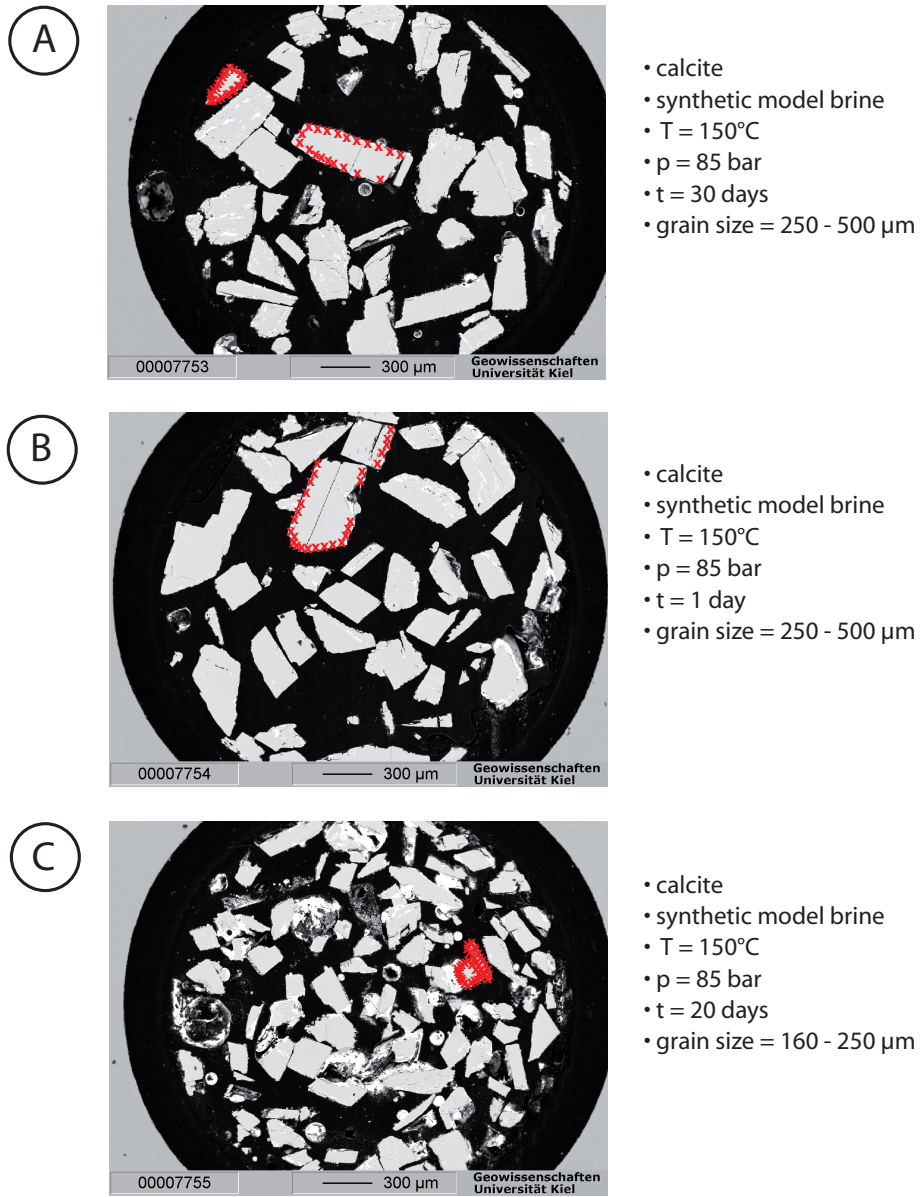


Figure A.6: Backscattered electron images of reacted calcite grains: red crosses describe the points of measuring (EMP laboratory, IfG, CAU Kiel)

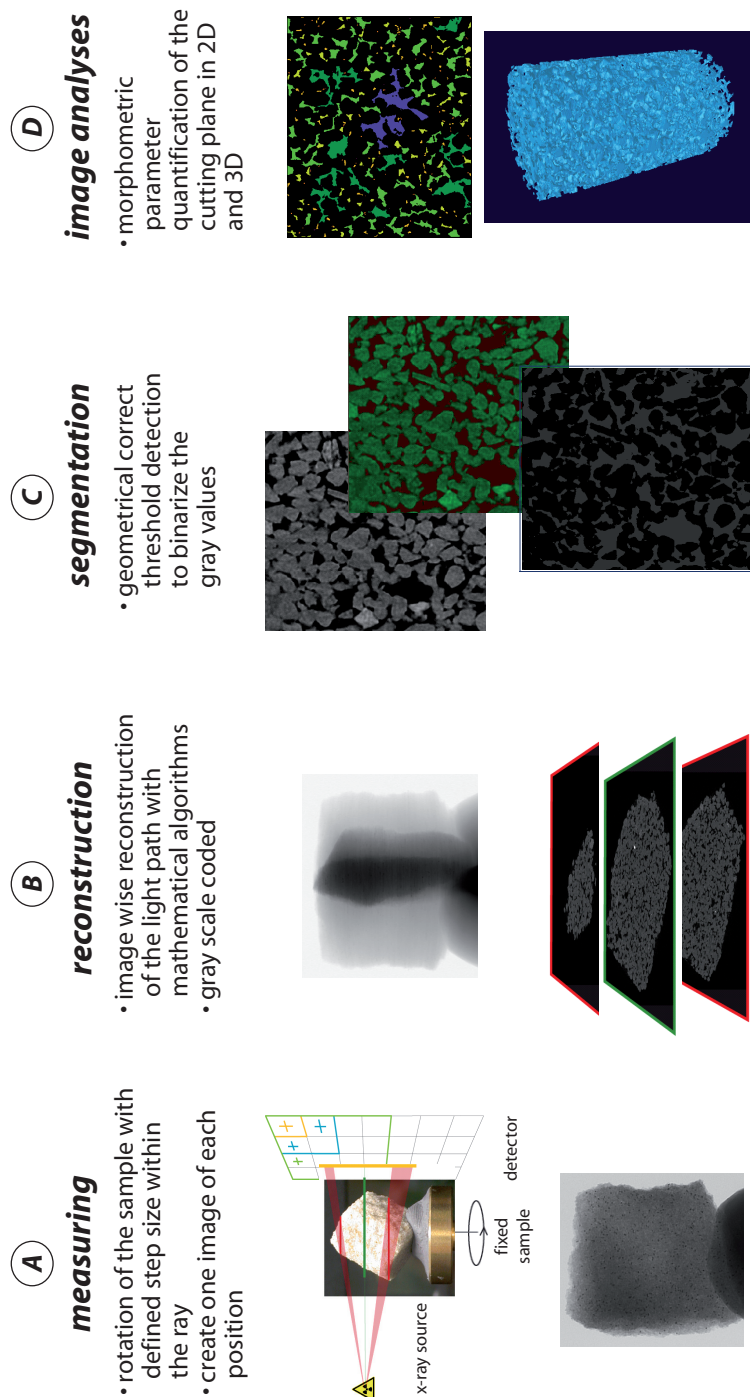


Figure A.7: Simplified illustration of the functionality of the micro computertomography: (A) sample measuring based on x-ray analyses, (B) gray scale coded sample reconstruction based on mathematical algorithms, (C) geometrical threshold detection to binarize the gray values, (D) morphometric parameter quantification of the cutting plane in 2D and 3D (provided by W.-A. Kahl)

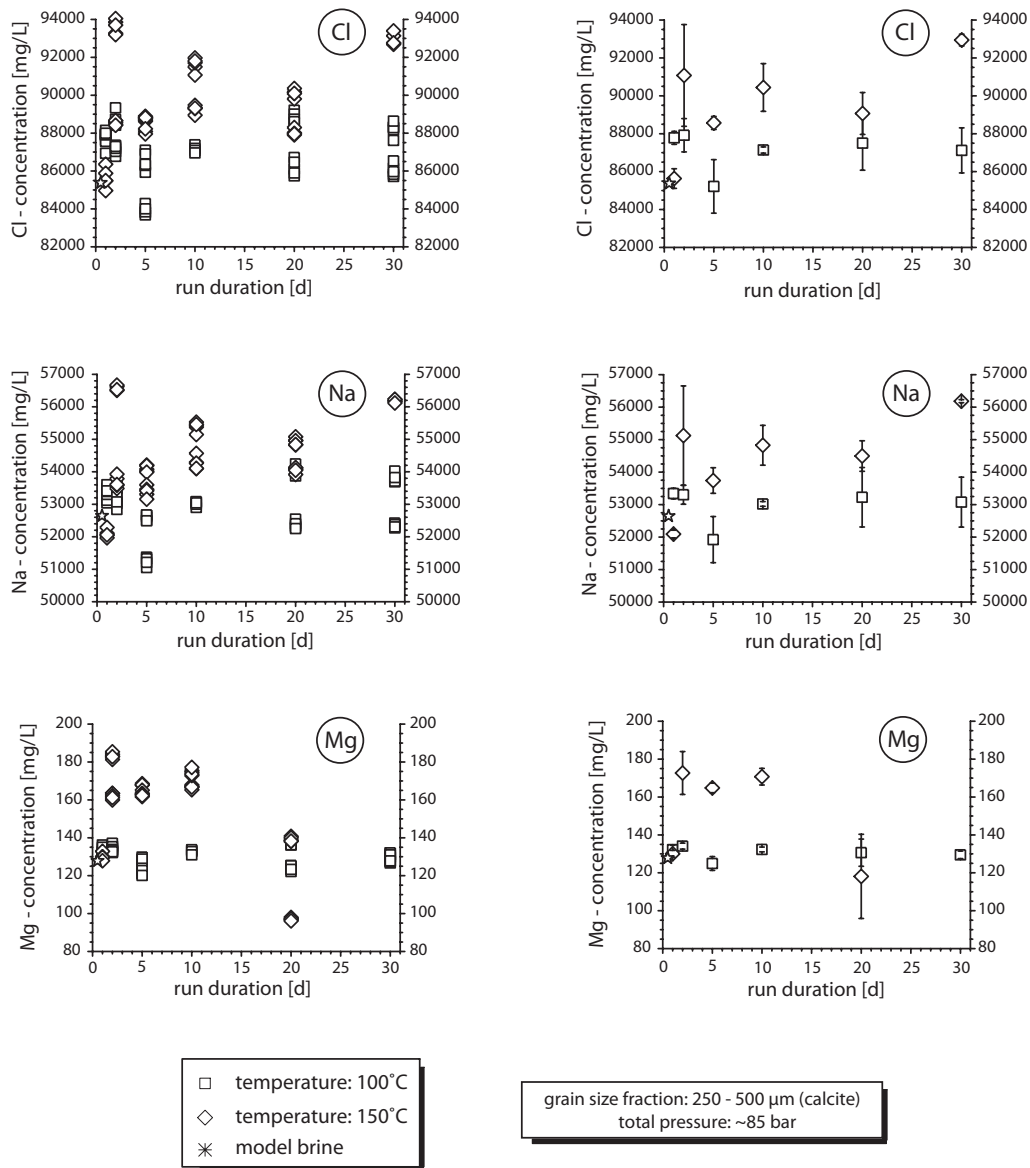


Figure A.8: Temperature dependent alteration of the model brine with increasing run duration (starting material: calcite): *left*: single measurements; *right*: averaged values; compare text for detailed descriptions of the shown data set. **Results:** (i) all analyzed components describe similar curve progressions with increasing run duration; (ii) no significant concentration changes with increasing run duration (ICP-OES laboratory, IfG, CAU Kiel)

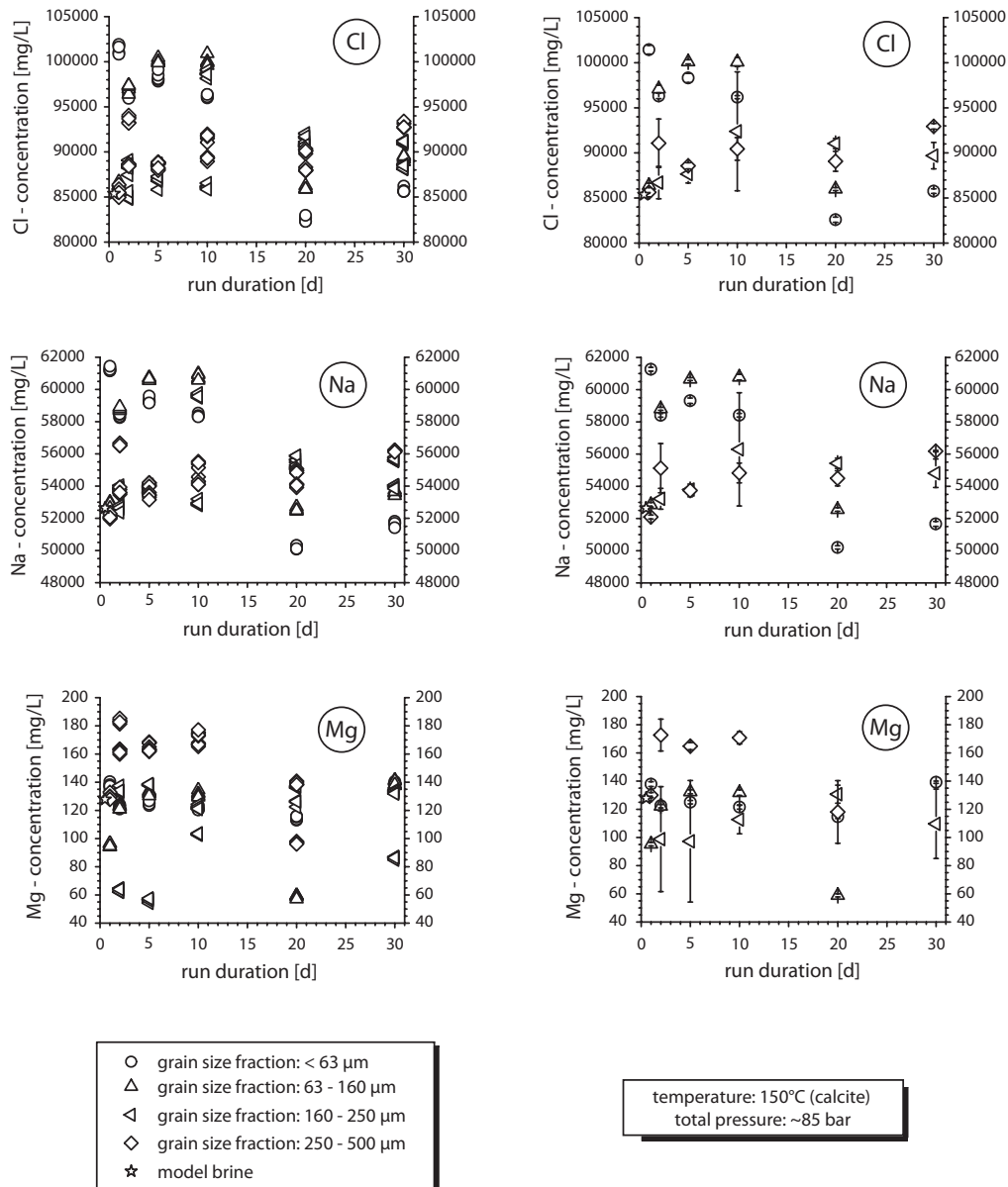


Figure A.9: Grain size dependent alteration of the model brine with increasing run duration (starting material: calcite): *left*: single measurements; *right*: averaged values; compare text for detailed descriptions of the shown data set. **Results:** (i) in relation to the main components Cl and Na the post-experimental fluid samples exhibit slightly increased concentrations in regard to the initial model brine; (ii) in relation to the minor component Mg significant differences between pre- and post-experimental fluid samples can be observed (ICP-OES laboratory, IfG, CAU Kiel)

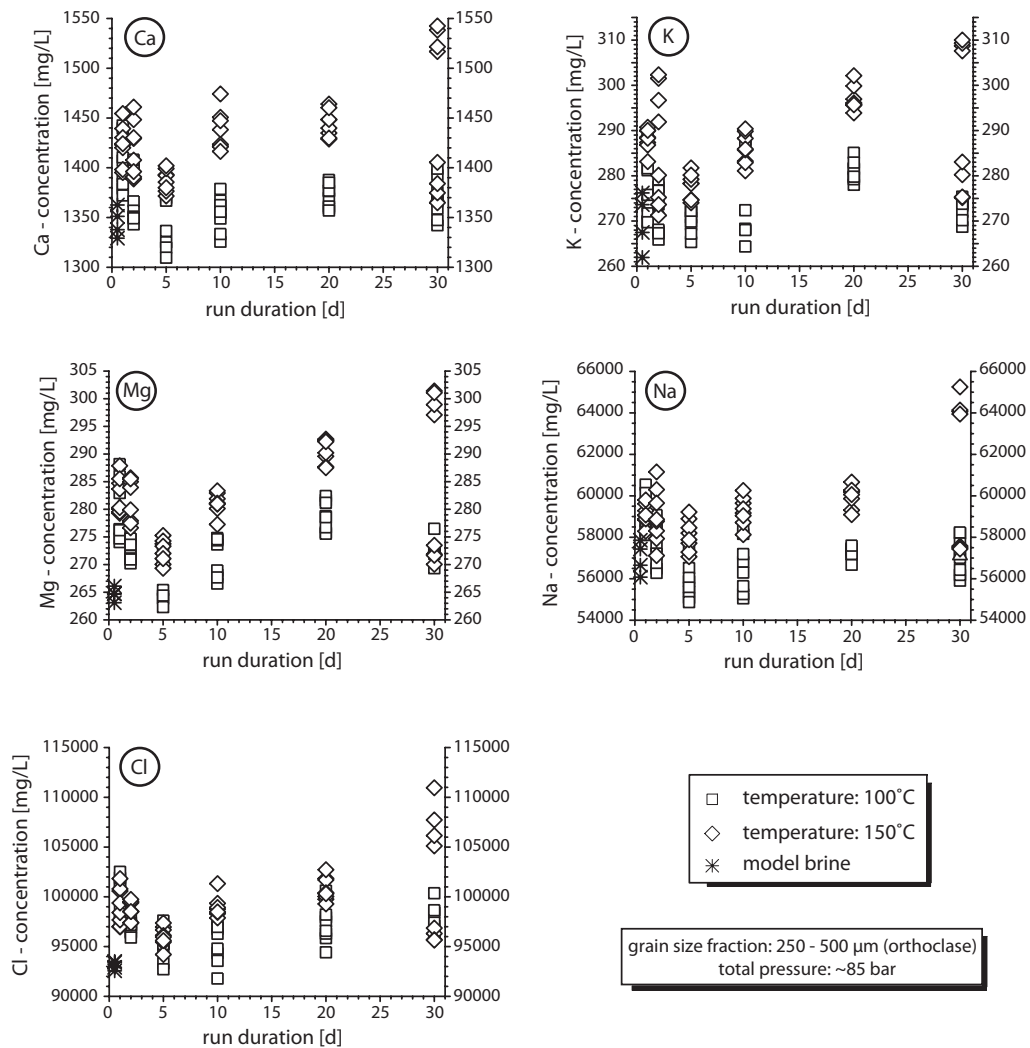


Figure A.10: Temperature dependent alteration of the model brine with increasing run duration - *single measurements* (starting material: orthoclase): compare text for detailed descriptions of the shown data set. **Results:** (i) all analyzed main components describe similar curve progressions with increasing run duration; (ii) no significant concentration changes with increasing run duration; (iii) fluid samples of experiments at 150 °C exhibit slightly increased element concentrations in regard to samples of experiments at 100 °C (ICP-OES laboratory, RWE Dea, Wietze)

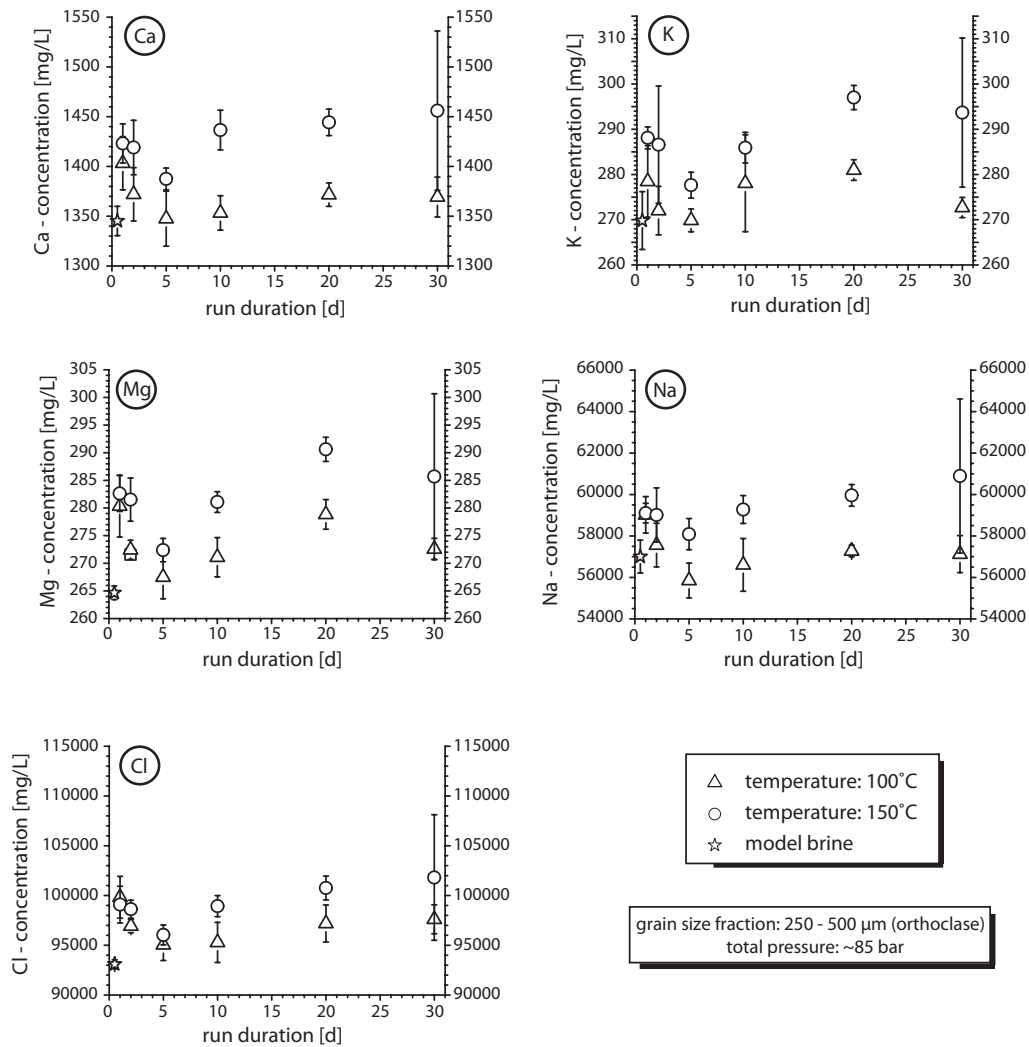


Figure A.11: Temperature dependent alteration of the model brine with increasing run duration - *average values* (starting material: orthoclase): compare text for detailed descriptions of the shown data set. **Results:** (i) all analyzed main components describe similar curve progressions with increasing run duration; (ii) no significant concentration changes with increasing run duration; (iii) fluid samples of experiments at 150 °C exhibit slightly increased element concentrations in regard to samples of experiments at 100 °C (ICP-OES laboratory, RWE Dea, Wietze)

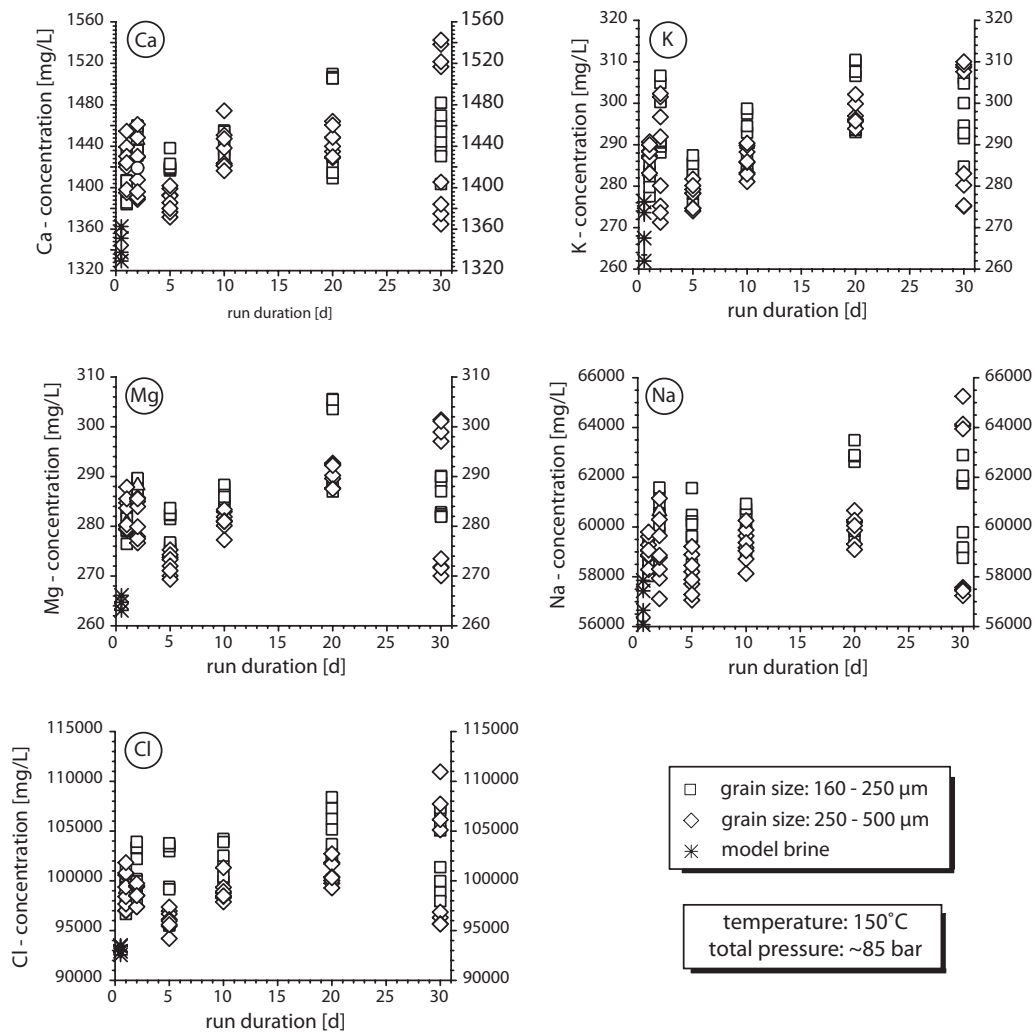


Figure A.12: Grain size dependent alteration of the model brine with increasing run duration - *single measurements* (starting material: orthoclase); compare text for detailed descriptions of the shown data set. **Results:** (i) all analyzed main components describe similar curve progressions with increasing run duration; (ii) no significant concentration changes with increasing run duration; (iii) no significant differences in concentration between both grain size fractions (ICP-OES laboratory, RWE Dea, Wietze)

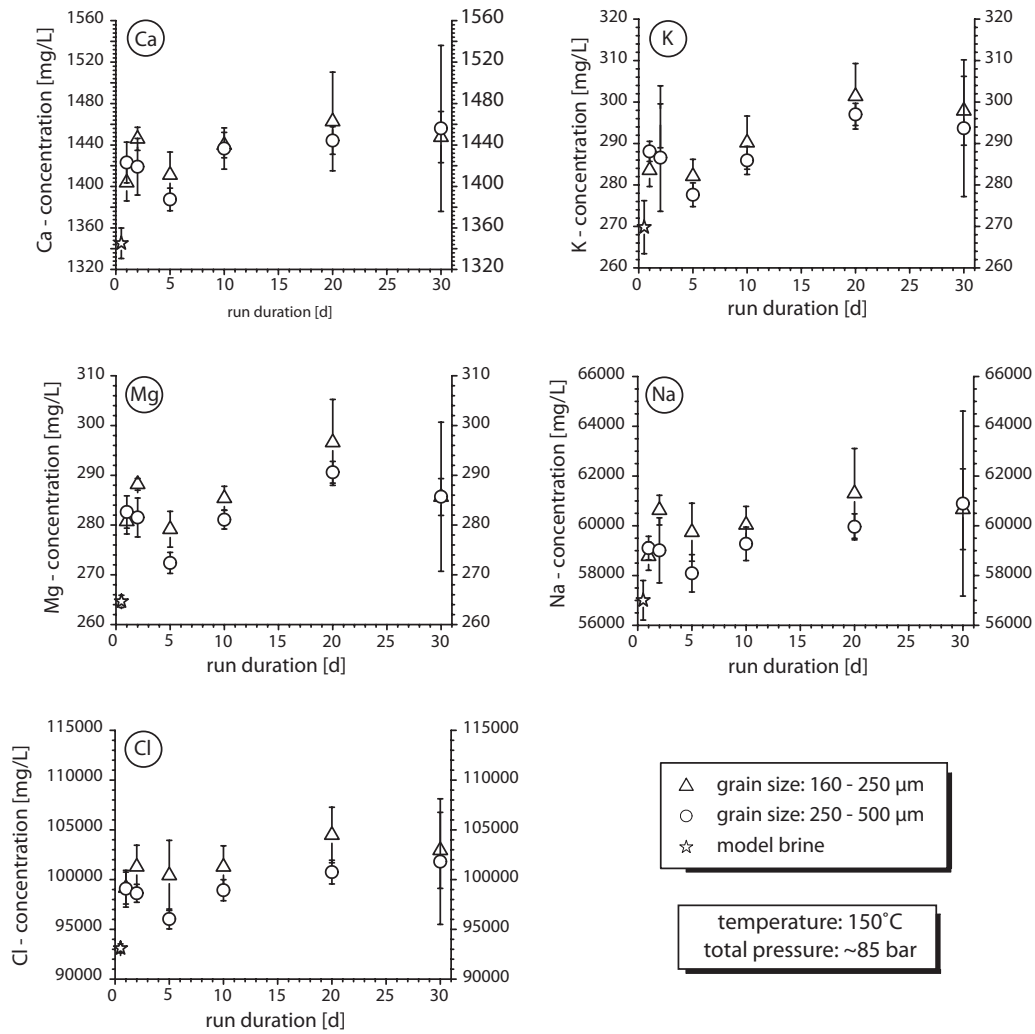


Figure A.13: Grain size dependent alteration of the model brine with increasing run duration - *average values* (starting material: orthoclase): compare text for detailed descriptions of the shown data set. **Results:** (i) all analyzed main components describe similar curve progressions with increasing run duration; (ii) no significant concentration changes with increasing run duration; (iii) no significant differences in concentration between both grain size fractions (ICP-OES laboratory, RWE Dea, Wietze)

Appendix B

Tables

Table B.1: Overview of compared mineral dissolution experiments and their corresponding references

mineral	quantity	references
aragonite <i>CaCO₃</i>	2	Chou et al. (1989), Cubillas et al. (2005)
calcite <i>CaCO₃</i>	14	Berner and Morse (1974), Plummer et al. (1978), Schott et al. (1989), Chou et al. (1989), Alkattan et al. (1998), Alkattan et al. (2002), Gledhill and Morse (2004), Palandri and Kharaka (2004), Cubillas et al. (2005), Pokrovsky et al. (2005), Gledhill and Morse (2006a), Yadav et al. (2008), Finneran and Morse (2009), Pokrovsky et al. (2009)
dolomite <i>(Ca, Mg)CO₃</i>	6	Gautelier et al. (1999), Lund et al. (1973), Pokrovsky et al. (2005), Gautelier et al. (2007), Yadav et al. (2008), Zhang et al. (2007)
magnesite <i>MgCO₃</i>	2	Pokrovsky et al. (2005), Chou et al. (1989)
witherite <i>BaCO₃</i>	1	Chou et al. (1989)
albite <i>NaAlSi₃O₈</i>	5	Oelkers et al. (1994), Stillings and Brantley (1995), Chen and Brantley (1997), Blake and Walter (1999), Harouiya and Oelkers (2004)

Continued on next page

Table B.1 – continued from previous page

mineral	quantity	references
anorthite $CaAl_2Si_2O_8$	2	Oelkers and Schott (1995), Sorai et al. (2007)
orthoclase $K/AlSi_3O_8/$	1	Blake and Walter (1999)
plagioclase (bytownite) $(Na, Ca)/(Al, Si)Si_3O_8$	1	Stillings and Brantley (1995)
plagioclase (labradorite) $(Na, Ca)/(Al, Si)Si_3O_8$	3	Stillings and Brantley (1995), Blake and Walter (1999), Carroll and Knauss (2005)
plagioclase (oligoclase) $(Ca, Na)Al(Si, Al)_3O_8$	1	Stillings and Brantley (1995)
K-feldspar $(Ba, Ca, Na, K, NH_4)(Al, B, Si)_4O_8$	3	Gautier et al. (1994), Stillings and Brantley (1995), Harouiya and Oelkers (2004)
quartz SiO_2	3	Dove and Crerar (1990), Blake and Walter (1999), Harouiya and Oelkers (2004)
kaolinite $Al_4(OH)_8Si_4O_{10}/$	1	Oelkers et al. (1994)
montmorillonite $(Na, Ca)_{0.3}(Al, Mg)_2Si_4O_{10}(OH)_2 \cdot 4 H_2O$	1	Golubev et al. (2006)

Table B.2: EMP measurements of unreacted carbonate samples regarding their chemical composition (EMP laboratory, IfG, CAU Kiel)

mineral	MgO [wt%]	CaO [wt%]	R^a [wt%]	total [wt%]	n^b
<i>calcite</i>					
grain 1	0.26	57.44	0.19	57.89	5
grain 2	0.26	58.09	0.12	58.47	6
grain 3	0.27	58.54	0.13	58.94	4
total	0.26	57.99	0.15	58.40	15
<i>dolomite</i>					
grain 1	21.86	30.94	0.21	53.01	5
grain 2	21.58	30.54	0.32	52.44	6
grain 3	21.49	30.46	0.55	52.50	5
grain 4	21.55	30.50	0.46	52.51	10
total	21.60	30.59	0.40	52.59	26

^a sum of residual components measured by EMP analyses^b number of measuring points within the grain

Table B.3: EMP measurements of unreacted feldspar samples regarding their chemical composition (EMP laboratory, IfG, CAU Kiel)

mineral	SiO ₂ [wt%]	Al ₂ O ₃ [wt%]	CaO [wt%]	Na ₂ O [wt%]	K ₂ O [wt%]	total [wt%]	n ^a
<i>anorthite</i>							
grain 1 (line A)	44.35	34.08	19.08	0.59	0.01	98.11	21
grain 1 (line B)	44.37	34.03	19.02	0.63	0.00	98.05	19
grain 2 (line A)	44.16	34.30	19.22	0.51	0.00	98.19	17
grain 2 (line B)	44.20	34.11	19.14	0.53	0.01	97.99	41
grain 3 (line A)	43.75	34.64	19.31	0.46	0.01	98.17	17
grain 3 (line B)	43.86	34.40	19.33	0.47	0.01	98.07	10
grain 4 (line A)	43.87	34.71	19.29	0.50	0.01	98.38	24
grain 4 (line B)	43.92	34.64	19.23	0.52	0.01	98.31	16
grain 5 (line A)	43.99	34.70	19.26	0.52	0.01	98.48	18
grain 5 (line B)	44.23	34.43	19.20	0.55	0.01	98.42	15
anorthite total	44.09	34.37	19.19	0.53	0.01	98.20	198
<i>orthoclase (Na commanding)</i>							
grain 1	68.71	18.91	0.06	10.99	0.68	99.34	13
grain 2	68.91	18.95	0.06	11.35	0.10	99.37	13
grain 3	68.88	18.75	0.08	11.16	0.57	99.44	9
grain 4	68.27	19.08	0.10	11.40	0.13	98.97	8
grain 5	68.75	19.05	0.14	11.05	0.64	99.63	1
total	68.76	18.93	0.07	11.27	0.29	99.32	44
<i>orthoclase (K commanding)</i>							
grain 1	64.72	17.89	0.00	0.21	17.33	100.15	12
grain 2	64.56	17.80	0.00	0.21	17.34	99.91	23
grain 3	64.54	17.77	0.01	0.17	17.36	99.85	50
grain 4	64.43	17.93	0.00	0.43	16.94	99.72	8
grain 5	64.71	17.82	0.00	0.19	17.33	100.05	13
total	64.61	17.82	0.00	0.21	17.31	99.96	106

^a number of measuring points within the grain

Table B.4: Overview of the accomplished monomineralic experiments and the appendant experimental conditions:
Cc - calcite, Do - dolomite, An - anorthite, Or - orthoclase

	initial weight [ml]	t [d]	p [bar]	gas phase	T [°C]	grain size fraction [μm]
	fluid	solid				<63 63 - 160 160 - 250 250 - 500
teflon						
reactors	37	1, 2, 5, 10, 20, 30, (180)	85	dry ice	100	Cc An Or
teflon						
reactors	37	1, 2, 5, 10, 20, 30, (180)	85	dry ice	150	Cc Cc Cc Do An Or
PARR						
reactor	195.14	5, 7, 11, 14	85	dry ice, CO ₂ , N ₂	150	Cc Do An Or

Table B.5: EMP measurements on a subset of reacted calcite grains and their relative deviation according to the chemical composition of the starting material (EMP laboratory, IfG, CAU Kiel)

	MgO [wt%]	CaO [wt%]	R ^a [wt%]	total [wt%]	n ^b
<i>calcite (250 - 500 μm, t = 1 day, T = 150°C, p = 85 bar)</i>					
grain 1	0.25	58.89	0.13	59.27	23
grain 2	0.24	59.31	0.12	59.67	5
total	0.25	58.96	0.13	59.34	28
starting material	0.26	57.99	0.15	58.40	15
relative deviation	0.96	1.017	0.87	1.016	
<i>calcite (250 - 500 μm, t = 30 days, T = 150°C, p = 85 bar)</i>					
grain 1	0.24	59.82	0.12	60.18	20
grain 2	0.46	59.42	0.14	60.02	26
total	0.36	59.60	0.13	60.09	46
starting material	0.26	57.99	0.15	58.40	15
relative deviation	1.38	1.028	0.87	1.029	
<i>calcite (160 - 250 μm, t = 2 days, T = 150°C, p = 85 bar)</i>					
grain 1	0.24	59.64	0.14	60.03	23
grain 2	0.27	58.17	0.18	58.62	16
total	0.25	59.04	0.16	59.45	39
starting material	0.26	57.99	0.15	58.40	15
relative deviation	0.96	1.018	1.067	1.018	
<i>calcite (160 - 250 μm, t = 20 days, T = 150°C, p = 85 bar)</i>					
grain 1	0.88	58.57	0.13	59.58	11
total	0.88	58.57	0.13	59.58	11
starting material	0.26	57.99	0.15	58.40	15
relative deviation	3.38	1.010	0.87	1.020	

^a sum of residual components measured by EMP analyses

^b number of measuring points within the grain

Table B.6: Results of ICP-OES measurements on post-experimental fluid samples of experiments with calcite; experimental conditions: teflon reactor, T: 100 °C, p: ~85 bar; grain size: 250 – 500 μm . (ICP-OES laboratory, IfG, CAU Kiel)

run duration [d]	series	Ca [mg/L]	Cl [mg/L]	K [mg/L]	Mg [mg/L]	Na [mg/L]
1	V-I	1397.58	88150.67	b.d.l. ^d	126.66	53303.33
		1390.58	88350.67	b.d.l.	125.66	53343.33
		1394.58	87840.67	b.d.l.	125.16	53053.33
		1387.58	88060.67	b.d.l.	125.46	53133.33
		1391.58	88140.67	b.d.l.	125.06	53503.33
	V-II	1395.58	87140.67	b.d.l.	127.66	53313.33
		1404.58	88120.67	b.d.l.	131.46	53423.33
		1394.58	87770.67	b.d.l.	128.16	53613.33
		1400.58	88110.67	b.d.l.	129.46	53403.33
		1400.58	88200.67	b.d.l.	130.26	53423.33
average ^a	1395.78	87988.67		127.50	53351.33	
SD ^b	5.18	341.79		2.29	164.98	
RSD ^c	0.37	0.39		1.80	0.31	
2	V-I	1421.58	88930.67	b.d.l.	131.06	53663.33
		1419.58	88720.67	b.d.l.	129.86	53723.33
		1425.58	89540.67	b.d.l.	132.36	53423.33
		1414.58	88750.67	b.d.l.	130.56	53513.33
		1411.58	88620.67	b.d.l.	129.06	53503.33
	V-II	1403.58	86980.67	b.d.l.	127.46	53113.33
		1408.58	87570.67	b.d.l.	128.96	53033.33
		1397.58	87240.67	b.d.l.	128.26	52853.33
		1396.58	87400.67	b.d.l.	128.06	53243.33
		1399.58	87500.67	b.d.l.	127.86	53083.33
average	1409.88	88125.67		129.35	53315.33	
SD	10.42	879.30		1.58	291.84	
RSD	0.74	1.00		1.22	0.55	

Continued on next page

Table B.6 – continued from previous page

run duration [d]	series	Ca [mg/L]	Cl [mg/L]	K [mg/L]	Mg [mg/L]	Na [mg/L]
5	V-I	1388.58	86140.67	b.d.l.	120.96	52523.33
		1389.58	86500.67	b.d.l.	123.86	52623.33
		1382.58	86560.67	b.d.l.	122.96	52673.33
		1391.58	87300.67	b.d.l.	125.06	52683.33
		1385.58	87110.67	b.d.l.	124.06	52503.33
	V-II	1350.58	84000.67	b.d.l.	116.26	51383.33
		1353.58	83890.67	b.d.l.	116.36	51333.33
		1350.58	84490.67	b.d.l.	119.16	51333.33
		1351.58	84050.67	b.d.l.	117.96	51063.33
		1352.58	84210.67	b.d.l.	115.36	51223.33
average	1369.68	85425.67		120.20	51934.33	
SD	19.03	1411.77		3.65	710.45	
RSD	1.39	1.65		3.04	1.37	
10	V-I	1438.58	87590.67	b.d.l.	128.56	53083.33
		1435.58	87400.67	b.d.l.	128.96	52913.33
		1436.58	87290.67	b.d.l.	127.96	53013.33
		1432.58	87290.67	b.d.l.	126.26	53093.33
		1433.58	87160.67	b.d.l.	126.26	53053.33
	V-II	819.58	76250.67	b.d.l.		47123.33
		809.58	75650.67	b.d.l.		47143.33
		810.58	76200.67	b.d.l.		46953.33
		812.58	75550.67	b.d.l.		47323.33
		812.58	75970.67	b.d.l.		47083.33
average	1124.18	81635.67		127.60	50078.33	
SD	328.05	6024.56		1.27	3114.38	
RSD	29.18	7.38		1.00	6.22	
20	V-I	1427.58	89410.67	b.d.l.	134.16	54033.33
		1426.58	89210.67	b.d.l.	133.66	53883.33
		1422.58	88750.67	b.d.l.	132.26	54063.33
		1419.58	88940.67	b.d.l.	131.46	54253.33
		1416.58	88810.67	b.d.l.	131.56	54253.33
	V-II	1435.58	86310.67	b.d.l.	117.46	52353.33
		1430.58	85950.67	b.d.l.	120.66	52553.33
		1440.58	86920.67	b.d.l.	118.86	52303.33
		1439.58	86670.67	b.d.l.	120.46	52413.33
		1425.58	86100.67	b.d.l.	118.56	52263.33
average	1428.48	87707.67		125.91	53237.33	
SD	8.12	1425.94		7.18	915.73	
RSD	0.57	1.63		5.70	1.72	

Continued on next page

Table B.6 – continued from previous page

run duration [d]	series	Ca [mg/L]	Cl [mg/L]	K [mg/L]	Mg [mg/L]	Na [mg/L]
30	V-I	1423.58	88380.67	b.d.l.	127.26	53703.33
		1423.58	87820.67	b.d.l.	124.86	53763.33
		1416.58	88530.67	b.d.l.	127.26	54033.33
		1425.58	88490.67	b.d.l.	126.26	53723.33
		1419.58	88840.67	b.d.l.	125.16	53833.33
	V-II	1419.58	85920.67	b.d.l.	121.96	52283.33
		1421.58	86350.67	b.d.l.	122.66	52403.33
		1426.58	86740.67	b.d.l.	126.26	52433.33
		1422.58	86030.67	b.d.l.	122.86	52383.33
		1418.58	86170.67	b.d.l.	123.06	52313.33
average	1421.78	87327.67		124.76	53087.33	
SD	3.19	1189.79		2.00	769.49	
RSD	0.22	1.36		1.60	1.45	

^a average of five single analyses calculated after equation 4.1 [mg/L]

^b standard deviation of five single analyses calculated after equation 4.2 [mg/L]

^c relative standard deviation [%]

^d below detection limit

Table B.7: Validation of the reproducibility of experimental data
(calcite: 250 – 500 μm , T: 100 °C)

t [d]		Ca [mg/L]	Cl [mg/L]	Mg [mg/L]	Na [mg/L]
1	average VI ^a	1392.38	88108.67	125.60	53267.33
	average VII ^b	1399.18	87868.67	129.40	53435.33
	deviation ^c	-0.49	0.27	-3.03	-0.32
2	average VI	1418.58	88912.67	130.58	53565.33
	average VII	1401.18	87338.67	128.12	53065.33
	deviation	1.23	1.77	1.88	0.93
5	average VI	1387.58	86722.67	123.38	52601.33
	average VII	1351.78	84128.67	117.02	51267.33
	deviation	2.58	2.99	5.15	2.54
10	average VI	1435.38	87346.67	127.60	53031.33
	average VII	812.98	75924.67		47125.33
	deviation	43.36	13.08		11.14
20	average VI	1422.58	89024.67	132.62	54097.33
	average VII	1434.38	86390.67	119.20	52377.33
	deviation	-0.83	2.96	10.12	3.18
30	average VI	1421.78	88412.67	126.16	53811.33
	average VII	1421.78	86242.67	123.36	52363.33
	deviation	0.00	2.45	2.22	2.69

^{a,b} average of five analyses of each individual fluid sample within experimental series V-I & V-II [mg/L], calculated after equation 4.1

^c deviation of experimental series V-II in regard to values of experimental series V-I [%], positive values: V-I > V-II, negative values: V-I < V-II

Table B.8: Results of ICP-OES measurements on post-experimental fluid samples of experiments with calcite; experimental conditions: teflon reactor, T: 150 °C, p: ~85 bar; grain size: 250 – 500 μm . (ICP-OES laboratory, IfG, CAU Kiel)

run duration [d]	series	Ca [mg/L]	Cl [mg/L]	K [mg/L]	Mg [mg/L]	Na [mg/L]
1	V-I	267.38	78610.67	b.d.l. ^d	-85.53	50203.33
		267.18	79280.67	b.d.l.	-83.35	50373.33
		265.08	78680.67	b.d.l.	-83.01	50443.33
		266.48	79130.67	b.d.l.	-83.00	50253.33
		266.08	79490.67	b.d.l.	-83.57	50383.33
	V-II	1262.58	84290.67	b.d.l.	97.16	51193.33
		1256.58	83410.67	b.d.l.	94.26	51133.33
		1245.58	82900.67	b.d.l.	94.16	51053.33
		1249.58	83810.67	b.d.l.	93.96	51373.33
		1245.58	83430.67	b.d.l.	92.16	51143.33
average ^a	1251.98	83568.67		94.34	51179.33	
SD ^b	7.44	517.22		1.79	119.50	
RSD ^c	0.59	0.62		1.90	0.23	
2	V-I	1497.58	91200.67	b.d.l.	147.36	55713.33
		1499.58	91790.67	b.d.l.	148.36	55593.33
		1492.58	91980.67	b.d.l.	149.66	55753.33
		1499.58	91130.67	b.d.l.	145.66	55613.33
		1493.58	91630.67	b.d.l.	147.06	55613.33
	V-II	1392.58	86370.67	b.d.l.	127.76	52873.33
		1387.58	86480.67	b.d.l.	127.66	53013.33
		1389.58	86580.67	b.d.l.	126.46	52573.33
		1385.58	86590.67	b.d.l.	124.26	52673.33
		1385.58	86350.67	b.d.l.	125.46	52693.33
average	1442.38	89010.67		136.97	54211.33	
SD	57.21	2685.59		11.31	1529.46	
RSD	3.97	3.02		8.26	2.82	

Continued on next page

Table B.8 – continued from previous page

run duration [d]	series	Ca [mg/L]	Cl [mg/L]	K [mg/L]	Mg [mg/L]	Na [mg/L]
5	V-I	1444.58	86820.67	b.d.l.	132.16	53163.33
		1440.58	86770.67	b.d.l.	132.86	53103.33
		1441.58	86730.67	b.d.l.	132.26	53293.33
		1438.58	86560.67	b.d.l.	129.36	53273.33
		1438.58	86620.67	b.d.l.	129.36	53073.33
	V-II	1420.58	86020.67	b.d.l.	127.56	52393.33
		1417.58	85890.67	b.d.l.	126.06	52683.33
		1414.58	86700.67	b.d.l.	127.66	52543.33
		1413.58	86750.67	b.d.l.	127.16	52503.33
		1413.58	86160.67	b.d.l.	126.56	52243.33
average	1428.38	86502.67		129.10	52827.33	
SD	13.33	344.28		2.53	394.61	
RSD	0.93	0.40		1.96	0.75	
10	V-I	1453.58	87270.67	b.d.l.	132.16	53373.33
		1445.58	86880.67	b.d.l.	131.36	53183.33
		1437.58	87230.67	b.d.l.	131.06	53653.33
		1442.58	87400.67	b.d.l.	129.66	53353.33
		1448.58	87250.67	b.d.l.	131.06	53193.33
	V-II	1487.58	89430.67	b.d.l.	139.76	54463.33
		1474.58	89000.67	b.d.l.	137.16	54523.33
		1485.58	89650.67	b.d.l.	138.86	54233.33
		1478.58	89900.67	b.d.l.	137.86	54613.33
		1492.58	89740.67	b.d.l.	141.46	54543.33
average	1464.68	88375.67		135.04	53913.33	
SD	21.08	1260.58		4.38	613.55	
RSD	1.44	1.43		3.25	1.14	
20	V-I	1342.58	88110.67	b.d.l.	103.06	54053.33
		1342.58	87740.67	b.d.l.	102.46	54163.33
		1345.58	88030.67	b.d.l.	105.06	54043.33
		1344.58	88290.67	b.d.l.	104.26	53913.33
		1338.58	88030.67	b.d.l.	102.56	53923.33
	V-II	1119.58	85840.67	b.d.l.	60.96	53163.33
		1117.58	85950.67	b.d.l.	61.56	53203.33
		1116.58	86230.67	b.d.l.	62.26	53003.33
		1117.58	85920.67	b.d.l.	61.56	53213.33
		1113.58	85890.67	b.d.l.	60.46	53133.33
average	1229.88	87003.67		82.42	53581.33	
SD	119.03	1105.79		22.22	470.22	
RSD	9.68	1.27		26.96	0.88	

Continued on next page

Table B.8 – continued from previous page

run duration [d]	series	Ca [mg/L]	Cl [mg/L]	K [mg/L]	Mg [mg/L]	Na [mg/L]
30	V-I	899.58	87410.67	b.d.l.	14.46	54843.33
		900.58	87640.67	b.d.l.	13.16	54533.33
		902.58	87810.67	b.d.l.	13.66	54663.33
		904.58	88200.67	b.d.l.	15.26	54633.33
		905.58	88370.67	b.d.l.	12.66	54453.33
	V-II	1445.58	91070.67	b.d.l.	132.36	55313.33
		1457.58	91330.67	b.d.l.	133.36	55253.33
		1442.58	90680.67	b.d.l.	129.26	55263.33
		1439.58	90620.67	b.d.l.	130.46	55313.33
		1439.58	90690.67	b.d.l.	132.36	55203.33
average	1444.98	89382.67		131.56	54947.33	
SD	7.47	1612.04		1.66	354.72	
RSD	0.52	1.80		1.26	0.65	

^a average of five single analyses calculated after equation 4.1 [mg/L]

^b standard deviation of five single analyses calculated after equation 4.2 [mg/L]

^c relative standard deviation [%]

^d below detection limit

Table B.9: Validation of the reproducibility of experimental data
(calcite: 250 – 500 μm , T: 150 °C)

t [d]		Ca [mg/L]	Cl [mg/L]	Mg [mg/L]	Na [mg/L]
1	average VI ^a	266.44	79038.67	-83.70	50331.33
	average VII ^b	1251.98	83568.67	94.34	51179.33
	deviation ^c	-369.89	-5.73	212.71	-1.68
2	average VI	1496.58	91546.67	147.62	55657.33
	average VII	1388.18	86474.67	126.32	52765.33
	deviation	7.24	5.54	14.43	5.20
5	average VI	1440.78	86700.67	131.20	53181.33
	average VII	1415.98	86304.67	127.00	52473.33
	deviation	1.72	0.46	3.20	1.33
10	average VI	1445.58	87206.67	131.06	53351.33
	average VII	1483.78	89544.67	139.02	54475.33
	deviation	-2.64	-2.68	-6.07	-2.11
20	average VI	1342.78	88040.67	103.48	54019.33
	average VII	1116.98	85966.67	61.36	53143.33
	deviation	16.82	2.36	40.71	1.62
30	average VI	902.58	87886.67	13.84	54625.33
	average VII	1444.98	90878.67		55269.33
	deviation	-60.09	-3.40		-1.18

^{a,b} average of five analyses of each individual fluid sample within experimental series V-I & V-II [mg/L], calculated after equation 4.1

^c deviation of experimental series V-II in regard to values of experimental series V-I [%], positive values: V-I > V-II, negative values: V-I < V-II

Table B.10: Results of ICP-OES measurements on post-experimental fluid samples of experiments with calcite; experimental conditions: teflon reactor, T: 150 °C, p: ~85 bar; grain size: 160 – 250 μm . (ICP-OES laboratory, IfG, CAU Kiel)

run duration [d]	series	Ca [mg/L]	Cl [mg/L]	K [mg/L]	Mg [mg/L]	Na [mg/L]
2	V-I	1443.58	87650.67	b.d.l. ^d	127.46	53803.33
		1449.58	88590.67	b.d.l.	128.86	53793.33
		1447.58	88440.67	b.d.l.	128.66	54043.33
		1453.58	89280.67	b.d.l.	132.76	53623.33
		1443.58	88830.67	b.d.l.	129.16	53893.33
	V-II	1124.58	85160.67	b.d.l.	59.66	52743.33
		1117.58	85010.67	b.d.l.	57.46	52613.33
		1123.58	85220.67	b.d.l.	59.86	52803.33
		1121.58	85090.67	b.d.l.	57.66	52653.33
		1122.58	85840.67	b.d.l.	59.26	52383.33
average ^a	1284.78	86911.67		94.08	53235.33	
SD ^b	171.64	1795.06		37.24	645.55	
RSD ^c	13.36	2.07		39.59	1.21	
5	V-I	1429.58	88830.67	b.d.l.	133.26	53933.33
		1421.58	88610.67	b.d.l.	133.16	53963.33
		1422.58	88750.67	b.d.l.	133.36	54083.33
		1427.58	88600.67	b.d.l.	133.76	53853.33
		1421.58	88890.67	b.d.l.	133.86	54013.33
	V-II	1050.58	86020.67	b.d.l.	49.66	53633.33
		1059.58	86990.67	b.d.l.	51.86	53793.33
		1057.58	87370.67	b.d.l.	52.66	53593.33
		1054.58	87100.67	b.d.l.	51.36	53503.33
		1059.58	87480.67	b.d.l.	52.66	53663.33
average	1240.48	87864.67		92.56	53803.33	
SD	194.09	1000.47		43.14	197.26	
RSD	15.65	1.14		46.61	0.37	
10	V-I	1669.58	98970.67	b.d.l.	119.46	59643.33
		1672.58	98360.67	b.d.l.	116.26	59693.33
		1670.58	99280.67	b.d.l.	117.46	59513.33
		1670.58	98850.67	b.d.l.	117.76	59773.33
		1667.58	98800.67	b.d.l.	116.46	59573.33

Continued on next page

Table B.10 – continued from previous page

run duration [d]	series	Ca [mg/L]	Cl [mg/L]	K [mg/L]	Mg [mg/L]	Na [mg/L]
	V-II	1320.58	86260.67	b.d.l.	98.26	52973.33
		1314.58	86410.67	b.d.l.	98.96	52833.33
		1310.58	86270.67	b.d.l.	97.96	52913.33
		1307.58	86740.67	b.d.l.	98.36	53203.33
		1312.58	86060.67	b.d.l.	98.66	52933.33
average		1491.68	92600.67		107.96	56305.33
SD		188.19	6596.05		10.07	3516.22
RSD		12.62	7.12		9.33	6.24
20	V-I	1414.58	91760.67	b.d.l.	121.26	55673.33
		1409.58	91170.67	b.d.l.	117.76	55483.33
		1406.58	91310.67	b.d.l.	117.76	55623.33
		1415.58	92260.67	b.d.l.	122.06	55883.33
		1412.58	91920.67	b.d.l.	121.56	55893.33
	V-II	1465.58	90860.67	b.d.l.	132.06	55163.33
		1461.58	90460.67	b.d.l.	131.36	55053.33
		1455.58	90950.67	b.d.l.	131.36	55153.33
		1454.58	90840.67	b.d.l.	132.26	55153.33
		1456.58	90970.67	b.d.l.	132.26	55313.33
average		1435.28	91250.67		125.97	55439.33
SD		25.09	562.91		6.38	315.95
RSD		1.75	0.62		5.06	0.57
30	V-I	1430.58	88310.67	b.d.l.	129.66	54023.33
		1421.58	88440.67	b.d.l.	127.96	54063.33
		1423.58	88810.67	b.d.l.	128.96	54053.33
		1422.58	88360.67	b.d.l.	127.76	53923.33
		1429.58	88690.67	b.d.l.	127.16	53863.33
	V-II	1384.58	91070.67	b.d.l.	82.26	55583.33
		1379.58	91290.67	b.d.l.	81.86	55803.33
		1374.58	91220.67	b.d.l.	81.96	55573.33
		1373.58	91450.67	b.d.l.	80.26	55623.33
		1379.58	91370.67	b.d.l.	81.66	55693.33
average		1401.98	89901.67		104.95	54820.33
SD		25.21	1464.02		24.63	884.40
RSD		1.80	1.63		23.47	1.61

^a average of five single analyses calculated after equation 4.1 [mg/L]

^b standard deviation of five single analyses calculated after equation 4.2 [mg/L]

^c relative standard deviation [%]

^d below detection limit

Table B.11: Validation of the reproducibility of experimental data
(calcite: 160 - 250 μm , T: 150 $^{\circ}\text{C}$)

t [d]		Ca [mg/L]	Cl [mg/L]	Mg [mg/L]	Na [mg/L]
2	average VI ^a	1447.58	88558.67	129.38	53831.33
	average VII ^b	1121.98	85264.67	58.78	52639.33
	deviation^c	22.49	3.72	54.57	2.21
5	average VI	1424.58	88736.67	133.48	53969.33
	average VII	1056.38	86992.67	51.64	53637.33
	deviation	25.85	1.97	61.31	0.62
10	average VI	1670.18	98852.67	117.48	59639.33
	average VII	1313.18	86348.67	98.44	52971.33
	deviation	21.37	12.65	16.21	11.18
20	average VI	1411.78	91684.67	120.08	55711.33
	average VII	1458.78	90816.67	131.86	55167.33
	deviation	-3.33	0.95	-9.81	0.98
30	average VI	1425.58	88522.67	128.30	53985.33
	average VII	1378.38	91280.67	81.60	55655.33
	deviation	3.31	-3.12	36.40	-3.09

^{a,b} average of five analyses of each individual fluid sample within experimental series V-I & V-II [mg/L], calculated after equation 4.1

^c deviation of experimental series V-II in regard to values of experimental series V-I [%], positive values: V-I > V-II, negative values: V-I < V-II

Table B.12: Results of ICP-OES measurements on post-experimental fluid samples of experiments with calcite; experimental conditions: teflon reactor, T: 150 °C, p: ~85 bar; grain size: 63 – 160 μm . (ICP-OES laboratory, IfG, CAU Kiel)

run duration [d]	Ca [mg/L]	Cl [mg/L]	K [mg/L]	Mg [mg/L]	Na [mg/L]
1	1375.58	86590.67	b.d.l. ^d	96.36	52853.33
	1367.58	86080.67	b.d.l.	94.26	53013.33
	1363.58	86280.67	b.d.l.	94.16	52843.33
	1364.58	86710.67	b.d.l.	96.76	52923.33
	1364.58	86290.67	b.d.l.	94.76	52633.33
average ^a	1367.18	86390.67		95.26	52853.33
SD ^b	4.93	255.24		1.22	140.53
RSD ^c	0.36	0.30		1.28	0.27
2	1438.58	97010.67	b.d.l.	122.56	58763.33
	1438.58	97410.67	b.d.l.	123.56	58883.33
	1436.58	96390.67	b.d.l.	120.86	58693.33
	1434.58	97260.67	b.d.l.	122.96	58793.33
	1428.58	97370.67	b.d.l.	121.06	58923.33
average	1435.38	97088.67		122.20	58811.33
SD	4.15	420.14		1.19	92.57
RSD	0.29	0.43		0.97	0.16
5	1530.58	99930.67	b.d.l.	133.26	60573.33
	1534.58	100190.67	b.d.l.	134.06	60743.33
	1533.58	100460.67	b.d.l.	131.76	60733.33
	1531.58	100040.67	b.d.l.	132.46	60553.33
	1533.58	99870.67	b.d.l.	130.36	60663.33
average	1532.78	100098.67		132.38	60653.33
SD	1.64	236.16		1.42	88.03
RSD	0.11	0.24		1.07	0.15
10	1488.58	99990.67	b.d.l.	132.56	60663.33
	1490.58	100910.67	b.d.l.	134.56	60723.33
	1480.58	100030.67	b.d.l.	131.96	60993.33
	1478.58	99850.67	b.d.l.	130.56	60923.33
	1479.58	99590.67	b.d.l.	129.46	60573.33
average	1483.58	100074.67		131.82	60775.33
SD	5.57	498.08		1.95	177.12
RSD	0.38	0.50		1.48	0.29

Continued on next page

Table B.12 – continued from previous page

run duration [d]	Ca [mg/L]	Cl [mg/L]	K [mg/L]	Mg [mg/L]	Na [mg/L]
20	1593.58	85860.67	b.d.l.	59.76	52613.33
	1595.58	86020.67	b.d.l.	59.36	52723.33
	1592.58	86260.67	b.d.l.	59.56	52513.33
	1590.58	85900.67	b.d.l.	58.66	52443.33
	1584.58	85880.67	b.d.l.	57.16	52493.33
average	1591.38	85984.67		58.90	52557.33
SD	4.21	166.37		1.06	111.49
RSD	0.26	0.19		1.80	0.21
30	2128.58	89620.67	b.d.l.	141.66	53773.33
	2112.58	88930.67	b.d.l.	138.66	53563.33
	2122.58	89210.67	b.d.l.	140.86	53603.33
	2138.58	89390.67	b.d.l.	137.56	53413.33
	2126.58	89520.67	b.d.l.	138.36	53653.33
average	2125.78	89334.67		139.42	53601.33
SD	9.44	273.00		1.75	131.42
RSD	0.44	0.31		1.26	0.25

^a average of five single analyses calculated after equation 4.1 [mg/L]

^b standard deviation of five single analyses calculated after equation 4.2 [mg/L]

^c relative standard deviation [%]

^d below detection limit

Table B.13: Results of ICP-OES measurements on post-experimental fluid samples of experiments with calcite; experimental conditions: teflon reactor, T: 150 °C, p: ~85 bar; grain size: <63 μm .
(ICP-OES laboratory, IfG, CAU Kiel)

run duration [d]	Ca [mg/L]	Cl [mg/L]	K [mg/L]	Mg [mg/L]	Na [mg/L]
1	1522.58	101020.67	260.37	137.76	61183.33
	1525.58	101820.67	263.57	140.36	61323.33
	1516.58	100830.67	b.d.l. ^d	135.76	61153.33
	1521.58	101910.67	262.47	138.16	61233.33
	1518.58	101630.67	263.37	137.26	61443.33
average ^a	1520.98	101442.67	262.45	137.86	61267.33
SD ^b	3.51	487.31	1.46	1.67	117.60
RSD ^c	0.23	0.48	0.56	1.21	0.19
2	1426.58	96580.67	b.d.l.	124.16	58523.33
	1429.58	96650.67	b.d.l.	123.16	58253.33
	1421.58	96200.67	b.d.l.	120.96	58323.33
	1422.58	96210.67	b.d.l.	122.96	58463.33
	1422.58	95940.67	b.d.l.	121.46	58473.33
average	1424.58	96316.67		122.54	58407.33
SD	3.39	294.67		1.31	113.71
RSD	0.24	0.31		1.07	0.19
5	1428.58	97840.67	b.d.l.	125.36	59253.33
	1428.58	98010.67	b.d.l.	125.16	59223.33
	1421.58	98110.67	b.d.l.	123.46	59343.33
	1424.58	98500.67	b.d.l.	124.46	59593.33
	1433.58	99110.67	b.d.l.	126.76	59163.33
average	1427.38	98314.67		125.04	59315.33
SD	4.55	506.69		1.22	168.43
RSD	0.32	0.52		0.97	0.28
10	1438.58	96090.67	b.d.l.	122.76	58533.33
	1431.58	95990.67	b.d.l.	123.66	58533.33
	1432.58	96350.67	b.d.l.	120.56	58333.33
	1432.58	96120.67	b.d.l.	120.76	58373.33
	1441.58	96370.67	b.d.l.	120.36	58303.33
average	1435.38	96184.67		121.62	58415.33
SD	4.44	167.87		1.49	110.54
RSD	0.31	0.17		1.23	0.19

Continued on next page

Table B.13 – continued from previous page

run duration [d]	Ca [mg/L]	Cl [mg/L]	K [mg/L]	Mg [mg/L]	Na [mg/L]
20	1981.58	82320.67	233.17	113.06	50213.33
	1991.58	82760.67	b.d.l.	113.66	50083.33
	1988.58	82620.67	235.27	115.86	50303.33
	1991.58	82290.67	234.67	115.26	50313.33
	1992.58	82970.67	b.d.l.	115.76	50113.33
average	1989.18	82592.67	234.37	114.72	50205.33
SD	4.51	290.29	1.84	1.28	105.69
RSD	0.23	0.35	0.46	1.12	0.21
30	2066.58	86210.67	245.27	140.46	51733.33
	2062.58	85600.67	243.27	139.36	51683.33
	2056.58	85680.67	b.d.l.	139.16	51813.33
	2051.58	85690.67	244.67	138.46	51683.33
	2059.58	85620.67	243.97	138.56	51413.33
average	2059.38	85760.67	244.30	139.20	51665.33
SD	5.72	254.46	0.87	0.80	150.57
RSD	0.28	0.30	0.35	0.58	0.29

^a average of five single analyses calculated after equation 4.1 [mg/L]

^b standard deviation of five single analyses calculated after equation 4.2 [mg/L]

^c relative standard deviation [%]

^d below detection limit

Table B.14: Results of ICP-OES measurements on post-experimental fluid samples of experiments with calcite; conditions: teflon reactor, T: 150 °C, without CO₂; grain size: 250 – 500 μm. (ICP-OES lab., IfG, CAU Kiel)

run duration [d]	Ca [mg/L]	Cl [mg/L]	K [mg/L]	Mg [mg/L]	Na [mg/L]
1	1461.58	87840.67	256.27	136.36	53473.33
	1460.58	87910.67	253.97	135.36	53543.33
	1466.58	88410.67	254.87	136.06	53423.33
	1465.58	88410.67	255.07	135.26	53473.33
	1461.58	88300.67	256.37	135.46	53403.33
average^a	1463.18	88174.67	255.31	135.70	53463.33
SD^b	2.70	277.72	1.01	0.48	54.31
RSD^c	0.18	0.31	0.40	0.36	0.10
2	1203.58	70890.67	208.37	81.56	43713.33
	1202.58	70520.67	208.07	80.16	43693.33
	1195.58	70570.67	207.27	79.16	43623.33
	1199.58	70570.67	206.87	80.26	43713.33
	1201.58	70650.67	207.27	79.06	43473.33
average	1200.58	70640.67	207.57	80.04	43643.33
SD	3.16	147.31	0.62	1.01	101.98
RSD	0.26	0.21	0.30	1.27	0.23
5	1432.58	86230.67	251.47	133.06	52773.33
	1428.58	86500.67	251.77	131.96	52703.33
	1428.58	86270.67	251.47	132.46	52743.33
	1420.58	86150.67	251.27	130.66	52553.33
	1424.58	86430.67	251.17	129.66	52503.33
average	1426.98	86316.67	251.43	131.56	52655.33
SD	4.56	144.84	0.23	1.38	119.87
RSD	0.32	0.17	0.09	1.05	0.23
10	1311.58	78950.67	230.67	102.66	48573.33
	1309.58	78820.67	229.17	100.46	48453.33
	1312.58	79030.67	230.47	100.36	48333.33
	1314.58	79460.67	231.87	101.16	48433.33
	1313.58	79120.67	231.37	100.46	48363.33
average	1312.38	79076.67	230.71	101.02	48431.33
SD	1.92	241.31	1.03	0.97	93.38
RSD	0.15	0.31	0.44	0.96	0.19

^a average of five single analyses calculated after equation 4.1 [mg/L]

^b standard deviation of five single analyses calculated after equation 4.2 [mg/L]

^c relative standard deviation [%]

Table B.15: Calcite dissolution rates and related parameters for determination

t^a [d]	Ca^b [mg/l]	Δc^c [mol]	S^d [m ² /g]	RS^e [m ²]	R_{Ca}^f [mol/(m ² ·s)]	$\log R_{Ca}^g$ [mol/(m ² ·s)]
<i>T: 100°C, p: ~85 bar, grain size: 250 – 500 μm</i>						
1	1395.78	-7.68E-06	0.0099 ^h	0.00183	-4.85E-08	
2	1409.88	-2.05E-06	0.0099	0.00183	-6.47E-09	
5	1369.68	-1.81E-05	0.0099	0.00183	-2.29E-08	
10	1435.38	8.14E-06	0.0099	0.00183	5.15E-09	-8.29
20	1428.48	5.38E-06	0.0099	0.00183	1.70E-09	-8.77
30	1421.78	2.71E-06	0.0099	0.00183	5.71E-10	-9.24
<i>T: 150°C, p: ~85 bar, grain size: 250 – 500 μm</i>						
1	1430.58	6.22E-06	0.0099 ^h	0.00183	3.93E-08	-7.41
2	1620.98	8.23E-05	0.0099	0.00183	2.60E-07	-6.58
5	1606.98	7.67E-05	0.0099	0.00183	9.70E-08	-7.01
10	1643.28	9.12E-05	0.0099	0.00183	5.77E-08	-7.24
20	1408.48	-2.60E-06	0.0099	0.00183	-8.23E-10	
30	1623.58	8.33E-05	0.0099	0.00183	1.76E-08	-7.76
<i>T: 150°C, p: ~85 bar, grain size: 160 – 250 μm</i>						
1						
2	1289.78	-5.00E-05	0.0163 ⁱ	0.00301	-9.60E-08	
5	1245.48	-6.77E-05	0.0163	0.00301	-5.20E-08	
10	1496.68	3.26E-05	0.0163	0.00301	1.25E-08	-7.90
20	1440.28	1.01E-05	0.0163	0.00301	1.94E-09	-8.71
30	1406.98	-3.20E-06	0.0163	0.00301	-4.10E-10	
<i>T: 150°C, p: ~85 bar, grain size: 63 – 160 μm</i>						
1	1367.18	-1.79E-05	0.016 ^j	0.00296	-7.00E-08	
2	1435.38	7.32E-06	0.016	0.00296	1.43E-08	-7.84
5	1532.78	4.33E-05	0.016	0.00296	3.39E-08	-7.47
10	1483.58	2.51E-05	0.016	0.00296	9.83E-09	-8.01
20	1591.38	6.50E-05	0.016	0.00296	1.27E-08	-7.90
30	2125.78	2.62E-04	0.016	0.00296	3.42E-08	-7.47
<i>T: 150°C, p: ~85 bar, grain size: < 63 μm</i>						
1	1520.98	3.89E-05	0.05 ^k	0.00925	4.88E-08	-7.31
2	1424.58	3.33E-06	0.05	0.00925	2.08E-09	-8.68
5	1427.38	4.36E-06	0.05	0.00925	1.09E-09	-8.96
10	1435.38	7.32E-06	0.05	0.00925	9.16E-10	-9.04
20	1989.18	2.12E-04	0.05	0.00925	1.33E-08	-7.88
30	2059.38	2.38E-04	0.05	0.00925	9.93E-09	-8.00

Continued on next page

Table B.15 – continued from previous page

t^a [d]	Ca^b [mg/l]	Δc^c [mol]	S^d [m ² /g]	RS^e [m ²]	R_{Ca}^f [mol/(m ² ·s)]	$\log R_{Ca}^g$ [mol/(m ² ·s)]
<i>T: 150°C, p: ~85 bar, grain size: 250 – 500 μm, without CO₂</i>						
1	1463.18	1.92E-05	0.0099 ^h	0.00183	1.22E-07	-6.91
2	1200.58	-8.56E-05	0.0099	0.00183	-2.71E-07	
5	1426.98	4.78E-06	0.0099	0.00183	6.05E-09	-8.22
10	1312.38	-4.10E-05	0.0099	0.00183	-2.59E-08	

^a experimental run duration

^b corrected Ca-concentration within the post-experimental fluid sample

^c Ca-concentration change in regard to the Ca-concentration within the initial model brine; normalized to the initial fluid volume

^d literature data of BET surfaces

^e estimated reactive surface of the calcite samples used within the present study; according to literature data of BET surfaces after Gledhill and Morse (2006b), Finneran and Morse (2009) and Eisenlohr et al. (1999); normalized to the initial solid weight

^f Ca dissolution rate after equation 4.3

^g logarithm of the dissolution rate

^h reactive surface of limestone after Eisenlohr et al. (1999); estimated surface as average of grain size fraction 250 – 350 μm & grain size fraction 350 – 500 μm

ⁱ reactive surface of limestone (180 – 250 μm) after Eisenlohr et al. (1999)

^j reactive surface of calcite (63 – 125 μm) after Finneran and Morse (2009)

^k reactive surface of calcite (32 – 63 μm) after Gledhill and Morse (2006b)

Table B.16: Results of ICP-OES measurements on post-experimental fluid samples of experiments with dolomite; experimental conditions: teflon reactor, T: 150 °C, p: ~85 bar; grain size: 250 – 500 μm . (ICP-OES laboratory, IfG, CAU Kiel)

run duration [d]	series	Ca [mg/L]	Cl [mg/L]	K [mg/L]	Mg [mg/L]	Na [mg/L]
1	V-I	1400.58	84800.67	246.57	140.36	51603.33
		1390.58	85070.67	247.57	142.06	51973.33
		1403.58	85830.67	249.37	145.46	51983.33
		1405.58	85550.67	247.77	144.66	51963.33
		1398.58	85020.67	248.67	143.66	51953.33
	V-II	1424.58	87840.67	258.57	172.26	53393.33
		1418.58	88140.67	259.37	173.36	53783.33
		1423.58	87730.67	256.87	170.36	53653.33
		1417.58	87810.67	257.87	171.86	53793.33
		1416.58	88050.67	258.57	170.86	53673.33
average ^a		1409.98	86584.67	253.12	157.49	52777.33
SD ^b		11.68	1434.61	5.49	15.10	942.26
RSD ^c		0.83	1.66	2.17	9.59	1.79
2	V-I	1369.58	85370.67	248.37	168.96	51823.33
		1363.58	85200.67	248.97	165.56	51773.33
		1357.58	85230.67	246.27	163.66	51873.33
		1358.58	84740.67	247.67	165.16	51783.33
		1358.58	84560.67	245.67	162.66	51653.33
	V-II	1401.58	88140.67	259.27	183.06	53573.33
		1407.58	88700.67	261.77	184.36	53733.33
		1403.58	88400.67	262.47	183.16	53593.33
		1400.58	88080.67	258.77	182.06	53523.33
		1399.58	88220.67	259.87	182.46	53783.33
average		1382.08	86664.67	253.91	174.11	52711.33
SD		21.97	1756.46	7.02	9.55	984.61
RSD		1.59	2.03	2.76	5.48	1.87

Continued on next page

Table B.16 – continued from previous page

run duration [d]	series	Ca [mg/L]	Cl [mg/L]	K [mg/L]	Mg [mg/L]	Na [mg/L]
5	V-I	1375.58	86570.67	250.87	182.46	53023.33
		1381.58	87230.67	252.97	185.26	52933.33
		1370.58	87030.67	252.97	181.86	52983.33
		1376.58	86750.67	252.17	183.46	52743.33
		1375.58	86860.67	254.17	181.76	52703.33
	V-II	1466.58	88000.67	258.07	156.86	53613.33
		1468.58	87980.67	258.97	157.46	53513.33
		1462.58	87640.67	256.67	157.96	53543.33
		1468.58	88510.67	258.57	158.06	53413.33
		1467.58	88010.67	258.77	157.96	53463.33
average	1421.38	87458.67	255.42	170.31	53193.33	
SD	47.96	657.72	3.11	13.37	350.52	
RSD	3.37	0.75	1.22	7.85	0.66	
10	V-I	1344.58	82740.67	242.97	169.66	50533.33
		1337.58	82620.67	241.37	166.56	50403.33
		1340.58	82330.67	241.37	165.86	50523.33
		1337.58	82780.67	243.27	167.16	50543.33
		1350.58	82870.67	243.77	169.16	50203.33
	V-II	1393.58	83850.67	247.67	175.16	51213.33
		1394.58	84470.67	246.97	176.96	51453.33
		1389.58	83890.67	247.77	176.46	51283.33
		1387.58	83690.67	246.67	174.86	51373.33
		1385.58	84030.67	248.27	175.26	51243.33
average	1366.18	83327.67	245.01	171.71	50877.33	
SD	25.69	735.56	2.73	4.43	474.18	
RSD	1.88	0.88	1.11	2.58	0.93	
20	V-I	1261.58	79500.67	232.37	142.36	48453.33
		1254.58	79600.67	232.67	141.66	48493.33
		1260.58	79400.67	231.17	141.16	48413.33
		1253.58	79360.67	230.27	138.66	48393.33
		1253.58	79530.67	233.17	140.76	48583.33
	V-II	1201.58	83970.67	223.77	140.66	51333.33
		1196.58	84060.67	223.47	138.56	51563.33
		1204.58	84350.67	225.27	140.76	51473.33
		1208.58	84540.67	225.47	140.76	51483.33
		1200.58	84440.67	224.57	140.96	51423.33
average	1229.58	81875.67	228.22	140.63	49961.33	
SD	28.95	2532.82	4.03	1.19	1576.63	
RSD	2.35	3.09	1.77	0.84	3.16	

Continued on next page

Table B.16 – continued from previous page

run duration [d]	series	Ca [mg/L]	Cl [mg/L]	K [mg/L]	Mg [mg/L]	Na [mg/L]
30	V-I	1433.58	91160.67	265.47	177.66	55063.33
		1423.58	91130.67	267.07	178.66	55103.33
		1421.58	90960.67	265.07	177.56	55133.33
		1425.58	91220.67	265.27	176.76	55063.33
		1423.58	91100.67	265.07	175.86	55223.33
	V-II	1430.58	90930.67	264.87	179.66	55193.33
		1437.58	91350.67	266.87	182.66	55083.33
		1423.58	90940.67	265.87	178.06	54803.33
		1427.58	90180.67	262.97	176.06	54863.33
		1427.58	91150.67	264.07	178.96	55123.33
average		1427.48	91012.67	265.26	178.19	55065.33
SD		5.09	320.93	1.21	1.99	133.57
RSD		0.36	0.35	0.46	1.12	0.24

^a average of five single analyses calculated after equation 4.1 [mg/L]

^b standard deviation of five single analyses calculated after equation 4.2 [mg/L]

^c relative standard deviation [%]

Table B.17: Validation of the reproducibility of experimental data (dolomite: 250 – 500 μm , T: 150 °C)

t		Ca	Cl	Mg	Na
[d]		[mg/L]	[mg/L]	[mg/L]	[mg/L]
1	average VI ^a	1399.78	85254.67	143.24	51895.33
	average VII ^b	1420.18	87914.67	171.74	53659.33
	deviation^c	-1.46	-3.12	-19.90	-3.40
2	average VI	1361.58	85020.67	165.20	51781.33
	average VII	1402.58	88308.67	183.02	53641.33
	deviation	-3.01	-3.87	-10.79	-3.59
5	average VI	1375.98	86888.67	182.96	52877.33
	average VII	1466.78	88028.67	157.66	53509.33
	deviation	-6.60	-1.31	13.83	-1.20
10	average VI	1342.18	82668.67	167.68	50441.33
	average VII	1390.18	83986.67	175.74	51313.33
	deviation	-3.58	-1.59	-4.81	-1.73
20	average VI	1256.78	79478.67	140.92	48467.33
	average VII	1202.38	84272.67	140.34	51455.33
	deviation	4.33	-6.03	0.41	-6.16
30	average VI	1425.58	91114.67	177.30	55117.33
	average VII	1429.38	90910.67	179.08	55013.33
	deviation	-0.27	0.22	-1.00	0.19

^{a,b} average of five analyses of each individual fluid sample within experimental series V-I & V-II [mg/L], calculated after equation 4.1

^c deviation of experimental series V-II in regard to values of experimental series V-I [%], positive values: V-I > V-II, negative values: V-I < V-II

Table B.18: Dolomite dissolution rates and related parameters for determination

t^a [d]	Ca^b [mg/l]	Δc_{Ca}^c [mol]	Mg^b [mg/l]	Δc_{Mg}^c [mol]	S^d [m ² /g]	RS^e [m ²]	R_{Ca}^f [mol/(m ² ·s)]	$\log R_{Ca}^g$ [mol/(m ² ·s)]	R_{Mg}^f [mol/(m ² ·s)]	$\log R_{Mg}^g$ [mol/(m ² ·s)]
1	1409.98	-2.37E-06	157.49	1.41E-05	0.0099 ^h	0.00183	-1.50E-08		8.89E-08	-7.05
2	1382.08	-1.56E-05	174.11	2.19E-05	0.0099	0.00183	-4.93E-08		6.94E-08	-7.16
5	1421.38	3.04E-06	170.31	2.01E-05	0.0099	0.00183	3.84E-09	-8.42	2.55E-08	-7.59
10	1366.18	-2.31E-05	171.71	2.08E-05	0.0099	0.00183	-1.46E-08		1.32E-08	-7.88
20	1229.58	-8.79E-05	140.63	6.07E-06	0.0099	0.00183	-2.78E-08		1.92E-09	-8.72
30	1427.48	5.93E-06	178.19	2.39E-05	0.0099	0.00183	1.25E-09	-8.90	5.03E-09	-8.30

^a experimental run duration

^b corrected Ca- and Mg-concentrations within the post-experimental fluid sample

^c Ca- and Mg-concentration change in regard to the Ca- and Mg-concentration within the initial model brine; normalized to the initial fluid volume

^d literature data of BET surfaces

^e estimated reactive surface of the starting materials used within the present study; according to literature data of BET surfaces after Eisenlohr et al. (1999); normalized to the initial solid weight

^f dissolution rates calculated after equation 4.3

^g logarithm of the dissolution rates

^h reactive surface of limestone after Eisenlohr et al. (1999); estimated surface as average of grain size fraction 250 – 350 μm & grain size fraction 350 – 500 μm

Table B.19: Results of ICP-OES measurements on post-experimental fluid samples of experiments with orthoclase; exp. conditions: teflon reactor, T: 100 °C, p: ~85 bar; grain size: 250 - 500 μm . (ICP-OES lab, RWE Dea, Wietze)

run duration [d]	series	Al [mg/L]	Ba [mg/L]	Ca [mg/L]	Cl [mg/L]	K [mg/L]	Mg [mg/L]	Na [mg/L]	Si [mg/L]	Sr [mg/L]
1	V-I	1.851	0.079	1391.25	97397.2	269.98	276.40	58300.4	b.d.l. ^a	0.662
		1.922	0.086	1379.14	97574.8	271.69	274.08	58889.1	b.d.l.	0.666
		1.867	0.082	1372.14	98087.7	269.73	274.73	58345.3	b.d.l.	0.672
		1.836	0.069	1383.61	98696.7	275.78	276.22	59038.7	b.d.l.	0.674
		2.550	b.d.l.	1407.21	101203.0	281.23	282.96	58110.8	b.d.l.	0.682
	V-II	2.704	b.d.l.	1439.69	101217.0	281.66	284.21	60539.3	b.d.l.	0.687
		2.709	b.d.l.	1442.47	101908.0	289.90	285.98	60136.1	b.d.l.	0.698
		2.706	b.d.l.	1410.47	102511.0	287.81	288.16	58788.2	b.d.l.	0.702
		2.268	0.079	1403.25	99824.4	278.47	280.34	59018.5		0.680
		0.430	0.007	26.76	2092.1	7.90	5.58	880.3		0.015
RSD^d		18.98	9.19	1.91	2.10	2.84	1.99	1.49		2.14
2	V-I	1.458	b.d.l.	1401.41	96383.2	277.55	274.66	59071.5	b.d.l.	0.653
		1.382	b.d.l.	1400.38	96877.2	279.18	272.69	58581.7	b.d.l.	0.647
		1.355	b.d.l.	1408.04	98043.9	273.71	274.70	58514.2	b.d.l.	0.636
		1.491	b.d.l.	1366.17	97398.6	276.71	273.58	57573.8	b.d.l.	0.640
		1.294	b.d.l.	1356.85	96483.8	267.67	270.23	57214.4	b.d.l.	0.639
	V-II	1.197	b.d.l.	1350.92	95907.4	265.90	271.58	56494.1	b.d.l.	0.642
		1.283	b.d.l.	1343.15	97173.0	268.08	271.11	56284.7	b.d.l.	0.638
		1.263	b.d.l.	1349.22	97183.6	267.31	270.92	56766.5	b.d.l.	0.650
		1.340		1372.02	96931.3	272.01	272.43	57562.6		0.643
		0.100		26.80	668.7	5.36	1.74	1052.3		0.006
RSD		7.48	1.95	0.69	1.97	0.64	1.83		0.96	

Continued on next page

Table B.19 – continued from previous page

run duration [d]	series	Al [mg/L]	Ba [mg/L]	Ca [mg/L]	Cl [mg/L]	K [mg/L]	Mg [mg/L]	Na [mg/L]	Si [mg/L]	Sr [mg/L]
5	V-I	3.477	2.204	1369.80	95355.7	272.21	272.63	55882.3	b.d.l.	0.691
		3.479	2.186	1376.87	95274.5	265.36	270.21	57468.7	b.d.l.	0.684
		3.503	2.225	1375.57	96363.9	270.78	270.12	56518.1	b.d.l.	0.697
		3.567	2.232	1366.91	97605.2	272.21	271.10	56043.9	b.d.l.	0.693
		2.509	b.d.l.	1325.14	93305.9	269.20	263.85	55390.7	b.d.l.	0.636
	V-II	2.628	b.d.l.	1336.47	92717.5	272.06	265.40	55572.0	b.d.l.	0.629
		2.552	b.d.l.	1319.79	94487.4	269.88	264.39	55080.2	b.d.l.	0.624
		2.663	b.d.l.	1309.66	95250.4	267.20	262.32	54875.6	b.d.l.	0.631
		3.047	2.212	1347.53	95045.1	269.86	267.50	55853.9		0.661
		0.494	0.021	27.64	1569.3	2.52	3.92	839.7		0.033
RSD	16.21	0.94	2.05	1.65	0.93	1.47	1.50		5.01	
10	V-I	3.539	b.d.l.	1367.01	97758.3	286.73	273.63	58165.2	b.d.l.	0.647
		3.557	b.d.l.	1378.66	94356.4	288.85	274.39	56820.1	b.d.l.	0.659
		3.503	b.d.l.	1362.46	96772.4	288.05	274.80	58421.2	b.d.l.	0.657
		3.529	b.d.l.	1354.54	96290.7	287.77	274.59	57189.2	b.d.l.	0.655
		3.978	b.d.l.	1325.71	93567.0	272.39	268.20	55055.0	b.d.l.	0.650
	V-II	4.105	b.d.l.	1349.01	94786.0	268.28	268.94	56297.9	b.d.l.	0.651
		4.033	b.d.l.	1355.79	91793.0	268.02	266.56	55260.8	b.d.l.	0.657
		3.995	b.d.l.	1333.38	96976.9	264.38	267.68	55642.0	b.d.l.	0.655
		3.780		1353.32	95287.6	278.06	271.10	56606.4		0.654
		0.268		17.32	2016.4	10.70	3.56	1273.4		0.004
RSD	7.09		1.28	2.12	3.85	1.31	2.25		0.63	

Continued on next page

Table B.19 – continued from previous page

run duration [d]	series	Al [mg/L]	Ba [mg/L]	Ca [mg/L]	Cl [mg/L]	K [mg/L]	Mg [mg/L]	Na [mg/L]	Si [mg/L]	Sr [mg/L]
20	V-I	3.293	2.061	1369.53	97964.1	285.08	278.78	57381.4	b.d.l.	0.665
		3.202	2.017	1359.32	95848.0	279.62	275.82	56679.1	b.d.l.	0.655
		3.269	2.023	1361.08	96303.6	281.69	275.58	57465.1	b.d.l.	0.645
		3.160	2.008	1357.04	94427.3	278.03	276.74	57281.5	b.d.l.	0.642
V-II	b.d.l.	4.017	b.d.l.	1376.56	97554.7	281.49	278.58	57191.6	b.d.l.	0.618
		4.006	b.d.l.	1376.99	96579.3	282.92	281.65	57436.7	b.d.l.	0.627
		4.161	b.d.l.	1387.73	98213.3	279.24	282.41	57194.2	b.d.l.	0.621
		4.068	b.d.l.	1385.05	100616.0	279.80	281.18	57597.1	b.d.l.	0.628
average		3.647	2.027	1371.66	97188.3	280.98	278.84	57278.3		0.638
SD		0.449	0.023	11.79	1855.8	2.28	2.68	279.3		0.017
RSD		12.31	1.15	0.86	1.91	0.81	0.96	0.49		2.65
30	V-I	3.202	2.124	1342.23	98439.3	273.41	269.35	57006.2	b.d.l.	0.671
		3.295	2.175	1366.97	97112.6	272.05	272.63	55909.9	b.d.l.	0.673
		3.228	2.129	1358.90	96443.5	274.12	271.94	56187.4	b.d.l.	0.671
		3.180	2.125	1347.43	96002.6	268.74	272.37	56433.7	b.d.l.	0.673
V-II	b.d.l.	3.532	b.d.l.	1392.95	98648.7	273.93	272.51	58187.3	b.d.l.	0.625
		3.710	b.d.l.	1371.15	96502.3	275.38	272.99	57336.2	b.d.l.	0.642
		3.617	b.d.l.	1375.63	97397.3	270.18	272.41	57711.4	b.d.l.	0.639
		3.649	b.d.l.	1399.10	100364.0	273.80	276.47	58231.5	b.d.l.	0.638
average		3.427	2.138	1369.30	97613.8	272.70	272.58	57125.5		0.654
SD		0.222	0.025	20.06	1454.8	2.23	1.94	893.5		0.020
RSD		6.48	1.15	1.46	1.49	0.82	0.71	1.56		3.04

^a below detection limit^b average of the eight single measurements calculated after equation 4.10 [mg/L]^c standard deviation of the eight single measurements calculated after equation 4.11 [mg/L]^d relative standard deviation [%]

Table B.20: Validation of the reproducibility of experimental data (orthoclase: 250 - 500 μm , T: 100 $^{\circ}\text{C}$)

t	Al	Ba	Ca	Cl	K	Mg	Na	Si	Sr
[d]	[mg/L]	[mg/L]	[mg/L]	[mg/L]	[mg/L]	[mg/L]	[mg/L]	[mg/L]	[mg/L]
1	average VI ^a	0.08	1381.54	97939.10	271.79	275.36	58643.38	b.d.l. ^d	0.67
	average VII ^b	b.d.l.	1424.96	101709.75	285.15	285.33	59393.60	b.d.l.	0.69
	deviation ^c	-42.71	-3.14	-3.85	-4.91	-3.62	-1.28		-3.55
2	average VI	1.42	1394.00	97175.73	276.79	273.91	58435.30	b.d.l.	0.64
	average VII	1.26	1350.04	96686.95	267.24	270.96	56689.93	b.d.l.	0.64
	deviation	11.41	3.15	0.50	3.45	1.08	2.99		0.27
5	average VI	3.51	1372.29	96149.83	270.14	271.01	56478.25	b.d.l.	0.69
	average VII	2.59	1322.77	93940.30	269.58	263.99	55229.63	b.d.l.	0.63
	deviation	26.19	3.61	2.30	0.21	2.59	2.21		8.86
10	average VI	3.53	1365.67	96294.45	287.85	274.35	57648.93	b.d.l.	0.65
	average VII	4.03	1340.97	94280.73	268.27	267.84	55563.93	b.d.l.	0.65
	deviation	-14.04	1.81	2.09	6.80	2.37	3.62		0.19
20	average VI	3.23	1361.74	96135.75	281.10	276.73	57201.78	b.d.l.	0.65
	average VII	4.06	1381.58	98240.83	280.86	280.95	57354.90	b.d.l.	0.62
	deviation	-25.75	-1.46	-2.19	0.09	-1.53	-0.27		4.33
30	average VI	3.23	1353.88	96999.50	272.08	271.57	56384.30	b.d.l.	0.67
	average VII	3.63	1384.71	98228.08	273.32	273.60	57866.60	b.d.l.	0.64
	deviation	-12.42	-2.28	-1.27	-0.46	-0.74	-2.63		5.36

^{a,b} average of four measurements of one individual fluid sample within experimental series V-I & V-II [mg/L], calculated after equation 4.10

^c deviation of experimental series V-II in regard to values of experimental series V-I [%],

positive values: V-I > V-II, negative values: V-I < V-II

^d below detection limit

Table B.21: Results of ICP-OES measurements on post-experimental fluid samples of experiments with orthoclase; exp. conditions: teflon reactor, T: 150 °C, p: ~85 bar; grain size: 250 - 500 μm . (ICP-OES lab, RWE Dea, Wietze)

run duration [d]	series	Al [mg/L]	Ba [mg/L]	Ca [mg/L]	Cl [mg/L]	K [mg/L]	Mg [mg/L]	Na [mg/L]	Si [mg/L]	Sr [mg/L]
1	V-I	5.163	2.519	1439.4	96976.6	289.93	284.71	58833.5	b.d.l. ^a	0.736
		5.309	2.503	1423.1	100584.0	290.72	283.66	59282.1	b.d.l.	0.739
		5.095	2.482	1430.3	100789.0	287.34	287.88	59051.7	b.d.l.	0.741
		5.041	2.476	1420.1	101834.0	283.13	285.53	59615.2	b.d.l.	0.731
		4.026	2.186	1454.5	97022.2	288.51	280.08	59800.1	b.d.l.	0.674
	V-II	4.183	2.174	1395.2	97678.2	286.81	279.29	58290.9	b.d.l.	0.669
		4.135	2.182	1398.2	98416.6	288.30	279.55	58884.1	b.d.l.	0.666
		4.059	2.163	1424.2	99383.0	290.03	280.31	59074.6	b.d.l.	0.659
		4.626	2.336	1423.1	99085.5	288.10	282.62	59104.0		0.702
		0.569	0.171	19.7	1848.7	2.42	3.25	472.7		0.038
RSD^d	12.30	7.32	1.38	1.87	0.84	1.15	0.80		5.36	
2	V-I	5.199	b.d.l.	1388.7	98512.9	271.26	277.91	57935.2	b.d.l.	0.695
		5.266	b.d.l.	1390.7	99403.2	275.21	276.65	57116.0	0.092	0.690
		5.193	b.d.l.	1407.7	97406.9	273.64	277.49	58308.4	0.306	0.664
		5.280	b.d.l.	1396.2	99520.8	280.13	279.92	58775.5	0.038	0.657
		3.948	2.126	1429.4	97382.0	291.92	285.71	58864.1	b.d.l.	0.698
	V-II	4.160	2.176	1448.4	98531.2	301.54	285.00	60299.5	b.d.l.	0.707
		4.169	2.184	1461.0	99737.3	296.70	283.95	61154.0	b.d.l.	0.720
		4.096	2.188	1430.3	98521.2	302.33	285.51	59650.4	b.d.l.	0.722
		4.664		1419.1	98626.9	286.59	281.52	59012.9		0.694
		0.614		27.3	902.9	12.96	3.91	1308.2		0.024
RSD	13.17		1.93	0.92	4.52	1.39	2.22		3.41	

Continued on next page

Table B.21 – continued from previous page

run duration [d]	series	Al [mg/L]	Ba [mg/L]	Ca [mg/L]	Cl [mg/L]	K [mg/L]	Mg [mg/L]	Na [mg/L]	Si [mg/L]	Sr [mg/L]	
5	V-I	4.775	2.206	1393.0	95454.7	278.34	273.75	57713.0	b.d.l.	0.681	
		4.716	2.175	1371.6	96963.9	281.75	270.05	58891.4	b.d.l.	0.681	
		4.846	2.206	1392.3	96677.4	274.71	275.26	57062.4	b.d.l.	0.665	
		4.926	2.167	1385.5	94205.6	278.25	274.27	58201.3	b.d.l.	0.669	
		2.941	b.d.l.	1399.1	97369.9	279.23	273.32	59218.0	b.d.l.	0.653	
	V-II	2.952	b.d.l.	1376.5	96110.8	280.16	269.34	57285.5	b.d.l.	0.653	
		2.952	b.d.l.	1402.0	95961.7	274.03	272.02	58460.3	b.d.l.	0.650	
		2.898	b.d.l.	1380.0	95599.3	274.62	271.09	57887.0	b.d.l.	0.651	
		3.876	2.189	1387.5	96042.9	277.64	272.39	58089.9			0.663
		1.007	0.020	10.9	995.8	2.86	2.11	751.3			0.013
RSD	25.98	0.94	0.79	1.04	1.03	0.77	1.29			1.98	
10	V-I	2.975	1.958	1450.7	98308.7	281.10	282.95	59643.5	2.179	0.658	
		3.015	1.959	1438.3	99346.7	283.23	281.91	58128.7	1.318	0.667	
		3.078	1.967	1447.3	97886.0	282.91	280.14	59170.6	1.562	0.663	
		3.150	2.000	1474.2	101327.0	285.73	283.35	59876.2	1.626	0.669	
		3.826	0.234	1421.6	98759.7	288.26	277.26	59375.3	5.558	0.708	
	V-II	3.817	0.214	1423.4	98439.9	285.92	280.96	58712.8	5.877	0.716	
		3.738	0.211	1421.1	98924.7	289.84	281.11	60258.6	5.538	0.708	
		3.811	0.219	1416.4	98486.0	290.38	280.98	59043.8	5.290	0.706	
		3.426	1.095	1436.6	98934.8	285.92	281.08	59276.2			0.687
		0.401	0.936	19.9	1059.7	3.39	1.88	672.9			0.025
RSD	11.72	85.49	1.39	1.07	1.18	0.67	1.14	58.07		3.58	

Continued on next page

Table B.21 – continued from previous page

run duration [d]	series	Al [mg/L]	Ba [mg/L]	Ca [mg/L]	Cl [mg/L]	K [mg/L]	Mg [mg/L]	Na [mg/L]	Si [mg/L]	Sr [mg/L]
20	V-I	3.946	2.592	1428.8	99751.8	295.84	292.51	60184.4	5.875	0.684
		3.936	2.611	1434.9	100031.0	296.95	289.59	60666.1	5.379	0.682
		4.005	2.655	1448.3	101837.0	299.87	292.70	60226.0	5.247	0.688
		3.922	2.658	1464.0	101697.0	302.13	292.43	60272.7	5.876	0.702
	V-II	5.847	0.228	1439.9	99288.2	295.58	287.69	59310.9	7.822	0.677
		6.021	0.213	1448.6	102722.0	296.10	290.22	59865.6	7.667	0.682
		5.917	0.189	1429.9	100404.0	293.89	287.52	59092.7	8.123	0.674
		6.141	0.193	1460.4	100319.0	295.70	292.23	60060.2	7.813	0.671
average		4.967	1.417	1444.3	100756.3	297.01	290.61	59959.8	6.725	0.683
SD		1.088	1.296	13.3	1190.6	2.67	2.18	522.4	1.235	0.010
RSD		21.91	91.40	0.92	1.18	0.90	0.75	0.87	18.36	1.41
30	V-I	3.033	0.116	1516.8	105115.0	308.72	297.08	64064.5	11.713	0.689
		3.102	0.092	1538.3	107727.0	307.61	298.94	64136.8	11.726	0.699
		3.228	0.106	1542.4	106152.0	309.29	301.41	65253.7	11.439	0.702
		3.025	0.114	1521.6	110959.0	310.01	301.09	63944.4	11.486	0.704
	V-II	3.253	2.039	1364.9	96307.1	275.17	270.04	57241.3	14.499	0.644
		3.413	2.063	1374.8	96861.0	275.34	271.86	57573.9	14.617	0.644
		3.327	2.061	1384.1	95690.5	280.24	271.68	57496.7	14.380	0.656
		3.427	2.120	1405.4	95652.3	283.05	273.49	57436.4	14.253	0.662
average		3.226	1.089	1456.0	101808.0	293.68	285.69	60893.5	13.014	0.675
SD		0.160	1.050	80.1	6309.1	16.49	14.98	3717.6	1.528	0.026
RSD		4.96	96.42	5.50	6.20	5.61	5.24	6.11	11.74	3.88

^a below detection limit^b average of the eight single measurements calculated after equation 4.10 [mg/L]^c standard deviation of the eight single measurements calculated after equation 4.11 [mg/L]^d relative standard deviation [%]

Table B.22: Validation of the reproducibility of experimental data (orthoclase: 250 - 500 μm , T: 150 $^{\circ}\text{C}$)

t	Al	Ba	Ca	Cl	K	Mg	Na	Si	Sr
[d]	[mg/L]	[mg/L]	[mg/L]	[mg/L]	[mg/L]	[mg/L]	[mg/L]	[mg/L]	[mg/L]
1	average VI ^a	2.50	1428.23	10045.90	287.78	285.44	59195.63	b.d.l. ^d	0.74
	average VII ^b	2.18	1418.02	98125.00	288.41	279.80	59012.43	b.d.l.	0.67
	deviation^c	20.40	0.72	1.92	-0.22	1.98	0.31		9.47
2	average VI	b.d.l.	1395.83	98710.95	275.06	277.99	58033.78	0.10	0.68
	average VII	2.17	1442.27	98542.93	298.12	285.04	59992.00	b.d.l.	0.71
	deviation	21.80	-3.33	0.17	-8.39	-2.54	-3.37		-5.21
5	average VI	4.82	1385.60	95825.40	278.26	273.33	57967.03	b.d.l.	0.67
	average VII	2.94	1389.40	96260.43	277.01	271.44	58212.70	b.d.l.	0.65
	deviation	39.04	-0.27	-0.45	0.45	0.69	-0.42		3.30
10	average VI	3.05	1452.61	99217.10	283.24	282.09	59204.75	1.67	0.66
	average VII	3.80	1420.63	98652.58	288.60	280.08	59347.63	5.57	0.71
	deviation	-24.34	88.86	0.57	-1.89	0.71	-0.24	-233.03	-6.81
20	average VI	3.95	1444.02	100829.20	298.70	291.81	60337.30	5.59	0.69
	average VII	5.98	1444.67	100683.30	295.32	289.42	59582.35	7.86	0.68
	deviation	-51.34	-0.05	0.14	1.13	0.82	1.25	-40.43	1.89
30	average VI	3.10	1529.77	107488.25	308.91	299.63	64349.85	11.59	0.70
	average VII	3.36	1382.30	96127.73	278.45	271.76	57437.08	14.44	0.65
	deviation	-8.33	-1835.28	9.64	9.86	9.30	10.74	-24.56	6.73

^{a,b} average of four measurements of one individual fluid sample within experimental series V-I & V-II [mg/L], calculated after equation 4.10

^c deviation of experimental series V-II in regard to values of experimental series V-I [%],

^d positive values: V-I > V-II, negative values: V-I < V-II

^d below detection limit

Table B.23: Results of ICP-OES measurements on post-experimental fluid samples of experiments with orthoclase; exp. conditions: teflon reactor, T: 150 °C, p: ~85 bar; grain size: 160 - 250 μm . (ICP-OES lab, RWE Dea, Wietze)

run duration [d]	series	Al [mg/L]	Ba [mg/L]	Ca [mg/L]	Cl [mg/L]	K [mg/L]	Mg [mg/L]	Na [mg/L]	Si [mg/L]	Sr [mg/L]
1	V-I	4.545	2.193	1434.45	96666.7	287.942	280.147	59600	b.d.l. ^a	0.706
		4.370	2.175	1396.76	99582.4	283.646	276.456	58817.5	b.d.l.	0.704
		4.425	2.198	1407.27	98031.4	285.326	283.062	59459.1	b.d.l.	0.713
		4.500	2.233	1422.44	97508.1	289.341	282.244	59084.6	b.d.l.	0.721
		3.843	2.423	1406.71	101465	282.901	284.313	58267.7	b.d.l.	0.666
	V-II	3.925	2.414	1384.08	99584.2	281.992	278.986	58030.8	b.d.l.	0.651
		3.796	2.437	1392.77	99965.2	277.569	279.197	58333.6	b.d.l.	0.655
		3.889	2.444	1385.66	100410	279.77	281.578	58644	b.d.l.	0.658
		4.162	2.315	1403.8	99151.6	283.56	280.75	58779.7		0.684
		0.325	0.124	17.7	1608.0	3.94	2.54	569.4		0.029
RSD^d	7.81	5.36	1.26	1.62	1.39	0.91	0.97		4.29	
2	V-I	3.481	2.542	1456	100176	288.134	287.055	61237.1	b.d.l.	0.697
		3.700	2.522	1444.34	99942.3	289.55	287.946	59782.4	b.d.l.	0.693
		3.681	2.531	1460.06	98113.9	290.526	289.019	60919.2	b.d.l.	0.703
		3.729	2.557	1438.81	99376.2	290.918	288.405	60070.9	b.d.l.	0.71
		3.874	2.399	1431.11	103268	300.56	286.612	61587.7	b.d.l.	0.71
	V-II	3.947	2.417	1459.41	103346	304.927	289.596	60557.1	b.d.l.	0.716
		3.864	2.380	1442.09	103921	300.295	289.685	60509.4	b.d.l.	0.715
		3.879	2.404	1435.9	102199	306.624	287.187	60376.9	b.d.l.	0.705
		3.769	2.469	1446.0	101292.8	296.44	288.19	60630.1	b.d.l.	0.706
		0.152	0.075	11.2	2161.2	7.46	1.18	595.7		0.008
RSD	4.02	3.04	0.77	2.13	2.52	0.41	0.98		1.16	

Continued on next page

Table B.23 – continued from previous page

run duration [d]	series	Al [mg/L]	Ba [mg/L]	Ca [mg/L]	Cl [mg/L]	K [mg/L]	Mg [mg/L]	Na [mg/L]	Si [mg/L]	Sr [mg/L]
5	V-I	5.340	2.081	1419.83	95508.9	278.148	276.292	59594.2	3.491	0.646
		5.304	2.056	1379.48	95586.5	275.618	275.462	58503.5	2.887	0.643
		5.362	2.101	1416.60	99395.8	279.419	276.765	60485.9	3.454	0.644
		5.355	2.106	1374.49	99145.2	285.713	274.963	57820.5	3.047	0.651
	V-II	3.865	0.149	1417.70	103515	285.155	281.455	61566.9	b.d.l.	0.666
		3.779	0.167	1438.24	102977	282.62	282.255	60227.3	b.d.l.	0.669
		3.795	0.145	1419.34	103477	287.45	282.406	59632.8	b.d.l.	0.653
		3.801	0.130	1423.06	103775	282.772	283.662	60107.9	b.d.l.	0.661
average		4.575	1.117	1411.1	100422.6	282.11	279.16	59742.4	3.220	0.654
SD		0.819	1.036	22.2	3522.9	4.08	3.60	1165.8	0.299	0.010
RSD		17.89	92.78	1.57	3.51	1.45	1.29	1.95	9.30	1.54
10	V-I	4.206	2.045	1430.77	98865.4	283.158	280.806	58994.7	6.551	0.662
		4.211	2.055	1420.75	98902.2	284.633	284.321	59483.3	6.867	0.664
		4.225	2.084	1436.24	99942.7	283.814	284.05	59156.2	6.815	0.653
		4.068	2.065	1448.68	100409	286.414	285.49	60492.1	6.386	0.661
	V-II	4.252	2.435	1441.85	104214	292.928	287.9	60454.1	1.124	0.7
		4.385	2.478	1455.24	103900	297.504	288.334	60728	1.059	0.701
		4.433	2.465	1431.58	101527	298.704	286.293	60086.1	1.278	0.709
		4.246	2.449	1454.11	102523	294.496	285.897	60930.4	0.926	0.7
average		4.253	2.260	1439.9	101285.4	290.21	285.39	60040.6	3.876	0.681
SD		0.113	0.212	12.3	2108.1	6.41	2.39	739.5	2.976	0.023
RSD		2.65	9.36	0.85	2.08	2.21	0.84	1.23	76.79	3.39

Continued on next page

Table B.23 – continued from previous page

run duration [d]	series	Al [mg/L]	Ba [mg/L]	Ca [mg/L]	Cl [mg/L]	K [mg/L]	Mg [mg/L]	Na [mg/L]	Si [mg/L]	Sr [mg/L]
20	V-I	4.584	b.d.l.	1409.13	102677	293.047	286.985	59490.4	10.49	0.632
		4.785	b.d.l.	1420.81	100119	296.23	288.822	60003	10.695	0.636
		4.768	b.d.l.	1429.75	103685	293.546	289.418	59223.7	10.936	0.629
		4.718	b.d.l.	1414.45	102281	293.69	289.081	59843.4	10.611	0.625
		6.268	2.731	1509.77	107285	309.938	305.575	62619.3	2.94	0.732
	V-II	6.314	2.699	1505.53	106218	310.454	304.014	63490.1	2.803	0.726
		6.488	2.685	1506.76	105168	306.589	303.557	62847.8	2.868	0.721
		6.482	2.700	1505.46	108401	307.609	305.432	62886.8	2.532	0.713
		5.551	2.704	1462.7	104479.3	301.39	296.61	61300.6	6.734	0.677
		0.900	0.019	47.6	2789.6	7.91	8.64	1806.3	4.225	0.050
RSD	16.21	0.72	3.25	2.67	2.62	2.91	2.95	62.73	7.36	
30	V-I	3.416	2.283	1403.55	98852.9	284.718	282.83	59093.8	17.247	0.64
		3.486	2.272	1435.86	99976.6	291.572	282.408	59179.1	16.734	0.648
		3.735	2.331	1430.42	101371	294.609	282.045	59790	16.728	0.65
		3.518	2.299	1444.6	97966.1	292.801	281.901	58762.5	16.254	0.655
		3.879	0.316	1461.13	105062	300.044	288.813	61756.9	9.444	0.724
	V-II	4.019	0.300	1469.57	107085	308.587	290.125	62890.3	9.167	0.711
		4.011	0.330	1454.07	107317	306.033	289.963	61792.6	9.069	0.717
		3.921	0.321	1481.96	105888	304.769	287.022	62062	9.512	0.713
		3.748	1.307	1447.6	102939.8	297.89	285.64	60665.9	13.019	0.682
		0.245	1.058	24.7	3821.4	8.30	3.70	1622.6	3.990	0.037
RSD	6.55	81.00	1.71	3.71	2.79	1.30	2.67	30.64	5.39	

^a below detection limit^b average of the eight single measurements calculated after equation 4.10 [mg/L]^c standard deviation of the eight single measurements calculated after equation 4.11 [mg/L]^d relative standard deviation [%]

Table B.24: Validation of the reproducibility of experimental data (orthoclase: 160 - 250 μm , T: 150 $^{\circ}\text{C}$)

t	Al	Ba	Ca	Cl	K	Mg	Na	Si	Sr
[d]	[mg/L]	[mg/L]	[mg/L]	[mg/L]	[mg/L]	[mg/L]	[mg/L]	[mg/L]	[mg/L]
1	average VI ^a	2.20	1415.23	97947.15	286.56	280.48	59240.30	b.d.l. ^d	0.71
	average VII ^b	2.43	1392.31	100356.10	280.56	281.02	58319.03	b.d.l.	0.66
	deviation ^c	13.38	-10.44	1.62	-2.46	-0.19	1.56		7.52
2	average VI	3.65	1449.80	99402.10	289.78	288.11	60502.40	b.d.l.	0.70
	average VII	3.89	1442.13	103183.50	303.10	288.27	60757.78	b.d.l.	0.71
	deviation	-6.67	5.44	0.53	-3.80	-0.06	-0.42		-1.53
5	average VI	5.34	1397.60	97409.10	279.72	275.87	59101.03	3.22	0.65
	average VII	3.81	1424.59	103436.00	284.50	282.44	60383.73	b.d.l.	0.66
	deviation	28.66	92.92	-1.93	-6.19	-2.38	-2.17		-2.52
10	average VI	4.18	1434.11	99529.83	284.50	283.67	59531.58	6.65	0.66
	average VII	4.33	1445.70	103041.00	295.91	287.11	60549.65	1.10	0.70
	deviation	-3.63	-19.13	-0.81	-3.53	-1.21	-1.71	83.52	-6.44
20	average VI	4.71	1418.54	102190.50	294.13	288.58	59640.13	10.68	0.63
	average VII	6.39	1506.88	106768.00	308.65	304.64	62961.00	2.79	0.72
	deviation	-35.52	-6.23	-4.48	-4.94	-5.57	-5.57	73.92	-14.67
30	average VI	3.54	1428.61	99541.65	290.93	282.30	59206.35	16.74	0.65
	average VII	3.96	1466.68	106338.00	304.86	288.98	62125.45	9.30	0.72
	deviation	-11.83	86.21	-2.67	-4.79	-2.37	-4.93	44.46	-10.49

^{a,b} average of four measurements of one individual fluid sample within experimental series V-I & V-II [mg/L], calculated after equation 4.10

^c deviation of experimental series V-II in regard to values of experimental series V-I [%],

^d positive values: V-I > V-II, negative values: V-I < V-II

^d below detection limit

Table B.25: Orthoclase dissolution rates and related parameters for determination

t^a [d]	Si ^b [mg/L]	Δc^c [mol]	S ^d [m ² /g]	RS ^e [m ²]	R _{Si} ^f [mol/(m ² ·s)]	log R _{Si} ^g [mol/(m ² ·s)]
<i>T: 150°C, p: ~85 bar, grain size fraction: 250 - 500 μm</i>						
1	b.d.l. ^h		0.053	0.0098		
2	b.d.l.		0.053	0.0098		
5	b.d.l.		0.053	0.0098		
10	3.62	5.20E-07	0.053	0.0098	6.14E-11	-10.21
20	6.73	9.67E-07	0.053	0.0098	5.71E-11	-10.24
30	13.01	1.87E-06	0.053	0.0098	7.36E-11	-10.13
<i>T: 150°C, p: ~85 bar, grain size fraction: 160 - 250 μm</i>						
1	b.d.l.		0.053	0.0098		
2	b.d.l.		0.053	0.0098		
5	b.d.l.		0.053	0.0098		
10	3.88	5.57E-07	0.053	0.0098	6.58E-11	-10.18
20	6.73	9.67E-07	0.053	0.0098	5.71E-11	-10.24
30	13.02	1.87E-06	0.053	0.0098	7.36E-11	-10.13

^a experimental run duration^b Si-concentration within the post-experimental fluid sample^c Si-concentration change in regard to the Si concentration within the initial model brine; normalized to the initial fluid volume^d BET surface of albite after Welch and Ullman (1996) (grain size: 125 - 250 μm)^e estimated reactive surface of the orthoclase samples used within the present study; according to the BET surface of albite after Welch and Ullman (1996); normalized to the initial solid weight^f Si dissolution rate after equation 4.12^g logarithm of the dissolution rate^h below detection limit

Eidesstattliche Erklärung

Hiermit versichere ich, Katja Beier, dass die vorliegende Abhandlung, abgesehen von der Beratung durch die angegebenen Betreuer, selbstständig und ohne unerlaubte Hilfe angefertigt und alle benutzten Quellen und Hilfsmittel vollständig angegeben wurden. Die Arbeit ist weder ganz noch in Teilen einer anderen Stelle im Rahmen eines Prüfungsverfahrens vorgelegt worden, veröffentlicht oder zur Veröffentlichung eingereicht. Auszüge dieser Arbeit wurden jedoch bereits auf nationalen und internationalen Tagungen präsentiert. Des Weiteren erkläre ich, dass die vorliegende Arbeit gemäß der Grundsätze zur Sicherung guter wissenschaftlicher Praxis der Deutschen Forschungsgemeinschaft erstellt wurde.

Kiel,

KATJA BEIER

Danksagung

Ohne die Hilfe vieler Kollegen und Freunde wäre diese Arbeit nicht möglich gewesen. Daher möchte ich folgenden Personen meinen herzlichsten Dank aussprechen:

- meiner Doktormutter Prof. Dr. Astrid Holzheid, welche mir die Bearbeitung des Themas anvertraute, mich wissenschaftlich betreute und mir stets mit Rat und Tat zur Seite stand. Vielen Dank!
- meinem Kollegen Dr. Wolf-Achim Kahl für die Hilfe und Unterstützung bei der gemeinsamen Bearbeitung des Projektes.
- allen Kollegen und HiWi der AG „Experimentelle & Theoretische Petrologie“ für die herzliche Aufnahme in die Arbeitsgruppe, die wissenschaftlichen und nicht-wissenschaftlichen Gespräche, die zahlreiche Hilfe bei der Durchführung der Experimente und der Korrektur meiner geistigen Ergüsse, sowie die stets freundschaftliche, moralische Unterstützung. Ihr habt mir das Leben hier viel leichter gemacht!
- allen Kollegen der Labore (EMP, SEM/XRD, ICP-OES, TIC-TOC) am Institut für Geowissenschaften, die mir bei der Ermittlung der Daten geholfen haben. Sie standen mir bei Fragen und Problemen jederzeit zur Verfügung!
- allen Kollegen der Werkstatt des Instituts für Geowissenschaften für die stete Bereitstellung der verschiedensten Arbeitsmaterialien und die Instandhaltung sowie Modifizierung der experimentellen Aufbauten.
- Frau Petra Götze, Herrn Dr. Christoph Kersten und Herrn Dr. Michael Zettlitzer der RWE Dea AG für die sehr gute Zusammenarbeit bei der Durchführung geochemischer Analysen und der steten Bereitschaft an wissenschaftlichen Gesprächen, die meine Arbeit sehr bereichert haben.
- Herrn Michael Schmidt von der Martin-Luther-Universität Halle-Wittenberg für den sehr guten wissenschaftlichen Austausch.
- meiner Familie und meinen Freunden, insbesondere Christian und Sissy, die mich trotz der großen Entfernung in jeder Hinsicht unterstützt haben und immer an mich geglaubt haben. Vielen lieben Dank!
- allen Kollegen und Freunden, die ich vergessen habe, die mich aber dennoch in verschiedenster Form wissenschaftlich und moralisch unterstützt haben.

Diese Arbeit wurde gefördert durch das Bundesministerium für Bildung und Forschung (BMBF), EnBW Energie Baden-Württemberg AG, E.ON Energie AG, E.ON Ruhrgas AG, RWE Dea AG, Vattenfall Europe Technology Research GmbH, Wintershall Holding AG und die Stadtwerke Kiel AG als Teil des Verbundprojektes CO₂-MoPa im Rahmen des Sonderprogramms GEOTECHNOLOGIEN.

Lebenslauf

Persönliche Daten

Name	Katja Beier
Anschrift	Peter-Hansen-Straße 125 24148 Kiel
Geburtsdatum	19. Juli 1983
Geburtsort	Gotha
Staatsangehörigkeit	deutsch
Familienstand	ledig

Schulausbildung

1990 – 1991	Polytechnische Oberschule VII, Gotha-Siebleben
1991 – 1994	Staatliche Grundschule, Gotha-Siebleben
1994 – 2002	Staatliches Gymnasium "Gustav-Freytag", Gotha-Siebleben

Hochschulausbildung

10/2002 – 02/2008	Studium der Geologie/Paläontologie an der Technische Universität Bergakademie Freiberg
09/2006 – 03/2007	Diplomarbeit an der Bundesanstalt für Geowissen- schaften & Rohstoffe (Hannover)
07/2007 – 09/2007	Diplomkartierung an der Technischen Universität Bergakademie Freiberg
seit 01. Mai 2008	Doktorarbeit an der Christian - Albrechts - Uni- versität zu Kiel, Institut für Geowissenschaften, AG „Experimentelle & Theoretische Petrologie“